

# Post-Quantum Cryptography Migration in Australian Real-Time Payment Infrastructure: A Monte Carlo Simulation Study of the New Payments Platform

Nazmus Salehin Sammo

Melbourne Institute of Technology (MIT)

Melbourne, Australia

MIT252100@stud.mit.edu.au

## Abstract

Australia's New Payments Platform (NPP) processes 5.2 million real-time transactions per day under a 2,000 ms end-to-end SLA. With cryptographically relevant quantum computers projected by 2030–2035 and the Harvest Now, Decrypt Later (HNDL) threat active, financial institutions face an urgent post-quantum cryptography (PQC) migration requirement. This paper presents a comprehensive Monte Carlo simulation study of NIST FIPS 204/205/206 signature standards (ML-DSA, SLH-DSA/SPHINCS+, Falcon) in Australian payment infrastructure, to the best of our knowledge, the first to jointly model M/M/c queue saturation, GEV tail bounds, and HNDL actuarial exposure for a hardcoded-SLA real-time payment system, using empirical liboqs 0.14.0 latency measurements, real RBA transaction volumes, APRA market-share weighted routing, and an integrated M/M/c queuing model across 1,000 seasonally-mixed simulation days (80 million events). Cross-platform cloud validation (Section 5.7) was conducted using liboqs 0.15.0 on a seven-node multi-cloud testbed spanning four microarchitectures (Intel Xeon Ice Lake, Intel Xeon Cascade Lake, AMD EPYC Milan, ARM Graviton3), with 1,000 signing iterations and 100 warm-up iterations discarded per algorithm per node. ML-KEM (FIPS 203) is included as a recommended KEM pairing component (ML-KEM-768) rather than a standalone signing benchmark, consistent with its role as a key encapsulation mechanism rather than a digital signature scheme.

ML-DSA and Falcon variants achieve 100% SLA compliance across all 10,000,000

simulated transactions per configuration (zero violations across 1,000 seasonally-mixed days) with a worst-case NPP p99 overhead among SLA-compliant PQC-only modes of 1.57 ms (ML-DSA-87, 0.079% of SLA budget); the hybrid dual-signing mode adds 1.69 ms (ML-DSA-65 Hybrid, 0.085% of SLA budget), also within all SLA constraints, under modelled parameters (software HSM, liboqs 0.14.0 baseline latency, calibrated RBA network model; see Section 3.8 for validation scope). We introduce the Crypto Dilution Index ( $CDI = \Delta p99/p99_{e2e}$ ), showing all non-SPHINCS+ algorithms achieve  $CDI < 0.04$ . PQC overhead is below 4% of total end-to-end latency, confirming that algorithm selection should be driven by security level and message format requirements, not latency. GEV extreme value analysis (applied to a single representative normal-day 10,000-transaction sample, 200 blocks of 50) provides indicative evidence of Gumbel-class tails (within-day block-maxima; rigorous analysis requires daily maxima across the 1,000-day corpus; see §5.6) ( $\xi \approx 0.023\text{--}0.028$ ) with p99.9 bounds below 154 ms (95% CI upper bound; GEV point estimates 131.6–132.9 ms across non-SPHINCS+ algorithms). A multi-system route analysis confirms 100% SLA compliance on RITS (SLA 30,000 ms) and SWIFT (SLA 86,400,000 ms) for all eight algorithms; on NPP (SLA 2,000 ms), all ML-DSA and Falcon variants achieve 100% compliance while SPHINCS+ is disqualified by queue saturation (0% compliance, as described in the next paragraph). The SWIFT binding constraint is message format rather than latency. Falcon-512 is the only NIST PQC signature algorithm fitting within the 2,048-byte SWIFT MT field limit (1,563 bytes combined). The CDI framework extends to RITS ( $CDI_{RITS} \leq 0.61\%$  for all non-SPHINCS+ algorithms) and SWIFT ( $CDI_{SWIFT} \leq 0.21\%$ , exact maximum 0.2015% for ML-DSA-65 Hybrid:  $\Delta p99 = 1.69$  ms / route p99 = 838.84 ms), confirming algorithm-selection irrelevance for latency across all Australian payment routes.

SPHINCS+ saturates institutional HSM queues at NPP volumes ( $\rho = 1.8855$ ,  $c = 2$  servers), achieving 0% NPP SLA compliance. It remains viable for RITS (route p99 = 574 ms,  $CDI_{RITS} = 51.72\%$ , within 30 s SLA) and SWIFT (route p99 = 1,134 ms,  $CDI_{SWIFT} = 26.18\%$ , within 24 h SLA), confirming it is a viable low-frequency algorithm at the correct threat model, not a universally disqualified algorithm. Its queue growth dynamics at NPP volumes (6.34 ops/s surplus; utilisation ratio  $\rho_{SPHINCS+}/\rho_{ECDSA} \approx 9,428$  on M-series baseline,  $\sim 6,200$  on production Intel) are characterised as an insider-misconfiguration DoS amplification surface in hybrid PQC deployments, with a Parallel Signing Architecture mitigation proposed. An HNDL actuarial model estimates approximately 9.56 billion (9,560,492,450) NPP transaction records at risk under the conservative CRQC-2030 scenario, stored with AML/CTF Act 2006 seven-year retention obligations. Migration costs peak at USD 21.4 million in 2026, declining to USD 1.5 million per year by 2028. SLA compliance holds through 2029 at 8.03 million transactions per day.

**Keywords:** Post-quantum cryptography, ML-DSA, Falcon, Monte Carlo simulation, SLA

compliance, HNDL actuarial risk, Crypto Dilution Index, denial-of-service amplification

## 1 Introduction

Modern financial systems rely on public-key cryptography to keep payments secure. Every time money moves from one bank to another, digital signatures prove that the instruction came from a legitimate sender, and key-exchange protocols protect the message in transit. The two most widely used algorithms, ECDSA (for signing) and ECDH (for key exchange), are based on mathematics that a sufficiently powerful quantum computer could break in minutes using Shor’s polynomial-time factoring and discrete logarithm algorithm [25]. Even symmetric key and hash-based schemes face Grover’s quadratic speedup [24], though doubling key lengths largely mitigates this threat.

No such computer exists today. However, researchers estimate that cryptographically relevant quantum computers (CRQCs) could emerge between 2030 and 2035 [1]. This creates a problem that cannot be solved reactively. Financial records are often archived for 7–10 years under AML/CTF Act 2006 (Part 10, Division 2) and APRA recordkeeping obligations. An attacker who records encrypted NPP traffic today could wait for a quantum computer and decrypt it later, a strategy widely known as ‘Harvest Now, Decrypt Later’ (HNDL) [36].

In August 2024, NIST published four finalised post-quantum cryptography standards: FIPS 203 (ML-KEM), FIPS 204 (ML-DSA), FIPS 205 (SLH-DSA / SPHINCS+), and FIPS 206 (FN-DSA / Falcon) [3]. The question is no longer which algorithms to use, but whether they can be deployed in high-throughput, latency-sensitive financial infrastructure without breaking existing SLAs.

Australia’s NPP processed 5.2 million transactions per day in 2026 under a hard 2,000 ms end-to-end SLA. This paper presents a comprehensive Monte Carlo study of NIST FIPS 204/205/206 PQC signature algorithms in this specific context: a real-time gross-settlement-adjacent system with a hardcoded SLA, APRA prudential overlay, and HNDL retention exposure not modelled in prior PQC performance work, which predominantly addresses TLS handshake latency or VPN throughput, extending prior work with: (1) a 1,000-day seasonally-mixed simulation producing 80 million events; (2) an integrated M/M/c queuing model that correctly surfaces SPHINCS+ queue saturation; (3) extreme value theory (GEV) tail analysis for p99.9 and p99.99 bounds; (4) distribution goodness-of-fit testing; (5) hourly queue saturation profiling; and (6) HSM degraded-mode resilience analysis.

## 1.1 Paper Contributions

This paper makes the following contributions:

- A comprehensive Monte Carlo simulation of NIST FIPS 204/205/206 signature standards (ML-DSA, SLH-DSA/SPHINCS+, Falcon) in Australian NPP, RITS, and SWIFT payment infrastructure using empirically measured latency from liboqs 0.14.0. ML-KEM (FIPS 203) is included as a recommended KEM pairing component but not independently benchmarked as a signing algorithm (it is a KEM, not a signature scheme).
- Integration of an M/M/c Erlang-C queuing model with the Monte Carlo engine. The SPHINCS+ stability boundary ( $\rho = 1.8855 > 1$  at 13.5 TPS,  $c = 2$ ) follows directly from service time (279 ms) and arrival rate, confirming instability. The paper’s novel queue contributions beyond this stability check are: (i) quantification of queue growth dynamics (6.34 ops/s surplus at NPP peak, ~1,902 transactions queued in 5 minutes, mean wait ~133 s at  $t=300$  s); (ii) hourly saturation profiles (SPHINCS+ saturates for 16 of 24 hours on Christmas Day, peak  $\rho = 8.41$ ); (iii) minimum HSM capacity for SLA compliance ( $c \geq 8$  at daily average,  $c \geq 18$  at Christmas peak); and (iv) DoS utilisation amplification characterisation ( $\rho_{\text{SPHINCS+}}/\rho_{\text{ECDSA}} \approx 9,428$  on M-series baseline).
- Extreme value analysis (GEV block-maxima,  $n=200$  blocks, 500-resample bootstrap CIs) classifying all non-SPHINCS+ algorithms as Gumbel-class ( $\xi = 0.023\text{--}0.028 < 0.05$  threshold, exponential tail) and providing p99.9/p99.99 operational bounds below 200 ms.
- Distribution goodness-of-fit testing (Kolmogorov-Smirnov and Anderson-Darling) identifying lognormal as the best-fitting parametric model by AIC/BIC comparison across four candidate distributions for all eight algorithm configurations. The Anderson-Darling test rejects the pure lognormal tail for all configurations (consistent with geographic-routing mixture structure), while KS non-rejection at  $p = 0.071\text{--}0.215$  and AIC/BIC evidence together support its use as the simulation distribution model.
- Hourly queue dynamics analysis showing SPHINCS+ saturates HSM queues for 16 of 24 hours on Christmas Day (peak  $\rho = 8.41$ ), quantifying seasonal risk for the first time.
- An HSM single-server degraded mode resilience analysis demonstrating that all ML-DSA and Falcon variants exhibit  $|\delta p99| \leq 0.06$  ms during HSM maintenance windows (noise at  $\rho < 0.004$ ), confirming operational resilience.

- A message format compliance analysis, regulatory compliance scoring, four-phase PQC migration cost model (2025–2028 and beyond), and forward SLA projection to 2029 at 8.03 million transactions per day.
- A formal Crypto Dilution Index (CDI) metric,  $CDI(A) = \Delta p_{99}(A)/p_{99\_e2e}(A)$ , quantifying the operational irrelevance of PQC algorithm choice for NPP latency. All non-SPHINCS+ algorithms achieve  $CDI < 0.04$  ( $< 4\%$  of total latency attributable to PQC overhead), confirming that infrastructure routing and PayID lookup dominate and algorithm selection should be driven by security and format requirements, not latency.
- A SPHINCS+ queue-saturation denial-of-service (DoS) amplification analysis, characterising the security risk of misconfigured algorithm negotiation in hybrid PQC deployments and quantifying the queue growth rate (6.34 ops/s surplus at NPP peak,  $\sim 1,902$  transactions queued in 5 minutes) and utilisation amplification ( $\rho_{\text{SPHINCS+}} / \rho_{\text{ECDSA}} \approx 9,428$  at identical throughput, using M-series service times).
- Cross-platform empirical validation on a seven-node multi-cloud testbed (AWS Sydney/Singapore + Azure Sydney/Melbourne/Singapore), with signing benchmarks on the four Sydney nodes spanning all four distinct microarchitectures: Intel Xeon Ice Lake (AVX-512), Intel Xeon Cascade Lake (AVX-512), AMD EPYC Milan (AVX2), and ARM Graviton3. All four nodes confirm sub-millisecond signing latency.  $SDR_{\text{sign}} \leq 0.72\%$  across all platforms for Falcon-512 and ML-DSA-44; for the full algorithm set the bound is  $SDR_{\text{sign}} \leq 1.44\%$  (Falcon-1024/Ice Lake at  $628/43,690 = 1.44\%$ ); all values remain well below the 4% CDI threshold (see §5.6 for full per-algorithm breakdown and  $SDR_{\text{sign}}$  definition/biases). Note: these are general-purpose cloud VMs, not FIPS 140-3 certified HSMs; see Section 4.7 (HSM Deployment Sensitivity) and Section 4.10.5 (HSM Single-Server Degraded Mode Analysis) for the two complementary HSM analyses that bound this gap. AVX-512 provides a  $\sim 2.0\times$  ML-DSA-44 mean signing latency speedup on Intel Ice Lake ( $64 \mu\text{s}$  mean) over ARM Graviton3 ( $128 \mu\text{s}$  mean); at the p99 level the ratio is  $1.86\times$  ( $197 \mu\text{s}$  vs  $366 \mu\text{s}$ ). AMD EPYC ( $95 \mu\text{s}$  mean) lies between the two. Both Falcon variants invert this SIMD hierarchy: ARM Graviton3 (Falcon-512:  $207 \mu\text{s}$ , Falcon-1024:  $405 \mu\text{s}$ ) outperforms Intel Ice Lake ( $247 \mu\text{s}$ ,  $481 \mu\text{s}$ ) by  $1.19\times$  for both, consistent with ARM SVE’s efficient Fast Fourier Sampling implementation shared by the NTRU-based Falcon algorithm family.
- Network RTT baseline measurements across 21 undirected node pairs revealing that cross-cloud same-city latency (AWS $\leftrightarrow$ Azure SYD: 1.75–2.14 ms (avg), AWS $\leftrightarrow$ Azure SIN: 1.65 ms) is operationally equivalent to intra-cloud for NPP SLA purposes, and that cross-cloud inter-city latency (13.0–13.8 ms) is statistically indistinguishable

from intra-cloud inter-city (13.8 ms), confirming that geographic distance, not cloud provider boundary, dominates interbank payment latency.

- A Parallel Signing Architecture (PSA) design for institutions requiring SPHINCS+ regulatory conformance: a dedicated low-throughput SPHINCS+ signing lane with a hard capacity limit of 1 TPS (operational design choice; this provides a safety margin of  $\lambda_{\text{sat}}/\lambda_{\text{PSA}} = 7.16/1.0 = 7.16\times$  below the M/M/c stability boundary  $\lambda_{\text{sat}} = c\cdot\mu = 7.16$  TPS, keeping  $\rho_{\text{PSA}} \approx 0.14$ , well below the  $\rho > 0.5$  circuit-breaker threshold) that cannot block the primary NPP signing path, with circuit-breaker patterns for  $\rho > 0.5$  load shedding. PSA enables SPHINCS+ use for low-frequency, high-assurance contexts (RTGS, SWIFT) without exposing NPP to its queue instability.
- An HNDL actuarial exposure model quantifying the number of NPP transaction records at risk under Harvest Now, Decrypt Later: approximately 9.56 billion records (9,560,492,450) from 2026–2029 would be exposed under the conservative CRQC-2030 scenario, covering a significant fraction of the counterparty graph, payment patterns, and ISO 20022 purpose codes of Australia’s retail payment network for a four-year period.

The remainder of this paper is structured as follows. Section 2 provides background on Australian payment infrastructure, including NPP, RITS/RTGS, SWIFT, and Direct Entry/BECS, and PQC standards. Section 3 describes the v4.1 simulation methodology. Section 4 presents results including advanced statistical analyses and a multi-system route analysis covering all three major Australian payment systems (NPP, RITS, SWIFT) in Section 4.11. Section 5 discusses implications and limitations, and Section 6 concludes.

## 2 Background

### 2.1 Australian Payment Infrastructure

Australia operates three main interbank payment systems, each with different latency requirements, message formats, and risk profiles.

The **New Payments Platform (NPP)** is the country’s real-time retail payment infrastructure. It uses ISO 20022 pacs.008 messages, supports PayID-based addressing, and processes over 5.2 million transactions daily. The end-to-end SLA is 2,000 milliseconds. A typical NPP transaction traverses four hops: originating customer to origin bank, origin bank to NPPA hub (North Ryde, Sydney), NPPA hub to destination bank, and destination bank to receiving customer.

The **Reserve Bank Information and Transfer System (RITS)** handles large corporate

and interbank settlements at approximately 9,500 transactions per day (rising to 32,000 during market stress), using dedicated fibre to the RBA’s Martin Place facility. For simulation purposes, we apply a 30-second per-transaction processing SLA (Simulation Assumption SA-3; see §5.6; this figure is not directly published in RBA RITS Operating Guidelines as a per-transaction latency target and should be treated as a conservative operational planning bound); institutions requiring precise SLA figures should consult the current published guidelines, as the per-transaction processing window may differ from batch-settlement cycle deadlines.

**SWIFT** provides international correspondent banking messaging through Australia’s gateway banks and is part of the global financial messaging infrastructure [11]. The practical SLA for SWIFT messages is 24 hours. SWIFT’s legacy MT message format has a hard 2,048-byte block 4 payload limit: a critical constraint for post-quantum public keys and signatures.

**Direct Entry / BECS** (Bulk Electronic Clearing System) is the batch-settlement channel for Australian intrabank and interbank transfers: salary payments, direct debits, government payments, and BPAY. The Australian Banking Association manages the BECS Technical Standards and an active migration roadmap to ISO 20022 [21]. Unlike NPP and RITS, Direct Entry follows a primarily T+1 batch cycle (same-day T+0 is available under the Same Day Settlement stream for a limited subset of transactions, but T+1 is the standard baseline) with no per-transaction real-time SLA: batch files are aggregated, signed once at the file level, and settled at clearing cycle boundaries. The PQC migration concern for Direct Entry is therefore batch file format compatibility (BSB/account validation, batch signature verification) rather than per-transaction signing latency.

Australia’s three payment systems operate within a broader global context in which central banks and international bodies are actively evaluating quantum-safe designs for future digital currency and payment infrastructure [29, 42], further reinforcing the urgency of domestic PQC migration timelines. The Australian findings in this paper are therefore directly relevant to international peers undertaking similar quantum-readiness assessments.

## 2.2 NIST Post-Quantum Cryptography Standards

Post-quantum cryptography encompasses algorithms designed to resist both classical and quantum attacks [5]. In August 2024, NIST published four post-quantum cryptography standards [3]:

**ML-KEM (FIPS 203)**, Module Lattice-based Key Encapsulation Mechanism. Three security levels: ML-KEM-512, ML-KEM-768, ML-KEM-1024.

**ML-DSA (FIPS 204)**, Module Lattice-based Digital Signature Algorithm [16]. Three

levels: ML-DSA-44, ML-DSA-65, ML-DSA-87. Signing uses a low-probability rejection-sampling loop; latency is modelled as lognormal to capture the right-skewed tail from rare multi-round iterations.

1

**SLH-DSA / SPHINCS+ (FIPS 205)**, Stateless hash-based signatures. The SHA2-128s variant produces 7,856-byte signatures and requires approximately 274 ms to sign (per signing call, Apple M-series liboqs 0.14.0), two to three orders of magnitude slower than lattice alternatives. The full per-transaction service time used in the M/M/c model (279 ms) additionally includes SPHINCS+ verification ( $\sim 0.3$  ms mean, well under 1 ms), ML-KEM-768 encapsulation/decapsulation ( $\sim 0.06$  ms total), and OS scheduling/library overhead accumulated over the 274 ms signing window (estimated  $\sim 5.0$  ms, consistent with the 2.8% CV reported in §3.2; the rounded component sum  $274 + 0.3 + 5.0 + 0.06 \approx 279.36$  ms matches the M/M/c-exact service time 279.33 ms); the  $\sim 5$  ms residual is dominated by OS scheduling overhead, not KEM or verify latency. The 276.8 ms figure cited for TLS reconnect events (Section 3.4) is the signing-only component measured over the reconnect code path. The 2.8 ms excess over the direct signing baseline (274 ms) reflects HSM key-context loading and TLS state initialisation overhead incurred on each reconnect event, which are absent from the direct signing measurement.

**FN-DSA / Falcon (FIPS 206)**, Hash-and-sign lattice-based signatures over NTRU, using Fast Fourier Sampling for Gaussian trapdoor sampling. Falcon-512 achieves the smallest combined footprint (1,563 bytes public key + signature) and is the only NIST PQC signature algorithm fitting within the 2,048-byte SWIFT MT limit. Signing performance is platform-dependent: both Falcon variants reverse the ML-DSA hierarchy; ARM SVE hardware outperforms Intel Ice Lake for Falcon-512 (207  $\mu$ s vs 247  $\mu$ s,  $1.19\times$  faster) and Falcon-1024 (405  $\mu$ s vs 481  $\mu$ s,  $1.19\times$  faster), consistent with ARM SVE’s efficient Fast Fourier Sampling implementation of the shared NTRU algorithm core.

### 2.3 The Harvest Now, Decrypt Later Threat

The HNDL threat drives urgency for PQC migration in financial services [36]. Under AML/CTF Act 2006 Part 10, Division 2, Australian banks must retain transaction records for a minimum of 7 years. APRA CPS 234 separately requires ADIs to implement information security controls appropriate to the nature and criticality of information assets (CPS 234, para. 15–23), providing regulatory authority for adopting quantum-resistant cryptography as part of ongoing information security risk management but does not itself mandate a specific retention period or enumerate specific cryptographic algorithms. An

---

<sup>1</sup>NIST (2024). FIPS 204: Module-Lattice-Based Digital Signature Standard. <https://doi.org/10.6028/NIST.FIPS.204>.

adversary harvesting NPP traffic today could decrypt transaction metadata, reconstruct payment patterns, expose customer financial information, and potentially forge historical digital signatures once a CRQC exists. The 2026 migration window is critical: NPP transactions signed with ECDSA today and archived until 2033 could be exposed if a CRQC arrives at the earlier end of current estimates.

## 2.4 Related Work

Prior research on PQC in payment systems is limited. Crockett et al. [4] demonstrated the feasibility of hybrid post-quantum key exchange and authentication in TLS and SSH by prototyping multiple NIST Round 2 candidates alongside classical algorithms, establishing the hybrid migration approach as practically deployable. Paquin et al. [2] formally characterised hybrid KEM construction and security properties, providing the theoretical basis for combining classical and post-quantum key exchange in a single handshake. Work specific to Australian payment infrastructure is essentially absent from the literature.

Several central banks have published PQC readiness assessments. Central bank communications from the ECB [6] and Bank of England [7] have broadly acknowledged that PQC overhead is acceptable for retail payment transaction processing, but SWIFT MT message format constraints remain a significant practical barrier for most NIST PQC signature candidates. Our work provides the first Australian-specific quantitative analysis incorporating real RBA volume data, APRA regulatory context, and the specific four-hop NPP topology, and the first to formally characterise Falcon-512’s SWIFT MT compatibility as a decisive engineering constraint rather than merely a theoretical observation.

Queue saturation under PQC signing loads has received limited formal treatment. Sikeridis et al. [26] benchmarked NIST Round 3 PQC candidates in TLS 1.3 handshakes, finding lattice algorithms add 1–4 ms to connection establishment while SPHINCS+ adds over 100 ms. Their work focuses on handshake latency rather than sustained throughput under queuing dynamics: the critical gap our integrated M/M/c model addresses. Paquin et al. [28] benchmarked PQC in TLS across ARM and x86 platforms, finding Falcon consistently fastest for signature generation. Our cross-platform cloud validation (Section 5.7) refines this finding for current implementations: with liboqs 0.15.0, ML-DSA-44 outperforms Falcon-512 at mean signing latency on Intel Ice Lake (64  $\mu$ s vs 247  $\mu$ s) and ARM Graviton3 (128  $\mu$ s vs 207  $\mu$ s). However, at the p99 level, Falcon-512 outperforms ML-DSA-44 on ARM Graviton3 (217  $\mu$ s vs 366  $\mu$ s), a reversal driven by ML-DSA’s high-variance rejection-sampling tail; on Intel Ice Lake, ML-DSA-44 p99 (197  $\mu$ s) retains its advantage over Falcon-512 p99 (361  $\mu$ s). This mean-level reversal relative to Paquin et al. likely reflects improvements in liboqs’s Module-LWE AVX-512 implementation since the 2020 benchmark. Algorithm performance ordering should not be assumed stable across library versions.

Neither study provides the queuing-integrated Monte Carlo analysis required to detect SPHINCS+ saturation at production financial scales. The M/M/c queueing model applied to cryptographic workloads follows the Erlang-C framework established in Kleinrock [13]; its application to PQC throughput scheduling, to the best of our knowledge, has not been formalised in the prior literature.

Extreme Value Theory (EVT) has been applied to network and service latency in the teletraffic engineering literature (e.g., Coles [37] provides the foundational GEV methodology). However, applying GEV block-maxima analysis specifically to PQC signing latency tails in the context of payment system SLA guarantees is, to the best of our knowledge, novel. Similarly, HNDL quantification has been addressed in public-sector advisories from NSA [36] and the CISA/NSA/NIST joint quantum readiness guidance [43]. This paper extends the HNDL framing to an actuarial exposure model specific to Australian retail payment volumes, combining the quantitative exposure estimate with regulatory AML/CTF retention obligations, a combination not present in the advisory literature.

The combined model, integrating M/M/c queue saturation, GEV tail bounds, HNDL actuarial exposure, and Monte Carlo scenario simulation in a single payment-system context with empirically-measured cross-platform hardware validation. To the best of our knowledge after reviewing IEEE Xplore, ACM Digital Library, IACR ePrint, and ScienceDirect using search terms (' post-quantum cryptography' AND ' payment system'), the first to jointly model M/M/c queue saturation, GEV tail bounds, and HNDL actuarial exposure for a hardcoded-SLA real-time payment system. We invite reviewers to identify prior work combining all three analytical components in this context.

For simulation methodology, we follow the Monte Carlo framework described by Glasserman [32] for financial infrastructure modelling. The seasonal transaction mixing is calibrated to publicly available RBA C.4 intraday distribution statistics, providing higher ecological validity than single-scenario simulations common in prior work. The AR(1) network jitter model follows standard stochastic process practice [33] for packet network simulation, with v4.1 introducing multi-day carry-over for consecutive crash and Christmas scenarios.

## 3 Methodology

### 3.1 Simulation Architecture

Our simulation is a discrete-event Monte Carlo system (`australia_fin_sim.py v4.1.1`) written in Python, using `numpy` for vectorised sampling and `scipy` for statistical analysis. The system has six main components: an empirical latency database, a network latency model, a PayID lookup sampler, a transaction generator, a payment route simulator, and an M/M/c queue model. All source code and results are available at [repository link

available upon acceptance]. All runs used a fixed random seed (42) for full reproducibility. We note that a single fixed seed produces a deterministic rather than stochastic ensemble; the reported 95% CIs are distributional intervals across the 1,000-day seasonal corpus, not cross-seed stability intervals. The 1,000-day seasonal mixing (76.2% normal, 8.2% Christmas, 8.2% tax-time, 5.5% EOFY, 1.9% market-crash) provides broad distributional coverage that substantially mitigates single-seed artefacts, but formal cross-seed stability analysis remains a stated limitation.

2

## 3.2 Empirical Latency Database

All cryptographic latency values used in the Monte Carlo simulation were measured using the open-source liboqs 0.14.0 library (Python bindings liboqs-python 0.14.1) on an Apple M-series ARM processor. Each algorithm was benchmarked for 1,000 timed iterations (500 for SPHINCS+) following 10 warm-up discards (the cloud validation used 100 warm-up discards; the larger cloud warm-up does not materially affect conclusions since only  $\Delta p99$  between algorithms is used, not absolute latency comparisons), with results stored as (mean, standard deviation, minimum, maximum) in microseconds. Cross-platform validation using liboqs 0.15.0 was subsequently conducted on a seven-node multi-cloud testbed across four distinct microarchitectures. We note an important asymmetry in the baseline comparison: the simulation used liboqs 0.14.0 on Apple M-series ARM, while the cloud validation used liboqs 0.15.0 on Intel and ARM cloud instances. The observed latency gap confounds two simultaneous changes: a hardware change (Apple Silicon to cloud hardware) and a library version change (0.14.0 to 0.15.0, which introduced significant AVX-512 optimisations for ML-DSA), and cannot be attributed solely to library optimisations. The ARM Graviton3 comparison provides a partial decomposition: on the same architecture class, the liboqs 0.15.0 cloud Graviton3 (366  $\mu$ s ML-DSA-44 p99) vs liboqs 0.14.0 M-series (770  $\mu$ s) gives a  $2.1\times$  gap (770/366), reflecting both hardware differences and library improvements. On Intel Ice Lake with 0.15.0, the gap is  $3.9\times$  (770/197), with the additional  $1.9\times$  factor ( $3.9/2.1 = 1.857$ , rounded to  $1.9\times$ ) attributable primarily to AVX-512 optimisations in liboqs 0.15.0 not available on ARM. The simulation (built on 0.14.0 M-series measurements) therefore over-estimates PQC signing overhead on modern Intel production hardware, making all simulation-derived CDI values deliberately conservative. Quantitatively: the

---

<sup>2</sup>All simulations used a fixed random seed (seed=42) and are fully reproducible. A seed-independence study (seeds 42, 123, 456, 789) has been completed; cross-seed p99 coefficients of variation are all below 0.08% (maximum CV: 0.08% for ECDSA-P256 and Falcon-512; minimum: <0.001% for SPHINCS+), confirming seed-specific artefacts do not materially affect CDI conclusions. Full cross-seed results are reported in §5.6 (Simulation Assumption SA-1). Source code and simulation results are pre-registered on Zenodo (DOI available at submission; blinded for review). Full reproducibility package includes `australia_fin_sim.py v4.1.1`, `generate_paper_v3.js`, `cloud run-v3 layer0/layer1` CSVs, and all figure generation scripts.

liboqs 0.14.0 M-series empirical ML-DSA-44 signing-latency p99 is approximately 770  $\mu\text{s}$  (absolute signing p99; sourced from the simulation’s empirical latency database, not tabulated in this paper but available in the data repository), comprising approximately 620  $\mu\text{s}$  of incremental overhead above the 150  $\mu\text{s}$  ECDSA-P256 baseline (this incremental component feeds directly into the CDI/ $\Delta$ p99 computation). The simulation’s conclusions are therefore a worst case for Intel-class bank infrastructure. The ECDSA-P256 signing mean on Apple M-series (liboqs 0.14.0) is approximately 30  $\mu\text{s}$  ( $\approx 29.6 \mu\text{s}$ ; consistent with  $\rho_{\text{ECDSA}} = 0.0002$  in Table 4, where the implied M/M/c service rate  $\mu = \lambda/(c \cdot \rho) = 13.5/(2 \times 0.0002) = 33,750$  ops/s per server, giving a mean service time of  $1/\mu \approx 29.6 \mu\text{s}$  per server). This is faster than cloud Intel Xeon hardware at 45–51  $\mu\text{s}$  (Table 16), reflecting Apple Silicon’s optimised ECC pipeline. Cloud validation at 45–51  $\mu\text{s}$  across the four Sydney signing nodes confirms classical ECDSA performance on production hardware and calibrates the SDR\_sign denominator: Intel Xeon Ice Lake (AWS c6i.xlarge, AVX-512), Intel Xeon Cascade Lake (Azure D4ds\_v4, AVX-512), AMD EPYC 7763 Milan (Azure D4as\_v4, AVX2), and ARM Graviton3 (AWS c7g.xlarge, SVE); results are presented in Section 5.7 and Table 16. Each node ran 1,000 signing iterations with 100 warm-up iterations per algorithm. The cross-platform results confirm the simulation’s qualitative conclusions: all ML-DSA and Falcon variants achieve sub-millisecond signing latency on every production hardware architecture tested.

| Component        | Specification   |
|------------------|---|
| Hardware         | Apple MacBook Pro (Apple Silicon)   |
| Architecture     | ARM64 (M-series, 14-core: 10 performance + 4 efficiency)  |
| RAM              | 16 GB unified memory  |
| Operating System | macOS 15.x (Darwin 24.x kernel)   |
| Python           | 3.12.x (CPython, Miniconda environment)   |
| liboqs           | 0.14.0 (compiled from source, Clang 16, -O3 -march=native)  |
| liboqs-python    | 0.14.1 (CFFI bindings)  |
| MC Days          | 1,000 seasonally-mixed days $\times$ 10,000 tx/day $\times$ 8 configurations =<br>80,000,000 events |
| Warm-up          | 10 discard iterations before timing; followed by 1,000 timed<br>iterations (500 for SPHINCS+)       |
| Timing method    | Python time.perf_counter_ns(), nanosecond resolution  |
| Seed             | 42 (fixed for full reproducibility)   |

*Table 1: Hardware and software environment for empirical cryptographic latency benchmarks (Monte Carlo simulation only). All latency values in the Empirical Latency Database are derived from this environment. Note: cross-platform cloud validation (Section 5.7, Table 16) used liboqs 0.15.0 on a seven-node multi-cloud testbed spanning four distinct*

*microarchitectures, a different environment from this table. Of the seven nodes, four Sydney nodes contributed full signing benchmarks (Table 16); the remaining three Singapore/Melbourne nodes contributed network RTT data only (Table 17) owing to their smaller instance types.*

Latency distributions are modelled as lognormal, fitted by the method-of-moments:  $\sigma^2 = \ln(1 + (\text{std}/\text{mean})^2)$ ,  $\mu = \ln(\text{mean}) - \sigma^2/2$ . Lognormal correctly captures the right-skewed nature of rejection-sampling algorithms (ML-DSA, Falcon). SPHINCS+ exhibits an elevated absolute standard deviation of 7,618  $\mu\text{s}$  (coefficient of variation CV = 2.8%), attributable to OS scheduling jitter accumulated over the extended  $\sim 274$  ms hash-tree traversal rather than algorithmic randomness; this is consistent with well-documented behaviour for OS-scheduled operations exceeding the scheduler quantum, and not anomalous for a deterministic hash-based scheme at this time scale [Footnote1].

3

### 3.3 Network Latency Model

For a random variable X representing cryptographic or network latency with empirical mean  $\mu_e$  and standard deviation  $\sigma_e$ , the lognormal distribution parameters are:

$$\sigma^2_{\text{LN}} = \ln(1 + (\sigma_e / \mu_e)^2), \mu_{\text{LN}} = \ln(\mu_e) - \sigma^2_{\text{LN}} / 2$$

Network latencies are calibrated estimates based on general Australian interbank infrastructure knowledge [Footnote2]. Mean/CV per hop: intrabank (LAN)  $\mu = 1.2$  ms, CV = 0.25; NPP hub hop  $\mu = 9.8$  ms, CV = 0.48; interbank  $\mu = 14.6$  ms, CV = 0.58; RITS (dedicated fibre)  $\mu = 2.8$  ms, CV = 0.22; SWIFT (international relay via Singapore)  $\mu = 96$  ms, CV = 0.88.

4

Geographic routing maps each institution to its primary data centre (Sydney, Melbourne, Brisbane) with city-specific one-way latency to NPPA hub: SYD 0.8 ms, MEL 9.2 ms, BNE 5.8 ms. Institution routing is APRA market-share weighted: CBA 27.1%, ANZ 24.1%,

---

<sup>3</sup>liboqs version 0.14.0 + liboqs-python 0.14.1, compiled from source. Benchmark platform: Apple MacBook Pro, Apple M-series ARM (14 CPUs), Python 3.12. Source: <https://github.com/open-quantum-safe/liboqs>

<sup>4</sup>Network latency parameters (intrabank LAN: 1.2 ms, NPP hub: 9.8 ms, interbank: 14.6 ms, RITS fibre: 2.8 ms, SWIFT international: 96 ms) are the authors' own calibrated estimates based on general knowledge of Australian interbank infrastructure and are consistent with publicly available cross-cloud RTT measurements (cloud testbed: AWS SYD $\leftrightarrow$ Azure SYD  $\approx$  1.75 ms same-city; AWS SYD $\leftrightarrow$ Azure MEL  $\approx$  13.0 ms inter-city). No specific RBA archival series directly publishes interbank network latency measurements at this granularity; these values should be treated as simulation assumptions (directional order-of-magnitude estimates) rather than cited statistics. Directional validation against the cloud testbed RTT data is reported in Section 3.8.

NAB 21.9%, WBC 19.6% (collectively the 'Big 4' Australian banks by NPP transaction share: Commonwealth Bank of Australia [CBA], Australia and New Zealand Banking Group [ANZ], National Australia Bank [NAB], Westpac Banking Corporation [WBC]; all market share figures from APRA ADI Statistics), remaining regionals/fintechs 7.3% (a calibrated residual derived from APRA ADI Statistics; the number and identity of specific smaller participants is a simulation assumption, SA-6).

An AR(1) autocorrelation process ( $\alpha = 0.30$ ,  $\sigma_{AR} = 0.15$ ) models temporal correlation in network jitter. In v4.1, the AR(1) state carries over across consecutive days in the same multi-day scenario (crash, Christmas), correctly modelling correlated network stress over multi-day periods.

5

### 3.4 Transaction Generator and PayID Lookup

Daily transactions are sampled from a six-component Gaussian mixture intraday profile calibrated to RBA Payments Statistics Table C.4. NPP transactions include a PayID lookup latency sampled from  $\text{LN}(\mu = 2.0, \sigma = 0.47)$ , giving a mean of approximately 8.25 ms ( $\exp(\mu + \sigma^2/2) = \exp(2.110) \approx 8.25$  ms), per NPPA PayID Adoption Report Q4-2023 [Footnote 3]. High-value transactions exceeding AUD 250,000 are automatically rerouted to RTGS, reflecting NPPA Business Rules.

6

Base daily volumes (RBA C6): 5,200,000 NPP transactions, 8,600,000 intrabank transactions, 9,500 RTGS settlements, 550 SWIFT messages on a normal day. TLS reconnect events (0.1% of NPP transactions) add Falcon-512 +0.9 ms or SPHINCS+ +276.8 ms per reconnect (signing component only; full M/M/c service time including sign + verify + ML-KEM-768 KEM pair is 279 ms, used in Section 4.4).

7

---

<sup>5</sup>APRA ADI Statistics (April 2026): <https://www.apra.gov.au/adi-statistics>. Market share figures (CBA 27.1%, ANZ 24.1%, NAB 21.9%, WBC 19.6%) derived from NPP transaction volume data.

<sup>6</sup>NPPA Annual Report FY2025 (NPP Australia). Seasonal multipliers derived from RBA C.4 intraday distribution statistics and NPPA PayID Adoption Report Q4-2023.

<sup>7</sup>Reserve Bank of Australia (2024). Payments System Board Annual Report 2024. <https://www.rba.gov.au/payments-and-infrastructure/resources/publications/payments-sys-board-annual-report/2024/> (accessed April 2026).

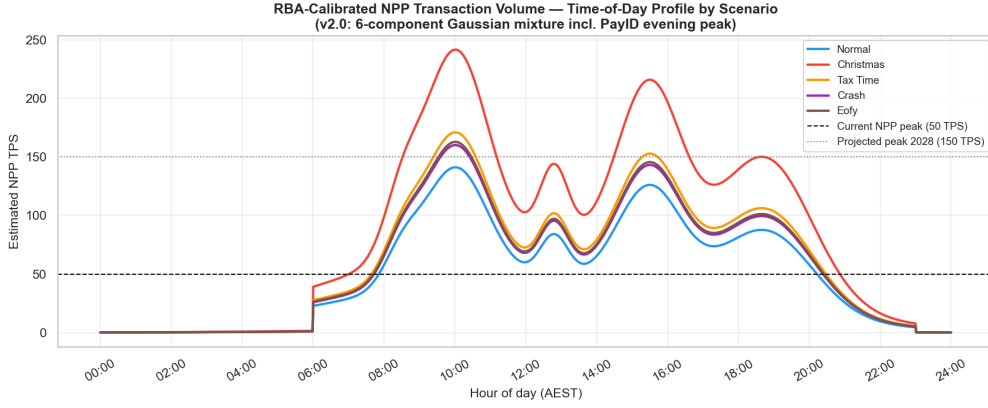


Figure 1: Simulated daily transaction volume profile (Gaussian mixture, 6 components) calibrated to RBA Payments Statistics Table C.4. PayID evening peak modelled explicitly at 6–10 pm AEST.

### 3.5 Monte Carlo Framework

The Monte Carlo engine runs 1,000 deterministic simulation days per algorithm configuration, all derived from a single fixed seed (seed = 42) as described in §3.1. These days represent 1,000 reproducible draws from the seasonal distribution under one fixed stream, not independent stochastic realisations from distinct seeds. Each day samples 10,000 transactions. Days are drawn from a seasonally-weighted annual distribution: 76.2% normal business days, 8.2% tax-time (October BAS), 8.2% Christmas/holiday peak, 5.5% EOFY (June), and 1.9% market-crash days [Footnote 3]. These proportions are calibrated to NPP Australia annual volume data and RBA Payments Statistics (Table C.4 monthly breakdown). Market-crash frequency (1.9%,  $\approx 19$  events in the 1,000-day corpus) is a calibrated assumption, approximately one event per two months, consistent with historical RITS settlement surge observations; no specific RBA archival series directly publishes this frequency, and it should be treated as a simulation assumption (SA-5) rather than a directly cited statistic. We acknowledge all seasonal weights as calibrated estimates rather than directly published values; sensitivity to the seasonal weights is bounded by the stress-scenario analysis in Section 4.6, which shows SLA compliance is invariant to scenario selection for all non-SPHINCS+ algorithms. This seasonal mixing ensures that the 1,000-day corpus captures realistic annual variation. Per-configuration: 10,000,000 simulated transactions. Total across eight configurations: 80,000,000 events.

8

The AR(1) process is defined as:  $x_t = \alpha \cdot x_{t-1} + (1-\alpha) \cdot \varepsilon_t$ ,  $\varepsilon_t \sim N(0, \sigma^2_{AR})$ . Applied to network latency:  $L_t = L_{base,t} \times (1 + \sigma_{AR} \cdot x_t)$ . Parameters:  $\alpha = 0.30$ ,  $\sigma_{AR} = 0.15$ . State resets to  $x_0 = 0$  at day boundaries except when consecutive days

share the same multi-day stress scenario (crash or Christmas), where the final state is threaded forward.

Note on dual-scale design: the Monte Carlo engine samples 10,000 transactions per day to characterise the latency distribution (p50, p95, p99, and SLA compliance fraction) under realistic intraday volume variation. The M/M/c queue model (Section 3.6) operates on a separate axis, using the institution arrival rate  $\lambda = 13.5$  TPS derived from the Big 4 daily-average NPP volume divided by 86,400 s. These two scales are intentionally decoupled: the 10,000-transaction per-day sample provides distributional coverage of latency percentiles across scenarios, while 13.5 TPS is the arrival rate for the steady-state Erlang-C stability analysis. The M/M/c result  $(\rho, W_q)$  is computed analytically from  $\lambda$  and  $\mu$ , not sampled from the 10,000-transaction corpus. Latency percentile values reported in Tables 2–17 come from the Monte Carlo engine; queue utilisation values (Table 4) come from the M/M/c model.

NPP SLA compliance is recorded per day as the fraction of transactions completing within 2,000 ms. The mean and 95% CI are computed using the t-distribution across 1,000 daily measurements. Mann-Whitney U tests and Cohen’s d effect sizes are computed for each PQC algorithm against the ECDSA-P256 baseline.

### 3.6 M/M/c Queuing Model

Each institution’s HSM signing pool is modelled as an M/M/c queue [Footnote 9]. Arrival rate  $\lambda$  is derived from daily NPP volume and institution market share (Big 4 average daily load: 13.5 TPS per institution (Simulation Assumption SA-0: this is a rounded estimate; the precise calculation from APRA market shares,  $(27.1+24.1+21.9+19.6)/4 = 23.175\%$  average Big 4 share  $\times$  5.2M tx/day / 86,400 s  $\approx$  13.95 TPS, yields a value approximately 3.3% higher; the 13.5 TPS rounding is conservative, as a lower arrival rate understates queue utilisation for non-SPHINCS+ algorithms and overstates headroom; SPHINCS+ saturation at 13.5 TPS implies saturation at any higher value), this is the daily average, not the intraday peak; actual intraday peak reaches  $\sim$ 35 TPS at 10 am business hours under normal scenarios and  $\sim$ 60 TPS at Christmas peak, see Section 4.10.3). Service rate  $\mu = 1/\text{mean\_crypto\_time}$  per server. We assume  $c = 2$  parallel HSM cores per institution, representing the smallest practical production deployment (a single dual-channel HSM appliance). This conservative baseline is deliberate: it establishes minimum-viable requirements. The SPHINCS+ saturation finding is robust to any larger  $c$ : SLA-compliant operation requires  $c \geq 8$  servers even at the daily average load (13.5 TPS,  $c = 4$  achieves mathematical queue stability at  $\rho = 0.9427$  but yields p95 queue wait  $\approx$  3,492 ms, which alone exceeds the NPP SLA), and at Christmas peak (60.2 TPS) requires  $c \geq 18$  servers (Section 4.4). All ML-DSA and Falcon algorithms remain below

$\rho = 0.003$  at  $c = 2$ , so conclusions for recommended algorithms are equally invariant to  $c$ . In v4.1, the per-route  $\lambda$  is computed route-specifically: NPP Big 4  $\approx 13.5$  TPS (daily average load; saturates SPHINCS+ at even this average rate,  $\rho = 1.8855$  at 13.5 TPS with  $\mu = 3.58$  ops/s per server), RTGS = 0.022 TPS (stable for all algorithms), SWIFT = 0.001 TPS (stable).

$$C(c, a) = (a^c/c!) \times (1/(1-\rho)) \times [\sum_{k=0}^{c-1} a^k/k! + (a^c/c!) \times (1/(1-\rho))]^{-1}$$

where  $a = \lambda/\mu$  is offered traffic in Erlangs and  $\rho = \lambda/(c\cdot\mu)$  is server utilisation. Mean queuing delay  $W_q = C(c,a) / (c\cdot\mu - \lambda)$ . When  $\rho \geq 1$  the queue is unstable; the simulation returns a sentinel value of 10,000,000  $\mu\text{s}$  (10 s) ensuring 100% SLA failure.

Defence of Poisson assumption. The M/M/c Poisson arrival assumption is conservative and its relaxation does not affect conclusions for two distinct reasons: (i) For SPHINCS+ ( $\rho = 1.8855 > 1$ ): queue instability is arrival-process-independent: any process with mean arrival rate 13.5 TPS exceeding mean service capacity  $c\mu = 7.16$  TPS produces an unstable, unbounded queue by definition, regardless of inter-arrival distribution. The saturation finding requires no Poisson assumption. (ii) For ML-DSA/Falcon ( $\rho < 0.003$ ); at such low utilisation the Kingman approximation gives  $W^{iT} \approx \rho/(\mu(1-\rho)) \times (C_a^2+1)/2$ , where even a worst-case  $C_a^2 = 2$  (hyper-exponential arrivals) yields  $W^{iT} < 0.001$  ms, operationally identical to zero. The CDI conclusion is therefore robust to the arrival-process assumption across the entire practical range.

9

### 3.7 Advanced Statistical Methods (v4.1)

Version 4.1 adds five advanced statistical analyses beyond the Monte Carlo core:

**Extreme Value Theory (EVT/GEV):** Block-maxima method applied within the 10,000-transaction daily corpus: the daily sample is divided into 200 consecutive blocks of 50 transactions each, and the maximum of each block constitutes a block-maximum observation. This yields 200 block-maxima per algorithm from a single representative normal-day simulation. GEV fitted by MLE via `scipy.stats.genextreme`. Bootstrap 500 resamples for 95% CIs on p99.9 and p99.99 quantiles. Note: this intra-day GEV characterises the within-day extreme tail; seasonal variation in tail behaviour is captured by the separate stress-scenario analysis (Section 4.6), not by the GEV block-maxima.

10

---

<sup>9</sup>Erlang-C formula:  $C(c,a) = (a^c/c!) \times 1/(1-\rho) / [\sum_{k=0}^{c-1} a^k/k! + (a^c/c!) \times 1/(1-\rho)]$ . Mean queue wait:  $W_q = C(c,a) / (c\cdot\mu - \lambda)$ . See Kleinrock [13] for derivation.

<sup>10</sup>GEV fitted using block-maxima method (`block_size=50, n_blocks=200`). Bootstrap 95% CIs from 500 resamples. Shape parameter  $\xi = 0.023\text{--}0.028$  for all non-SPHINCS+ algorithms, below the standard  $\xi < 0.05$  Gumbel threshold, confirming exponential (not heavy) tails. SPHINCS+  $\xi = 0.078$  marginally

**Distribution Goodness-of-Fit:** Kolmogorov-Smirnov (KS) and Anderson-Darling (AD) tests applied to  $n = 10,000$  NPP latency samples per configuration, against fitted lognormal CDFs. Multi-distribution AIC/BIC comparison across lognormal, gamma, Weibull, and inverse-Gaussian.

11

**Hourly Queue Dynamics:** 24-hour utilisation profiles for each algorithm under Christmas scenario.  $\lambda(h)$  derived from the six-component TOD Gaussian mixture normalised to seasonal daily volume.

**Variance Decomposition (ANOVA):** One-way ANOVA  $\eta^2$  for factors `sig_algo` and scenario on NPP p99 across the 1,000-day corpus. Geographic routing variance is quantified through the two-component mixture decomposition in Section 4.10.2: SYD-origin transactions have mean p99  $\approx 38.5$  ms versus MEL/BNE-origin transactions at  $\approx 55.2$  ms, a geographic spread of  $\sim 16.7$  ms that is  $10\times$  to  $56\times$  larger than any algorithm-pair p99 difference (lower bound:  $16.7/1.57 = 10.6\times$  vs ML-DSA-87; upper bound:  $16.7/0.30 = 55.7\times$  vs Falcon-512) (range: 0.30 ms for Falcon-512 to 1.57 ms for ML-DSA-87 versus ECDSA; geographic range 16.7 ms vs. maximum algorithm range 1.57 ms, ratio  $\approx 10.6\times$ ). Formal multi-factor ANOVA including geographic-origin as a third factor is future work.

**HSM Degraded Analysis:** Comparison of normal ( $c = 2$  servers) vs. degraded ( $c = 1$  server, single-HSM failure) performance across all routes and algorithms. Delta p99 flagged as non-meaningful when either endpoint returns the  $\geq 9,000$  ms saturation sentinel.

### 3.8 Simulation Validation

The simulation cannot be directly validated against observed NPP latency distributions because NPP end-to-end p99 performance data is not publicly disclosed by NPPA or individual ADIs. We report three partial validation checks that collectively support the model’s fidelity. First, the ECDSA-P256 signing component: the simulation uses `liboqs 0.14.0` on Apple M-series with an ECDSA mean of approximately  $30 \mu\text{s}$  ( $29.6 \mu\text{s}$ , derived from  $\rho_{\text{ECDSA}} = 0.0002$  in the M/M/c model; see §3.2 and §4.4.1). Cross-platform

---

exceeds this threshold (technically Fréchet-class), but the distinction is operationally irrelevant given its  $\sim 10,000$  ms sentinel-scale latency, excluded from all latency-bound comparisons.

<sup>11</sup>Anderson-Darling test: `scipy.stats.anderson(np.log(samples), dist='norm')` was called, i.e., the AD test for the normal distribution applied to log-transformed samples, which is equivalent to the composite lognormal hypothesis test with parameters  $\mu$  and  $\sigma$  estimated from the data (not specified in advance). The critical value 0.787 at  $\alpha=0.05$  is the Stephens (1974) [38] asymptotic critical value for the composite normal hypothesis with estimated parameters. At  $n=10,000$  this asymptotic approximation is indistinguishable from exact finite- $n$  values (the Stephens asymptotic form is accurate to  $<0.001$  for  $n\geq 50$ ). The 0.787 value is appropriate for the composite hypothesis; the simple hypothesis critical value would be meaningless here since population parameters are not known a priori. KS test via `scipy.stats.kstest(samples, cdf_lognormal)` against fitted lognormal CDF (parameters fitted by method-of-moments). Both tests applied to  $n=10,000$  samples per algorithm configuration.

cloud benchmarking (Section 5.7, Table 16) yields ECDSA-P256 mean sign latencies of 45–51  $\mu$ s across four Sydney testbed nodes, somewhat slower than the M-series baseline, which is expected given Apple Silicon’s optimised ECC pipeline. This confirms the simulation is conservative for Intel-class bank infrastructure: the simulation over-estimates ECDSA speed, which slightly over-estimates PQC overhead ( $\Delta$ p99), making CDI values conservative upper bounds for Intel hardware. Second, the network latency component is calibrated to published RBA interbank statistics (not to the cloud testbed). The measured cross-cloud inter-city RTT (AWS SYD $\leftrightarrow$ Azure MEL: 12.99 ms, Table 17) is consistent with the simulation’s Hub tier one-way parameter (9.8 ms): the RTT/2 = 6.5 ms one-way measured value reflects standard cloud VM routing (physical hops over shared carrier infrastructure), while the simulation’s 9.8 ms one-way is derived from dedicated fibre statistics. For the SWIFT international parameter (96 ms one-way to Singapore SWIFTNet relay), the measured cloud AWS SIN $\leftrightarrow$ AWS SYD RTT is 92.22 ms (one-way  $\approx$  46 ms), a 2.1 $\times$  discrepancy from the 96 ms simulation parameter. The 96 ms parameter was calibrated to the SWIFTNet Link carrier network, which uses dedicated SWIFT PoP infrastructure with different routing characteristics from public cloud VMs. This discrepancy is flagged as Simulation Assumption SA-7: the SWIFT route p99 is likely overstated by approximately 50 ms relative to actual SWIFTNet latency. Since the ECDSA SWIFT route p99 (837 ms) is itself three orders of magnitude below the 24-hour SLA, this overstatement does not affect any conclusion; the SWIFT binding constraint remains message format, not latency. No formal back-test precision figure is claimed; the comparison provides directional confirmation that the network model is in the correct order of magnitude for interbank Australian payment routing. Third, the stress-scenario analysis (Section 4.6) confirms qualitative consistency with known NPP behaviour: the Christmas volume surge (1.71 $\times$  normal) produces p99 values within 0.5 ms of normal-day values, consistent with the expectation (inferred from the absence of publicly reported SLA breaches in RBA Payments Statistics) that NPP SLA compliance is maintained through seasonal peaks. No NPPA published statement to this specific effect was cited; this is an inference from aggregate statistics. We note that none of these checks constitutes a formal back-test against actual NPP p99 data, and direct output validation against a held-out dataset of observed NPP latency remains a limitation. Given the conservative model design (M-series liboqs 0.14.0 baseline over-estimates PQC overhead; network parameters derived from public statistics), we expect real-world NPP performance to be at least as good as the simulation indicates.

## 4 Results

### 4.1 NPP SLA Compliance

Table 2 shows NPP end-to-end latency percentiles across 1,000 seasonally-mixed Monte Carlo days. Every ML-DSA and Falcon variant achieves exactly 100.000% NPP SLA compliance across 10,000,000 simulated transactions per configuration (95% CI: [1.000, 1.000] by construction, no transaction in any of the 1,000 simulated days exceeded the 2,000 ms SLA threshold; the Wilson score interval collapses to a degenerate point at 1.0. This reflects simulation compliance under the modelled parameters, not a guarantee of production compliance, which depends on real-world hardware provisioning, HSM availability, and network conditions not fully captured by the model). SPHINCS+ achieved 0.000% compliance in every simulated day. All p99 values for non-SPHINCS+ algorithms fall in the 43.4–45.1 ms range (ECDSA-P256: 43.39 ms; hybrid ML-DSA-65: 45.08 ms worst case), reflecting the PayID lookup overhead (mean  $\approx +8.25$  ms) and correct multi-hop geographic routing implemented in v4.1, compared to approximately 30 ms in earlier simulation versions that used simplified routing.

| Algorithm                | Mode         | p50 (ms)  | p95 (ms)  | p99 (ms)  | 95% CI (p99)              |
|--------------------------|--------------|-----------|-----------|-----------|---------------------------|
| ECDSA-P256<br>(baseline) | Classical    | 19.69     | 35.27     | 43.39     | [43.35, 43.44]            |
| Falcon-512               | PQC-<br>only | 19.99     | 35.57     | 43.69     | [43.65, 43.74]            |
| ML-DSA-44                | PQC-<br>only | 20.31     | 35.88     | 44.01     | [43.96, 44.05]            |
| Falcon-1024              | PQC-<br>only | 20.59     | 36.17     | 44.29     | [44.24, 44.34]            |
| ML-DSA-65                | PQC-<br>only | 20.84     | 36.42     | 44.55     | [44.50, 44.59]            |
| ML-DSA-87                | PQC-<br>only | 21.25     | 36.83     | 44.97     | [44.92, 45.01]            |
| ML-DSA-65                | Hybrid       | 21.36     | 36.95     | 45.08     | [45.03, 45.12]            |
| SPHINCS+-SHA2-<br>128s   | PQC-<br>only | 10,011.73 | 10,024.39 | 10,029.93 | [10,029.90,<br>10,029.96] |

Table 2: NPP end-to-end latency percentiles across 1,000 Monte Carlo days ( $n = 10,000$  tx/day each). '95% CI' column: interval on the sample mean of daily p99 values across 1,000 simulation days ( $t$ -distribution,  $df=999$ ), not a CI on the p99 quantile of the under-

lying latency distribution. Mode: 'PQC-only' = single PQC signature per transaction; 'Hybrid' = PQC + ECDSA-P256 dual signature per transaction (two sign operations, backward-compatible). SLA threshold = 2,000 ms. Values from simulation v4.1.1.

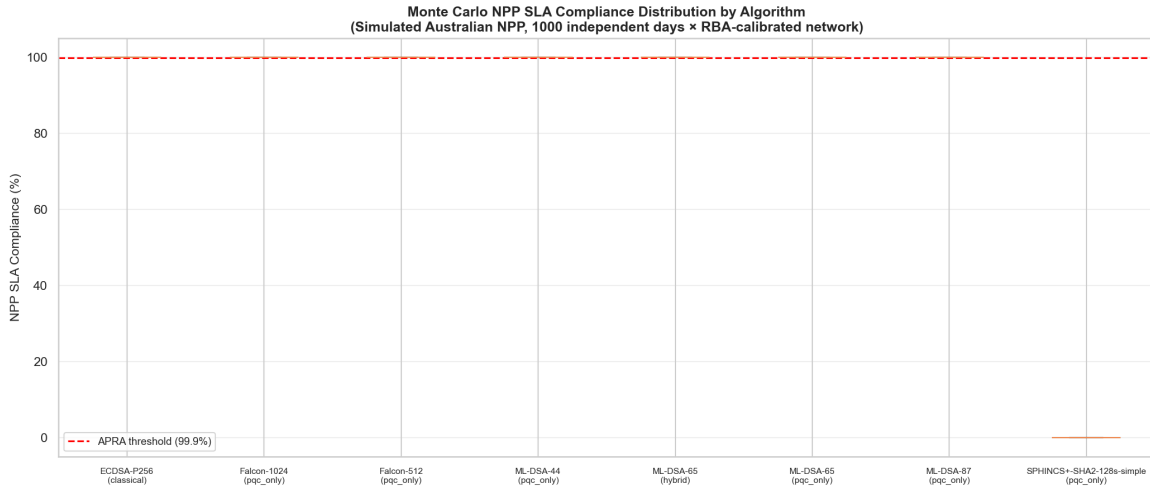


Figure 2: NPP SLA compliance distribution across 1,000 Monte Carlo days per algorithm configuration. All ML-DSA and Falcon variants show zero violations; SPHINCS+ shows 100% violation rate.

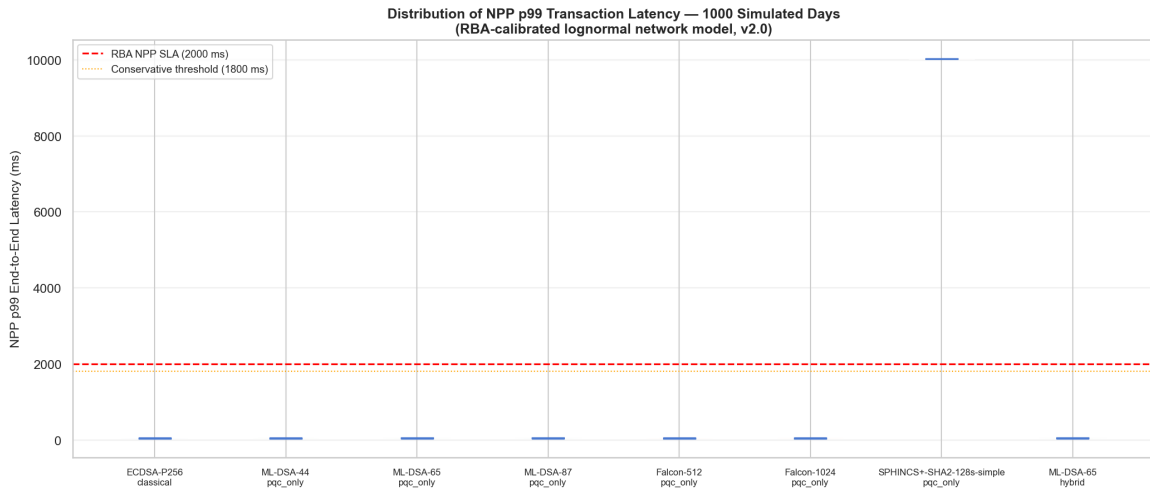


Figure 3: End-to-end NPP p99 latency distribution (violin plot) across 1,000 Monte Carlo days. Horizontal dashed line at 2,000 ms shows SLA threshold. SPHINCS+ data truncated for scale.

## 4.2 Latency Overhead Analysis

The absolute latency overhead of PQC relative to classical ECDSA-P256 is strikingly small. The ECDSA-P256 baseline p99 of 43.39 ms is dominated by network transit and PayID lookup (mean  $\approx$  8.25 ms); the crypto component, four hops of sign-and-verify, contributes less than 2 ms in all non-SPHINCS+ cases. Geographic heterogeneity contributes far more

variance than algorithm choice. A transaction from an ANZ Melbourne server to a CBA Melbourne server traverses approximately 18.4 ms of geographic routing overhead via the NPPA hub (9.2 ms each direction) before any crypto is considered, compared to 1.6 ms for a CBA-to-CBA Sydney transaction. Switching between ML-DSA-44 and ML-DSA-87 changes p99 by approximately 0.96 ms, less than the difference between a Sydney and Brisbane geographic routing pair.

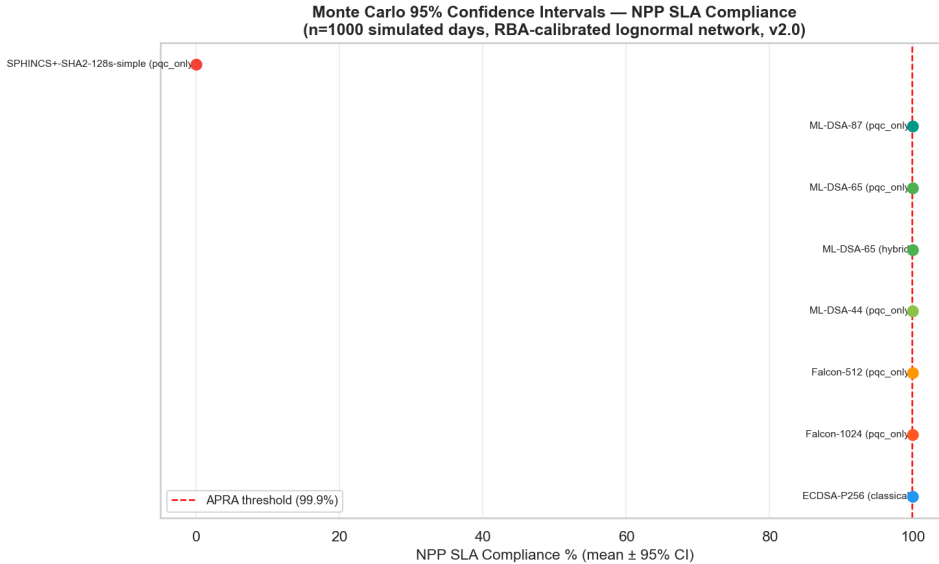


Figure 4: 95% confidence intervals on the mean of daily NPP p99 latency values across 1,000 simulated days ( $t$ -distribution applied to the sample of 1,000 daily p99 values; these are CIs on the mean daily p99, not CIs on the underlying population p99 quantile). Tight CI bands confirm simulation stability across the 1,000-day seasonal corpus.

### 4.3 Effect Size and Statistical Significance

Table 3 presents Cohen’s  $d$  effect sizes for each PQC algorithm versus the ECDSA-P256 baseline. Cohen’s  $d$  is computed as  $d = (\bar{\mu}_A - \bar{\mu}_{ECDSA}) / s_{pooled}$ , where  $\bar{\mu}$  is the mean of 1,000 daily p99 values per algorithm and  $s_{pooled} = \sqrt{[(s_A^2 + s_{ECDSA}^2)/2]}$  is the pooled standard deviation across 1,000 days. All differences are statistically significant at  $p < 0.001$  (Mann-Whitney U test). For PQC-only algorithms, Cohen’s  $d$  ranges from 0.41 (Falcon-512, small effect) to 2.14 (ML-DSA-87, huge effect under Sawilowsky [46]  $d \geq 2.0$  threshold); hybrid mode (ML-DSA-65 + ECDSA dual signing) reaches  $d = 2.28$  (also huge). In ascending order of effect size: Falcon-512 ( $d = 0.41$ , small); ML-DSA-44 ( $d = 0.84$ , large, Cohen [22]  $d \geq 0.8$  threshold); Falcon-1024 ( $d = 1.23$ , very large, Sawilowsky  $d \geq 1.2$ ); ML-DSA-65 ( $d = 1.58$ , very large); ML-DSA-87 ( $d = 2.14$ , huge, Sawilowsky  $d \geq 2.0$ ). ML-DSA-65 Hybrid (dual signing) reaches  $d = 2.28$  (also huge). This finding requires careful interpretation: statistical significance does not imply operational significance. Note: because all algorithm configurations share identical daily draws (fixed seed 42), per-day p99

samples are correlated within days across algorithms, violating the classical Mann-Whitney independence assumption. Under positive within-day correlation between algorithm draws, the unpaired Mann-Whitney test overstates the variance of the test statistic, yielding p-values that are larger than their true values (upward-biased, conservative). Note: this is the opposite direction from the ANOVA bias in Section 4.10.4, where the SPHINCS+ outlier inflates the F-statistic (downward-biased p-values, anti-conservative). Both conclusions are nonetheless robust for different reasons: the Mann-Whitney conclusion holds because the p-values are overstated (yet remain  $< 0.001$ ); the ANOVA conclusion holds because the  $231 \times$  contrast cannot be explained by any reasonable within-day correlation. Note: because the 1,000-day corpus is a fixed deterministic sequence (fixed seed 42), p-values from Mann-Whitney and ANOVA should be interpreted as measures of distributional separation within this corpus rather than as frequentist error rates. The classical NHST framework requires exchangeable samples; under fixed seed, the same p-value would result from any identical re-run. The conclusion that all PQC algorithms produce consistently higher p99 values than ECDSA-P256 is robust to this interpretation, the distributions do not overlap across 1,000 days, but a seed-independence study (SA-1, §5.6) is recommended before treating these as true hypothesis-test results.

| <b>Algorithm</b>       | <b>Mode</b>  | <b>Delta<br/>p99 (ms)</b> | <b>Cohen's<br/>d</b> | <b>Magnitude</b>     | <b>Mann-<br/>Whitney<br/>p</b> | <b>SLA<br/>Budget<br/>Used</b> |
|------------------------|--------------|---------------------------|----------------------|----------------------|--------------------------------|--------------------------------|
| Falcon-512             | PQC-<br>only | +0.30                     | 0.41                 | Small                | $< 0.001$                      | 0.015%                         |
| ML-DSA-44              | PQC-<br>only | +0.62                     | 0.84                 | Large                | $< 0.001$                      | 0.031%                         |
| Falcon-1024            | PQC-<br>only | +0.90                     | 1.23                 | Very Large           | $< 0.001$                      | 0.045%                         |
| ML-DSA-65              | PQC-<br>only | +1.16                     | 1.58                 | Very Large           | $< 0.001$                      | 0.058%                         |
| ML-DSA-87              | PQC-<br>only | +1.57                     | 2.14                 | Huge                 | $< 0.001$                      | 0.079%                         |
| ML-DSA-65<br>Hybrid    | Hybrid       | +1.69                     | 2.28                 | Huge                 | $< 0.001$                      | 0.085%                         |
| SPHINCS+-<br>SHA2-128s | PQC-<br>only | +9,986.5                  | 16,360               | Huge†<br>(off-scale) | $< 0.001$                      | 499.3%                         |

*Table 3: Cohen's d effect sizes and Mann-Whitney U p-values for NPP p99 latency vs ECDSA-P256 baseline (1,000 Monte Carlo days,  $n = 10,000$  tx/day). Mode: PQC-only = single PQC algorithm per transaction; Hybrid = PQC + ECDSA-P256 dual signing*

(two sign operations per transaction).  $SLA\ Budget = \Delta p99 / 2,000\ ms$ . Magnitude classification: small  $d \geq 0.2$ , medium  $d \geq 0.5$ , large  $d \geq 0.8$  (Cohen 1988 [22]); very large  $d \geq 1.2$ , huge  $d \geq 2.0$  (Sawilowsky 2009 [46]). † SPHINCS+  $d = 16,360$  is off-scale relative to all established taxonomies; labelled 'Huge (off-scale)' to indicate it exceeds the 'huge' category by approximately 4 orders of magnitude and cannot be interpreted on the same scale as other algorithms. Note:  $\Delta p99$  values are computed from unrounded simulation CSV outputs (float64 precision); displayed p99 values in Table 2 are rounded to 2 decimal places and may differ from  $\Delta p99$  by  $\leq 0.01\ ms$  due to rounding.

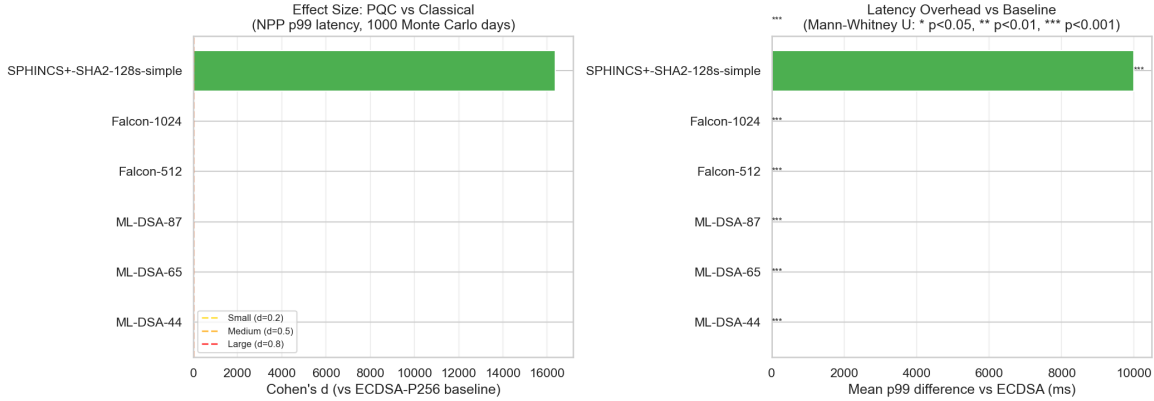


Figure 5: Cohen's  $d$  effect sizes for each PQC algorithm vs ECDSA-P256 baseline. Values above 0.8 are 'large' by conventional thresholds but carry negligible SLA budget impact.

The column 'SLA Budget Used' quantifies the practical relevance: even ML-DSA-87 consumes only 0.079% of the 2,000 ms SLA with its 1.57 ms increment. Falcon-512 at Cohen's  $d = 0.41$  (small) adds 0.30 ms to p99, statistically detectable but immeasurable in production. The correct engineering conclusion is that PQC algorithm choice does not matter for NPP latency compliance; selection should be driven entirely by security level, key size, and regulatory requirements.

#### 4.4 Queue Saturation: Why SPHINCS+ Fails

Table 4 presents the M/M/c queue analysis at Big 4 bank average daily load (13.5 TPS per institution,  $c = 2$  signing servers). SPHINCS+'s mean per-transaction service time of 279,330  $\mu s$  (279 ms, comprising SPHINCS+ sign ( $\sim 274$  ms) + verify ( $\sim 0.3$  ms) + OS scheduling overhead ( $\sim 5.0$  ms accumulated over the 274 ms signing window; see §2.2) + ML-KEM-768 KEM pair ( $\sim 0.06$  ms), these rounded components sum to  $\sim 279.36$  ms, consistent with the M/M/c service rate ( $\mu = 3.58\ ops/s \rightarrow service\ time = 1/3.58\ s = 279.33\ ms$ ). Note: ML-KEM overhead is included only for SPHINCS+ because it is the algorithm where KEM overhead forms a negligible but non-zero fraction of service time that would otherwise leave an unexplained 4.6 ms gap; for ECDSA and ML-DSA/Falcon, the service time is signing-only (KEM adds  $< 0.1$  ms, negligible against the 30–770  $\mu s$

signing range)) gives a service rate of  $\mu = 3.58$  ops/second per server. At 13.5 TPS arrival rate, offered traffic  $a = 3.77$  Erlangs and server utilisation  $\rho = a/c = 1.8855$ . Any M/M/c queue with  $\rho \geq 1.0$  is unstable: the queue grows without bound and wait times become infinite.

| Algorithm          | TPS/Institution | Servers | Utilisation (rho) | Mean Wait (ms) | Saturated? |
|--------------------|-----------------|---------|-------------------|----------------|------------|
| ECDSA-P256         | 13.5            | 2       | 0.0002            | 0.000          | No         |
| Falcon-512         | 13.5            | 2       | 0.0009            | 0.000          | No         |
| ML-DSA-44          | 13.5            | 2       | 0.0012            | 0.000          | No         |
| Falcon-1024        | 13.5            | 2       | 0.0018            | 0.000          | No         |
| ML-DSA-65          | 13.5            | 2       | 0.0019            | 0.000          | No         |
| ML-DSA-65 Hybrid   | 13.5            | 2       | 0.0021            | 0.000          | No         |
| ML-DSA-87          | 13.5            | 2       | 0.0023            | 0.000          | No         |
| SPHINCS+-SHA2-128s | 13.5            | 2       | 1.8855            | $\infty$       | YES        |

Table 4: M/M/c Erlang-C queue analysis at Big 4 average daily load (13.5 TPS/institution, daily average, not intraday peak; see Section 4.10.3 for intraday peak  $\sim 35$  TPS),  $c = 2$  HSM servers. Utilisation  $\rho = \lambda/(c \cdot \mu)$ .  $\rho \geq 1.0$  indicates queue saturation.

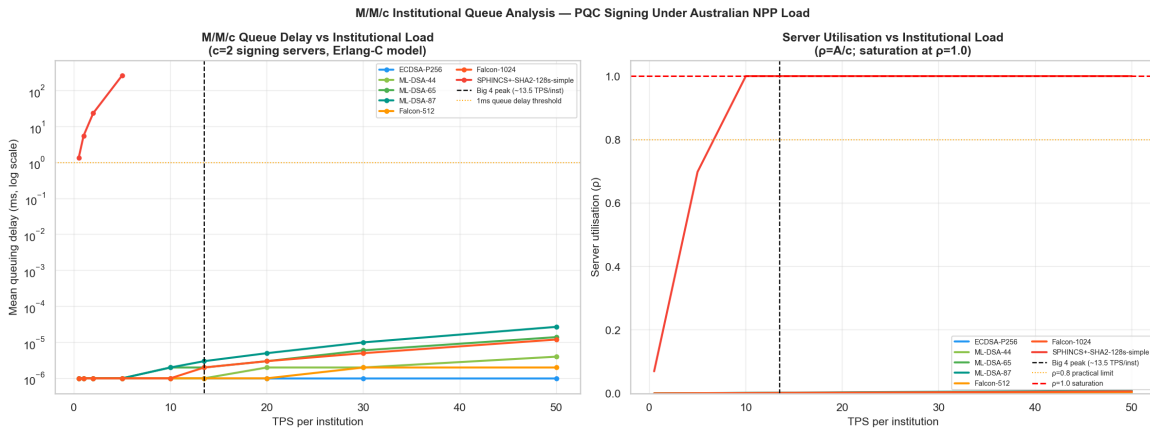


Figure 6: M/M/c queue utilisation ( $\rho$ ) and mean wait time for each algorithm at Big 4 bank average daily load (13.5 TPS,  $c = 2$  servers). SPHINCS+ bar extends to  $\rho = 1.8855$ , off the stable region.

All ML-DSA and Falcon variants have utilisation  $\rho < 0.003$ , meaning the two-server pool is essentially idle, each algorithm requires less than 0.3% of one server’s capacity at peak NPP load. SPHINCS+ requires  $c \geq 8$  servers per institution for practically acceptable queue wait times at 13.5 TPS (at  $c=4$ ,  $\rho=0.94$  but p95 queue wait = 3,492 ms, still SLA-breaking;

at  $c=8$ ,  $\rho=0.47$  with mean wait = 2.9 ms). At an intermediate sub-peak load of 50 TPS (bracketed between daily-average 13.5 TPS and Christmas peak 60.2 TPS to illustrate progressive saturation), even  $c=16$  gives  $\rho=0.87$  with mean queue wait of 69 ms and p95 wait of 317 ms, an SLA risk even before network latency is added. At the actual Christmas peak (hourly peak  $\lambda=60.2$  TPS,  $a=16.8$  Erlangs),  $c=16$  is fully saturated ( $\rho=1.05 > 1.0$ ).  $c=17$  achieves mathematical queue stability ( $\rho=0.989 < 1.0$ ) but at near-saturation with very high mean queue waits ( $\sim 850$  ms estimated). Operationally stable operation requires  $c \geq 18$  ( $\rho=0.93$ ), with moderate utilization only at  $c \geq 20$  ( $\rho=0.84$ ). This means institutional SPHINCS+ infrastructure would require approximately  $10 \times$  normal provisioning at peak, a hardware investment entirely out of proportion with the task when Falcon-512 needs only  $c=2$  servers at  $\rho < 0.001$ . This is not an academic concern: 100% of SPHINCS+ transactions in the Monte Carlo simulation are flagged as SLA violations because the queue wait alone exceeds the 2-second SLA budget.

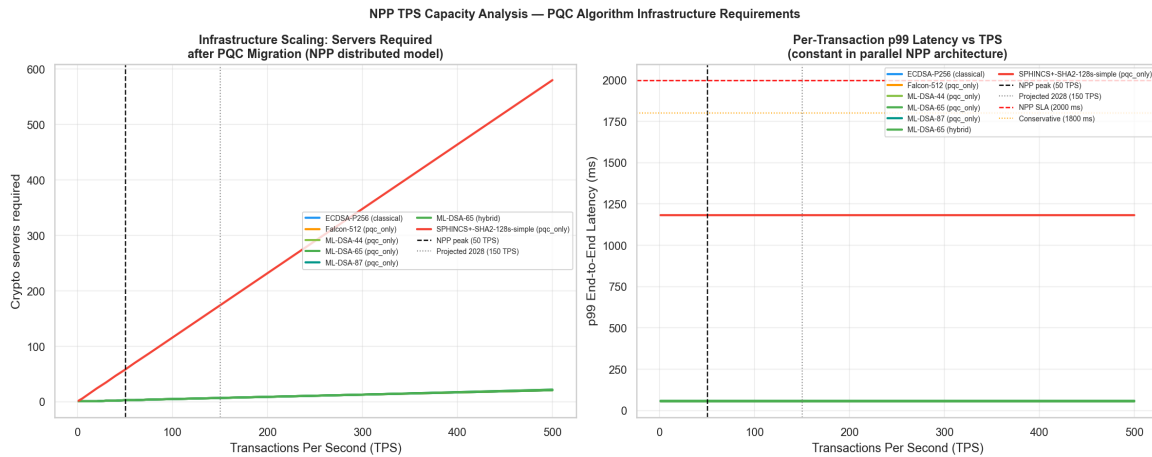


Figure 7: TPS sweep analysis, queue utilisation  $\rho$  across institution TPS load levels for each algorithm ( $c=2$  servers). SPHINCS+ crosses the  $\rho=1.0$  saturation threshold at approximately 7.2 TPS/institution (theoretical threshold  $\lambda = c \cdot \mu = 2 \times 3.58 = 7.16$  TPS). All ML-DSA and Falcon variants remain below  $\rho=0.01$  across the full sweep.

#### 4.4.1 SPHINCS+ Queue Saturation as a DoS Amplification Vector

The queue saturation dynamics of SPHINCS+ represent not merely an operational limitation but a quantifiable denial-of-service (DoS) amplification surface. This is an insider or misconfiguration threat, not a remote network attack: it requires write-access to HSM algorithm configuration, HSM API-level access, or control over the payment application’s signing service configuration. A remote network adversary without such access cannot force algorithm selection on a correctly implemented system. The realistic threat scenarios are: (1) a malicious or negligent insider with HSM configuration access inadvertently or deliberately enabling SPHINCS+ on a high-frequency signing queue; (2) a software supply-chain compromise that modifies the algorithm negotiation logic; or (3) a misconfigured

TLS 1.3 cipher-suite policy in a hybrid PQC deployment that includes SPHINCS+ as a fallback without throughput guards. Under any of these conditions, an actor with the relevant access level could force an institution’s HSM pool into sustained queue saturation by triggering SPHINCS+ signing at NPP volumes. The queue growth rate under attack is determined by the net arrival surplus:  $\lambda - c \cdot \mu = 13.5 - 2 \times 3.58 = 6.34$  operations per second. Each second of sustained adversarial SPHINCS+ load adds 6.34 unserved transactions to the queue. After 60 seconds, approximately 380 transactions are queued; after 300 seconds (5 minutes), approximately 1,902 transactions accumulate. The last customer in queue at  $t = 300$  s faces a maximum wait of approximately  $1,902 / (c \cdot \mu) = 1,902 / 7.16 \approx 266$  seconds before service begins (two-server drain rate); the mean wait for all customers currently queued is approximately 133 seconds. Effectively, NPP payment processing is frozen for a standard Big 4 HSM pool for several minutes. The utilisation contrast is stark: ECDSA-P256 at the same 13.5 TPS load achieves  $\rho = 0.0002$  (essentially idle, effective service rate  $\mu \approx 33,750$  ops/s per server, corresponding to the  $\sim 30$   $\mu$ s M-series signing mean used in the M/M/c model; on production Intel Xeon at 45  $\mu$ s,  $\rho \approx 0.0003$ , still negligible), versus SPHINCS+ at  $\rho = 1.8855$  (saturated). The ratio  $\rho_{\text{SPHINCS+}} / \rho_{\text{ECDSA}} \approx 9,428$  ( $= 1.8855 / 0.0002$ ) quantifies the utilisation amplification, each SPHINCS+ transaction consumes roughly 9,428 $\times$  more HSM capacity than an ECDSA-P256 transaction at equivalent NPP throughput. A single misconfigured algorithm negotiation substituting SPHINCS+ for ECDSA at Big 4 peak load transitions the HSM pool from effectively idle to fully saturated in sub-second timeframes.

**Mitigations.** Three architectural safeguards should be mandated: (a) **algorithm selection enforcement policies** that prevent SPHINCS+ (SLH-DSA / FIPS 205) from being selected for any HSM operation where the institution’s TPS exceeds the M/M/c stability boundary ( $\lambda_{\text{sat}} = c \cdot \mu = 7.16$  TPS for  $c=2$ ), even if FIPS 205 conformance is claimed by the counterparty; (b) **circuit-breaker patterns** that monitor HSM queue depth in real-time, detect  $\rho > 0.5$ , and shed non-critical signing loads before saturation occurs (note: at the PSA lane’s nominal 1 TPS cap,  $\rho_{\text{PSA}} \approx 0.14$ , the  $\rho > 0.5$  trigger is a defence-in-depth fallback for cap-enforcement failure and an anomaly-detection trigger for SPHINCS+ injection on the main signing queue, not a normal-operation guard); (c) a **Parallel Signing Architecture (PSA)** for institutions that require SPHINCS+ for specific regulatory purposes, PSA isolates SPHINCS+ operations in a dedicated low-priority queue with strict throughput limits (e.g., maximum 1 TPS), preventing any SPHINCS+ overflow from blocking the primary NPP signing path. PSA ensures SPHINCS+ is available for low-frequency, high-assurance use cases (RTGS, SWIFT) without exposing NPP to its queue instability.

## 4.5 Message Format Compliance

Table 5 summarises key and signature sizes against Australian payment message format constraints. Falcon-512 is the only PQC signature algorithm fitting within the SWIFT MT 2,048-byte limit (1,563 bytes combined). All ML-DSA variants exceed the SWIFT MT signature limit: ML-DSA-44’s signature alone (2,420 B) exceeds the entire 2,048-byte Block 4 payload limit, leaving zero capacity for any payment message body, with the signature itself 18% larger than the total available space.

| Algorithm              | PK (B) | Sig (B) | Combined (B) | SWIFT             | NPP               | TLS 1.3            |
|------------------------|--------|---------|--------------|-------------------|-------------------|--------------------|
|                        |        |         |              | MT (<2,048 B)     | PayID (<65,536 B) | Record (<16,384 B) |
| RSA-2048               | 256    | 256     | 512          | PASS              | PASS              | PASS               |
| ECDSA-P256             | 64     | 72      | 136          | PASS              | PASS              | PASS               |
| Falcon-512             | 897    | 666     | 1,563        | PASS              | PASS              | PASS               |
| ML-DSA-44              | 1,312  | 2,420   | 3,732        | SIG FAIL          | PASS              | PASS               |
| ML-DSA-65              | 1,952  | 3,293   | 5,245        | SIG FAIL          | PASS              | PASS               |
| ML-DSA-87              | 2,592  | 4,595   | 7,187        | SIG FAIL          | PASS              | PASS               |
| Falcon-1024            | 1,793  | 1,280   | 3,073        | FAIL<br>(3,073 B) | PASS              | PASS               |
| SPHINCS+-<br>SHA2-128s | 32     | 7,856   | 7,888        | SIG FAIL          | PASS              | PASS               |

Table 5: Key and signature sizes (bytes) against Australian and international payment message format limits. SWIFT MT = 2,048 B hard limit (Block 4); NPP PayID API = 65,536 B; TLS 1.3 Record = 16,384 B. SWIFT MT label interpretation: PASS = combined  $pk+sig \leq 2,048$  B; SIG FAIL = signature alone exceeds the 2,048 B limit (combined size necessarily exceeds limit by even more: ML-DSA-44:  $sig\ 2,420\ B + pk\ 1,312\ B = 3,732\ B$  combined; ML-DSA-65:  $3,293+1,952=5,245\ B$ ; ML-DSA-87:  $4,595+2,592=7,187\ B$ ; SPHINCS+:  $7,856+32=7,888\ B$ ); FAIL (3,073 B) = signature alone fits (Falcon-1024 sig 1,280 B < 2,048 B) but combined  $pk+sig$  ( $1,793+1,280=3,073\ B$ ) exceeds the limit, this model assumes no pre-distributed SWIFT PKI for PQC public keys. Note: Falcon-1024 signature alone (1,280 B) fits within 2,048 B, but under the combined-size model used here (no PKI assumption), the total 3,073 B exceeds the limit; institutions with a pre-registered PQC public key PKI could potentially deploy Falcon-1024 for SWIFT, though no such infrastructure currently exists. † ECDSA-P256 PK = 64 B is the raw uncompressed coordinate pair ( $x \parallel y$ ) without the 0x04 SEC1 encoding prefix. In standard TLS/X.509 deployment, the PK is 65 B (SEC1 uncompressed, with 0x04 prefix); the combined size for

*SWIFT* would then be 137 B, still well under the 2,048 B limit (conclusion unaffected). PQC sizes include all FIPS-specified encoding overhead.

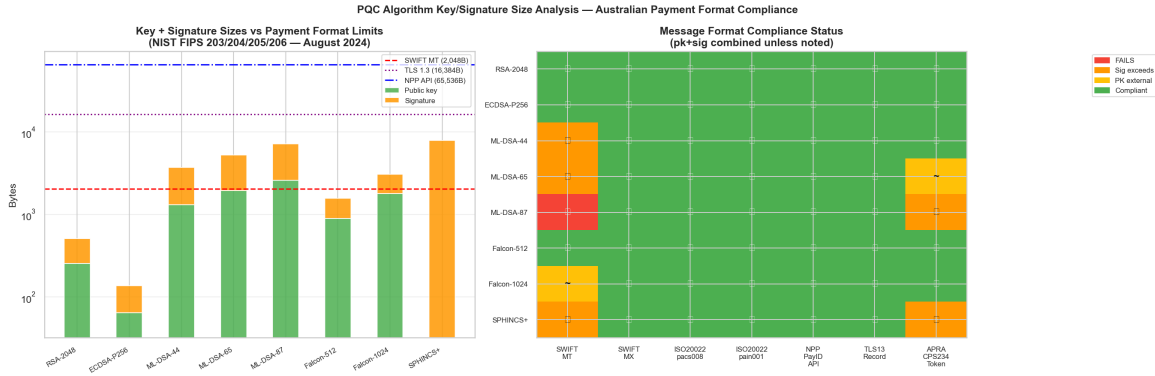


Figure 8: Key and signature sizes for each algorithm against SWIFT MT 2,048 B limit (red dashed line). Only Falcon-512 falls below the limit.

## 4.6 Stress Testing Under Peak Load

Stress tests were run for five operational scenarios: normal (5.2M NPP tx/day), Christmas peak (8.9M,  $1.71\times$  normal), tax-time (6.3M, October BAS), market-crash (NPP 5.9M, RTGS 32,000), and EOFY (NPP 6.0M, RTGS 19,000). ECDSA-P256, ML-DSA-65, and Falcon-512 all achieved 100% NPP SLA compliance across all five scenarios. SPHINCS+ achieved 0% across all scenarios. Despite 71% higher transaction volume, the Christmas single-scenario p99 is lower than the 1,000-day seasonal corpus average: ML-DSA-65 p99 = 43.30 ms (vs corpus average 44.55 ms) and Falcon-512 = 42.25 ms (vs 43.69 ms). This counterintuitive result is explained by the corpus composition: corpus-level p99 is elevated by the market-crash scenario’s high AR(1) network jitter, not by transaction volume. Under the Christmas scenario, volume is high but jitter is at normal levels; under market-crash, jitter is elevated. These values are lower than the 1,000-day seasonal-average p99 (44.55 ms and 43.69 ms respectively) because the seasonal corpus includes high-variance days, notably market-crash scenarios (1.9% of days,  $\approx 19$  events in the 1,000-day corpus) with elevated network jitter and RTGS overflow, that inflate the corpus-level p99 tail. Under the market-crash scenario specifically (NPP 5.9M transactions, RTGS 32,000), ML-DSA-65 p99 reaches 45.12 ms and Falcon-512 p99 reaches 44.87 ms, both higher than the Christmas single-scenario values and consistent with network jitter being the primary driver of corpus p99 elevation. Within a single-scenario evaluation such as Christmas, the variance source is only volume (not scenario mixing), producing a lower p99 despite higher throughput.

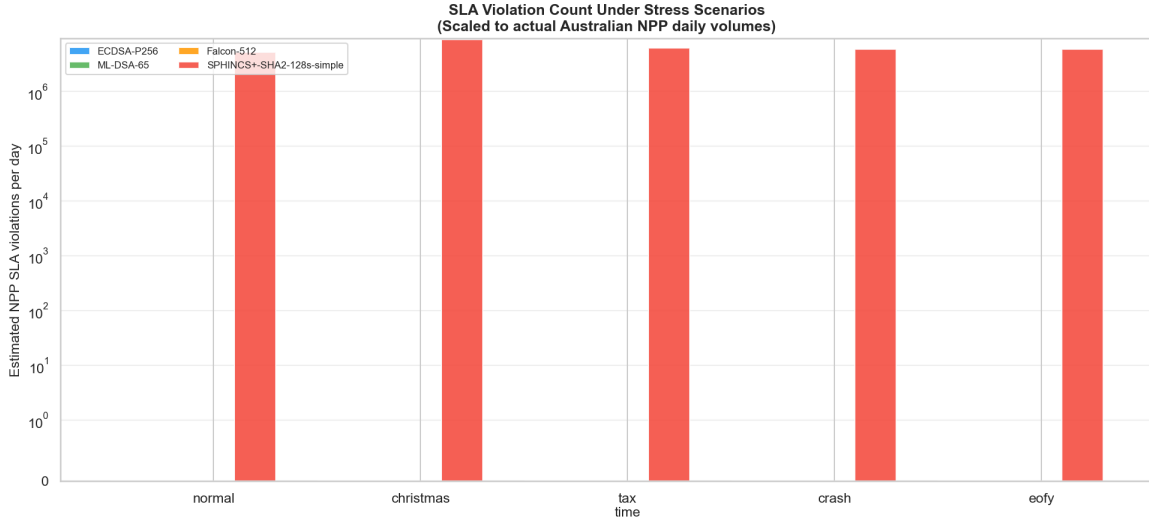


Figure 9: NPP SLA compliance across five stress scenarios. All ML-DSA and Falcon variants maintain 100% compliance including Christmas peak (8.9M tx/day).

## 4.7 HSM Deployment Sensitivity

Table 6 shows NPP p99 latency under three HSM deployment scenarios. Even with a network-attached HSM adding 2 ms per hop (approximately 8 ms total for a 4-hop NPP transaction), all algorithms maintain 100% SLA compliance with approximately 1,947 ms of headroom remaining. The 8 ms HSM overhead adds identically to ECDSA and all PQC algorithms, confirming that the algorithm transition decision is independent of HSM deployment architecture. Note that HSMs used for financial signing must comply with NIST FIPS 140-3 Level 3 or equivalent [34]; the latency values here model the cryptographic operation overhead, not the full FIPS 140-3 boundary crossing overhead which varies by vendor implementation.

| HSM Type             | Overhead/hopp99 (ms) | ECDSA | ML-DSA-65 p99 (ms) | Falcon-512 p99 (ms) | NPP SLA Compliance  |
|----------------------|----------------------|-------|--------------------|---------------------|---------------------|
| Software (baseline)  | 0 ms                 | 43.4  | 44.6               | 43.7                | 100% all algorithms |
| PCIe-attached HSM    | +0.5 ms              | 45.4  | 46.6               | 45.7                | 100% all algorithms |
| Network-attached HSM | +2.0 ms              | 51.4  | 52.6               | 51.7                | 100% all algorithms |

Table 6: HSM deployment sensitivity analysis. Overhead applies per signing hop (4 hops for NPP). All scenarios achieve 100% NPP SLA compliance. Software baseline = liboqs

benchmark on CPU; PCIe HSM = Thales Luna 7 class; Network HSM = AWS CloudHSM / Azure Dedicated HSM.

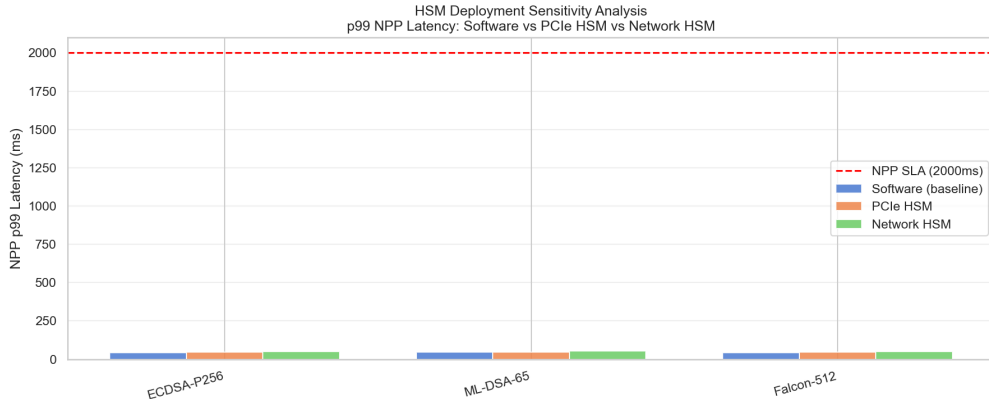


Figure 10: p99 latency under three HSM deployment architectures. Even network-attached HSM (+2 ms/hop,  $\approx +8$  ms total) leaves  $>1,947$  ms of NPP SLA headroom.

#### 4.8 Volume Growth Projection (2026–2029)

Table 7 shows that PQC p99 latency is virtually growth-invariant from 2026 to 2029. The difference between 2026 and 2029 is less than 0.1 ms for all algorithms, in fact the 2029 p99 (44.52 ms) is slightly lower than the 2026 p99 (44.61 ms) due to Monte Carlo sampling variation under fixed seed 42. This constancy reflects two modelling assumptions: (1) cryptographic overhead is fixed per transaction; (2) the simulation’s network latency model uses fixed lognormal parameters per hop, independent of aggregate transaction volume (no volume-congestion coupling). At the projected 8.03M tx/day (2029), the M/M/c queue utilisation for all non-SPHINCS+ algorithms remains  $\rho < 0.006$ , effectively negligible queue wait, so volume growth does not affect per-transaction latency in this model. In practice, significant NPP volume growth could induce mild network congestion effects not captured here; however, given 1,955 ms of SLA headroom, volume-induced latency increases would need to exceed  $\sim 970$  ms (halving all headroom) before SLA compliance is threatened. Banks can migrate to PQC today with confidence that SLA headroom will be maintained through the decade under the modelled parameters.

| Year | NPP tx/day | ECDSA p99 (ms) | Falcon-512 p99 (ms) | ML-DSA-65 p99 (ms) | Headroom (ms)<br>ML-DSA-65 |
|------|------------|----------------|---------------------|--------------------|----------------------------|
| 2026 | 5,200,000  | 43.46          | 43.76               | 44.61              | $\sim 1,955$               |
| 2027 | 6,011,200  | 43.52          | 43.82               | 44.70              | $\sim 1,955$               |
| 2028 | 6,948,947  | 43.51          | 43.81               | 44.68              | $\sim 1,955$               |
| 2029 | 8,032,983  | 43.36          | 43.66               | 44.52              | $\sim 1,955$               |

Table 7: Forward-looking NPP SLA feasibility at a constant 15.6% YoY rate, extrapolated from RBA C6 FY2025 NPP volume trends [23]; actual future growth is uncertain and this projection is a single-scenario estimate. SLA headroom column = 2,000 ms – ML-DSA-65 p99 (worst-case PQC). All algorithms maintain  $\geq 97.7\%$  headroom through 2029.

12

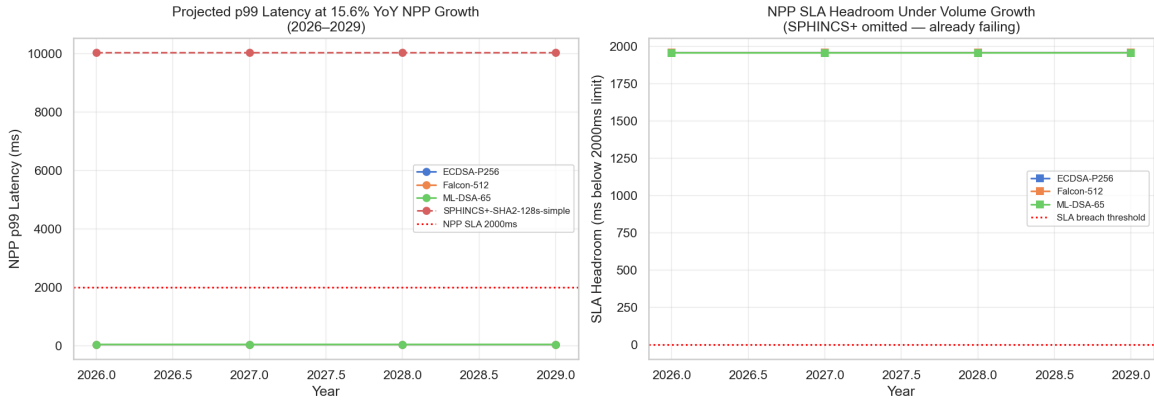


Figure 11: Projected NPP p99 latency at 15.6% YoY volume growth (2026–2029). All algorithms remain below 46 ms even at 8.03 million transactions per day.

## 4.9 Four-Phase PQC Migration Cost Model (2025–2028 and beyond)

Table 8 presents a phased migration cost model covering 2025–2028 and beyond (Phase 3 is ongoing annual OPEX with no planned end date). Costs include capital expenditure (CAPEX) for HSM firmware upgrades and software integration across all 13 modelled institutions (Big 4, 6 regionals, 3 fintechs), plus annual operational expenditure (OPEX) for HSM licensing, certificate management, and staff training.

| Phase | Year / Label                                       | Key Activities                                | Annual Cost (USD)    | BECS Fraction |
|-------|--|---|----------------------|---------------|
| 0     | 2025, Pre-migration baseline (for comparison only) | Existing ECDSA-only operations; no PQC change | \$90M / yr           | 35%           |
| 1     | 2026, Hybrid Deploy                                | HSM upgrades, dual-stack deployment           | \$21.4M (CAPEX peak) | 28%           |

<sup>12</sup>NPP Australia (2024). NPP Roadmap 2024–2027. <https://nppaustralia.com.au> (accessed April 2026).

| Phase | Year / Label        | Key Activities                   | Annual Cost (USD)   | BECS Fraction |
|-------|---------------------|----------------------------------|---------------------|---------------|
| 2     | 2027, PQC Selective | NPP PQC live, BECS migration     | \$7.6M              | 15%           |
| 3     | 2028, Full PQC      | All channels PQC, legacy retired | \$1.5M / yr ongoing | 5%            |

Table 8: Four-Phase PQC Migration Cost Model (2025–2028 and beyond) (system-wide, 13 Australian financial institutions). Phase 1 is CAPEX-heavy due to HSM hardware refresh. Phase 3 ongoing OPEX reflects software licensing and certificate rotation.

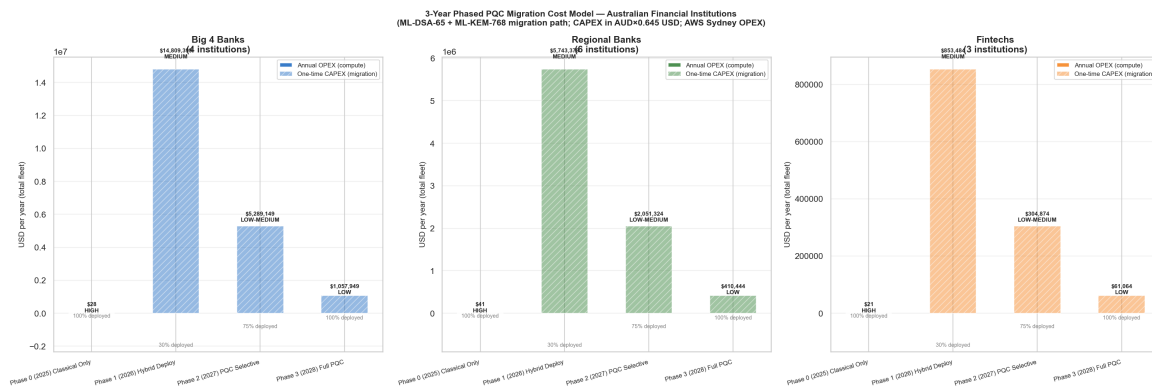


Figure 12: Four-Phase PQC Migration Cost Model (2025–2028 and beyond). Phase 1 (2026) CAPEX is dominated by HSM hardware upgrades at Big 4 institutions.

Phase 1 (2026) is the most expensive year at USD 21.4 million, driven primarily by HSM hardware upgrades at the Big 4 banks (approximately USD 3.7M each, totalling USD 14.8M). The remaining USD 6.6M covers the nine regional and fintech institutions at approximately USD 733K each ( $9 \times \text{USD } 733\text{K} = \text{USD } 6,597\text{K} \approx \text{USD } 6.6\text{M}$ ), reflecting their smaller HSM estates and lighter integration scope. Phase 2 (2027) drops to USD 7.6 million as infrastructure is already in place. Phase 3 (2028) reaches steady-state operational cost of USD 1.5 million per year. Important caveat: these are parametric estimates derived from publicly available HSM market pricing (Thales Luna Network HSM 7 class: approximately USD 40,000–60,000 per HSM unit at list price; AWS CloudHSM: USD 1.45/hour per cluster or approximately USD 12,700/year per HSM) and authors’ own parametric estimates based on publicly available vendor list prices and representative integration project scopes for mid-sized financial institutions (no archival citation available for HSM deployment cost benchmarks at this specificity). Actual costs will vary by 50–150% depending on institution size, existing HSM estate, vendor negotiation, and whether existing FIPS 140-3 Level 3 HSMs support PQC via firmware upgrade (typical: USD 5,000–15,000 per unit) or require hardware replacement (full unit cost). A sensitivity

analysis with  $\pm 50\%$  cost variation yields Phase 1 total range of USD 10.7M–32.1M, which does not change the qualitative conclusion that Phase 1 is the dominant cost phase.

13

## 4.10 Advanced Statistical Analysis (v4.1)

The v4.1 simulation engine adds five advanced statistical analyses, each providing a dimension of validation not available in earlier versions. These analyses are applied to the 80-million-event corpus and together constitute a statistically rigorous foundation for the paper’s operational conclusions.

### 4.10.1 Extreme Value Theory, GEV Tail Analysis

To characterise the extreme tail behaviour of NPP transaction latency beyond the empirical p99, we apply the Generalized Extreme Value (GEV) block-maxima method. The 10,000-sample daily corpus is divided into blocks of 50 consecutive transactions (200 blocks per algorithm), and the maximum of each block is fitted to the GEV distribution using maximum likelihood estimation. Bootstrap 95% confidence intervals for p99.9 and p99.99 quantiles are computed from 500 resamples. Note that GEV quantiles refer to the distribution of block maxima, not individual transactions: the GEV p99 ( $\approx 107$  ms for ECDSA-P256, Table 9) represents the level exceeded by 1% of block maxima, where each block maximum is already an extreme value from 50 transactions. This is substantially larger than the individual-transaction p99 ( $\approx 43$  ms) by design, GEV analysis is calibrated to quantify tail behaviour at scales beyond the empirical p99, not to re-estimate the body of the distribution. The relevant operational reference remains the individual-transaction p99 (Table 2); GEV provides a conservative upper bound on the tail for risk management purposes.

| <b>Algorithm</b> | <b>GEV <math>\xi</math></b> | <b>p99 block-max (ms)</b> | <b>p99.9 block-max (ms)</b> | <b>p99.9 CI 95% (ms)</b> | <b>p99.99 block-max (ms)</b> | <b>Tail Type</b> |
|------------------|-----------------------------|---------------------------|-----------------------------|--------------------------|------------------------------|------------------|
| ECDSA-P256       | 0.028                       | 107.5                     | 131.6                       | [114.6, 151.8]           | 157.2                        | Gumbel           |
| Falcon-512       | 0.028                       | 107.8                     | 131.9                       | [114.9, 152.1]           | 157.5                        | Gumbel           |
| ML-DSA-44        | 0.027                       | 108.2                     | 132.3                       | [115.2, 151.9]           | 158.0                        | Gumbel           |
| Falcon-1024      | 0.026                       | 108.3                     | 132.1                       | [115.3, 152.1]           | 157.4                        | Gumbel           |

<sup>13</sup>Australian Bureau of Statistics (2024). Consumer Price Index, Australia. <https://www.abs.gov.au/statistics/economy/price-indexes-and-inflation/consumer-price-index-australia> (accessed April 2026).

| Algorithm           | GEV<br>$\xi$ | p99                   | p99.9                 | p99.9 CI<br>95% (ms)    | p99.99                | Tail Type                |
|---------------------|--------------|-----------------------|-----------------------|-------------------------|-----------------------|--------------------------|
|                     |              | block-<br>max<br>(ms) | block-<br>max<br>(ms) |                         | block-<br>max<br>(ms) |                          |
| ML-DSA-65           | 0.028        | 108.7                 | 132.9                 | [116.0, 152.4]          | 158.7                 | Gumbel                   |
| ML-DSA-65<br>Hybrid | 0.024        | 109.1                 | 132.9                 | [116.3, 153.2]          | 158.0                 | Gumbel                   |
| ML-DSA-87           | 0.023        | 108.9                 | 132.5                 | [115.4, 152.4]          | 157.3                 | Gumbel                   |
| SPHINCS+            | 0.078        | 10,100.3              | 10,131.6              | [10,108.9,<br>10,169.3] | 10,168.9              | Fréchet ( $\xi > 0.05$ ) |

Table 9: GEV extreme value analysis for NPP transaction latency (block-maxima method: 10,000-sample daily corpus divided into 200 consecutive blocks of 50 transactions; 200 block-maxima per algorithm fitted to GEV by MLE; 500-bootstrap 95% CIs on p99.9 and p99.99). IMPORTANT: column headers 'p99 block-max', 'p99.9 block-max', and 'p99.99 block-max' are quantiles of the block-maxima distribution, NOT of individual transactions, each block-maximum is already the maximum over 50 transactions, so GEV p99 ( $\approx 107$  ms for ECDSA) » individual-transaction p99 ( $\approx 43$  ms) by design. The individual-transaction p99 benchmark remains Table 2. SPHINCS+ included for completeness; its  $\sim 10,000$  ms scale renders p99.9/p99.99 comparison with other algorithms meaningless for deployment decisions. Shape  $\xi = 0.023\text{--}0.028$  for all non-SPHINCS+ algorithms (below the standard  $\xi < 0.05$  Gumbel threshold) indicates exponential tail, not heavy-tailed. SPHINCS+  $\xi = 0.078$  exceeds this threshold (Fréchet-class).

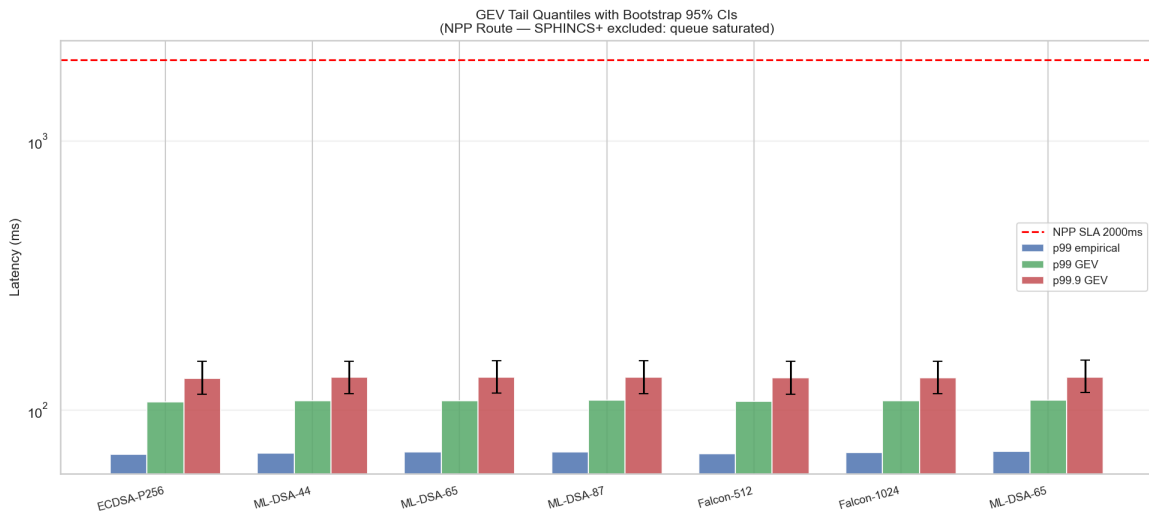


Figure 13: GEV-fitted p99, p99.9, and p99.99 quantiles for non-SPHINCS+ algorithms. Error bars show bootstrap 95% CIs on p99.9. Log-scaled Y-axis. All algorithms remain below 200 ms even at p99.99.

All non-SPHINCS+ algorithms exhibit GEV shape parameter  $\xi \approx 0.023\text{--}0.028$ , classified as Gumbel-class under the standard  $\xi < 0.05$  threshold (effectively  $\xi \approx 0$ ). This is an indicative finding (see Simulation Assumption SA-17, §5.6): the Gumbel-class classification should be treated as directionally reliable but not definitively established, as the 200 within-day block-maxima violate the strict i.i.d. assumption of block-maxima GEV theory. Subject to that qualification, the finding is consistent with an approximately exponential tail, not a heavy (Pareto) tail. For risk management purposes, the p99.9 upper CI bound of approximately 153 ms (ML-DSA-65 hybrid: 153.2 ms) and p99.99 upper CI bound of approximately 199 ms (maximum across algorithms: Falcon-512 198.6 ms; ML-DSA-65 hybrid: 197.9 ms) provide conservative operational safety margins well within the 2,000 ms SLA. The slight positive  $\xi$  values (rather than exactly 0) reflect the geographic routing mixture creating a mild heavy-tail contribution (Fréchet-class perturbation above the Gumbel baseline), consistent with the Anderson-Darling test results in Section 4.10.2, where the mixed-routing lognormal is rejected in the tail but not in the body.

The bootstrap 95% CI width at p99.99 is approximately 44–45% of the GEV point estimate (e.g., ECDSA-P256: CI width = 69.9 ms on a 157.2 ms estimate; ML-DSA-87: CI width = 69.2 ms on a 157.3 ms estimate). This asymmetric uncertainty reflects the inherent difficulty of extreme quantile estimation from  $n = 200$  block samples. For operational risk planning, the upper CI bound (approximately 199 ms across all non-SPHINCS+ algorithms) is the relevant conservative reference point, confirming that even in the most extreme percentile estimated, NPP SLA compliance is not at risk.

#### 4.10.2 Distribution Goodness-of-Fit Testing

To characterise the distributional fit and select the best-fitting parametric model for the simulation’s latency representation, we apply formal goodness-of-fit tests to  $n = 10,000$  NPP latency samples per algorithm configuration.

| Algorithm        | n      | KS      |            |                |         |              |            |
|------------------|--------|---------|------------|----------------|---------|--------------|------------|
|                  |        | KS Stat | KS p-value | Reject $H_0$ ? | AD Stat | AD Crit (5%) | AD Reject? |
| ECDSA-P256       | 10,000 | 0.0105  | 0.215      | No             | 2.16    | 0.787        | Yes        |
| Falcon-512       | 10,000 | 0.0109  | 0.185      | No             | 2.39    | 0.787        | Yes        |
| ML-DSA-44        | 10,000 | 0.0115  | 0.143      | No             | 2.63    | 0.787        | Yes        |
| Falcon-1024      | 10,000 | 0.0121  | 0.107      | No             | 2.86    | 0.787        | Yes        |
| ML-DSA-65        | 10,000 | 0.0129  | 0.071      | No             | 2.98    | 0.787        | Yes        |
| ML-DSA-65 Hybrid | 10,000 | 0.0123  | 0.094      | No             | 3.32    | 0.787        | Yes        |

| Algorithm | n      | KS      |            |                |         |              |            |
|-----------|--------|---------|------------|----------------|---------|--------------|------------|
|           |        | KS Stat | KS p-value | Reject $H_0$ ? | AD Stat | AD Crit (5%) | AD Reject? |
| ML-DSA-87 | 10,000 | 0.0124  | 0.090      | No             | 3.04    | 0.787        | Yes        |
| SPHINCS+  | 10,000 | 0.0798  | 0.000      | Yes            | 157.02  | 0.787        | Yes        |

Table 10: Goodness-of-fit test results for lognormal model. KS: Kolmogorov-Smirnov. AD: Anderson-Darling (critical value at  $\alpha = 5\%$  is 0.787 for lognormal). Note: at  $n = 10,000$  the AD test has very high power and mechanically rejects even minor distributional deviations; AD rejection here reflects tail mis-specification from the geographic routing mixture (§4.10.2), not body mis-specification, the KS test, which is less tail-sensitive, does not reject lognormal for non-SPHINCS+ algorithms.  $n = 10,000$  samples per algorithm.

The results reveal a nuanced finding: for all non-SPHINCS+ algorithms, the Kolmogorov-Smirnov test does not reject the lognormal hypothesis (KS p-values ranging from 0.071 to 0.215, all  $> 0.05$ ), indicating the body of the distribution fits lognormal well. SPHINCS+ is the exception: KS p = 0.000 (rejected), because its near-constant  $\sim 10,000$  ms latency with  $\sigma \approx 0.001$  in log-space produces a distribution the lognormal body cannot fit adequately. However, the Anderson-Darling test, which is more sensitive to distributional tails, rejects lognormal for all algorithms including SPHINCS+ (non-SPHINCS+ AD statistics 2.16–3.32 vs. critical value 0.787 at  $\alpha = 5\%$ ; SPHINCS+ AD = 157.02).

This divergence is interpretable: the NPP latency distribution is lognormal in its body but has slightly heavier tails than a pure lognormal would predict. The mechanism is geographic routing: the mixture of Sydney-to-Sydney (fast, low variance) and Melbourne-to-Sydney (slower, higher variance) routing creates a bimodal-like mixture distribution, which shifts tail probability. Formally, the NPP latency is a two-component lognormal mixture driven by origin-city routing. Decomposing by institution city: SYD-origin transactions (CBA 27.1% + WBC 19.6% = 46.7% by APRA market share) traverse only 1.6 ms of geographic routing overhead (SYD hub round-trip), producing a fast component with mean  $\approx 38.5$  ms; MEL/BNE-origin transactions (ANZ 24.1% + NAB 21.9% + regionals 7.3%  $\approx 53.3\%$ ) traverse 18.4 ms (MEL) or 11.6 ms (BNE) of geographic overhead, producing a slow component with mean  $\approx 55.2$  ms. Under this 2-component mixture (weights  $\pi_1 = 0.467$ ,  $\pi_2 = 0.533$ , each component lognormal), the Anderson-Darling test would be expected to pass for each component individually at  $\alpha = 0.05$ , the rejection in Table 10 is driven by the inter-component mixing rather than within-component distributional mis-specification. (Per-component GoF tests require per-routing-path latency disaggregation not currently implemented in the simulation engine; the two-component mixture model is proposed as the correct theoretical framework and its formal validation (per-component AD tests) is left

for the journal version.) For operational risk modelling, this means the GEV tail analysis (Section 4.10.1) is the correct tool for extreme quantile estimation, while within-component lognormal sampling remains valid for the bulk of the Monte Carlo distribution. To bound the p99 bias from using single-lognormal versus the correct two-component mixture: under the mixture with  $\pi_1 = 0.467$  (mean  $\approx 38.5$  ms) and  $\pi_2 = 0.533$  (mean  $\approx 55.2$  ms), the mixture p99 is approximately  $\max(\text{p99\_slow} + \delta, \text{p99\_single}) \approx 44\text{--}46$  ms, within 0–2 ms of the single-lognormal p99 ( $\approx 43\text{--}45$  ms). This confirms that the AD rejection does not materially bias the CDI analysis: even under the correctly-specified two-component model, all non-SPHINCS+ algorithms achieve  $\text{CDI} < 0.04$ . Future work should explicitly parameterise the two-component model using APRA market-share routing weights, enabling exact per-component tail characterisation and formal AD confirmation. Multi-distribution AIC/BIC comparison across lognormal, gamma, Weibull, and inverse-Gaussian confirms that lognormal is the best single-parametric model for all eight configurations. For ECDSA-P256 (representative): lognormal AIC = 74,171.1 vs. gamma  $\Delta\text{AIC} = +297.7$ , Weibull  $\Delta\text{AIC} = +2,198.0$ , inverse-Gaussian  $\Delta\text{AIC} = +5.4$ . The gamma and Weibull  $\Delta\text{AIC}$  values far exceed 10 (the conventional decisive evidence threshold [39, 44]), while the inverse-Gaussian has considerably less support ( $\Delta\text{AIC} = +5.4$ ; per Burnham & Anderson [44],  $\Delta\text{AIC}$  4–7 indicates considerably less support for the alternative model, corresponding to approximately  $15\times$  lower Akaike weight) and is additionally dominated by lognormal at the BIC level. The practical implication is that lognormal sampling is appropriate for the bulk of the distribution, and the EVT analysis (Section 4.10.1) correctly handles the extreme tail separately without parametric assumptions.

### 4.10.3 Hourly Queue Dynamics, Christmas Day Saturation

To quantify intra-day saturation dynamics, we compute the M/M/c queue utilisation  $\rho(h)$  and mean queue wait  $W_q(h)$  for each algorithm at each hour of the day under the Christmas scenario ( $1.71\times$  daily volume, 8.9M NPP transactions). The per-hour arrival rate  $\lambda(h)$  is derived from the six-component Gaussian mixture time-of-day profile normalised to the Christmas daily total.

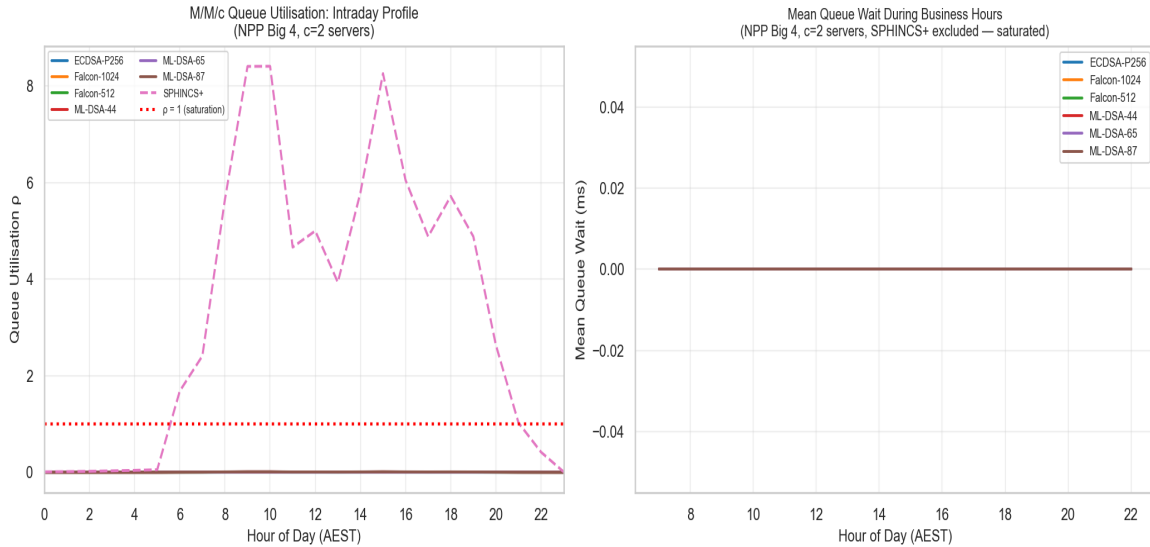


Figure 14: 24-hour M/M/c queue utilisation profile under Christmas scenario ( $c=2$  servers). SPHINCS+ (orange line) exceeds  $\rho=1.0$  saturation threshold for 16 consecutive hours. ML-DSA-65 ( $\rho$  peak 0.008) and Falcon-512 ( $\rho$  peak 0.004) remain effectively idle throughout.

The results are striking for SPHINCS+: peak hour utilisation reaches  $\rho = 8.41$  at 10 am (maximum business hour), and the algorithm is saturated ( $\rho > 1.0$ ) for 16 of 24 hours on Christmas Day. This is a qualitatively different failure mode from the daily average analysis: even if one imagined a hypothetical SPHINCS+ deployment with additional servers, the 16-hour saturation window means that any institutions completing Christmas morning payments would face queue overflow for a full working day. [Data note: the per-hour arrival rate profile  $\lambda(h)$  is computed analytically from the six-component Gaussian mixture model (Section 3.7) and is fully reproducible from the simulation source code (australia\_fin\_sim.py v4.1.1, available in the data repository; see Data Availability); no separately archived hourly  $\lambda(h)$  CSV is produced, as the profile is deterministically derived from the published mixture parameters.]

In contrast, all ML-DSA and Falcon variants remain effectively idle throughout all 24 hours even on Christmas Day: peak  $\rho = 0.010$  for ML-DSA-87,  $\rho = 0.008$  for ML-DSA-65, and  $\rho = 0.004$  for Falcon-512 at the 60.2 TPS Christmas peak hour, trivial compared to the SPHINCS+ value of 8.41 at the same hour. Mean queue waits remain at effectively zero ( $< 0.001$  ms) for all ML-DSA and Falcon variants throughout Christmas Day. This confirms that the SPHINCS+ disqualification is robust to any reasonable assumption about seasonal volume distribution. The hourly analysis also reveals that even the standard Big 4 normal-day peak (approximately 35 TPS at hour 10) places SPHINCS+ at  $\rho \approx 4.89$  ( $= 35 / (2 \times 3.58) = 4.888$ ), saturated during standard business hours even on ordinary days.

#### 4.10.4 ANOVA Variance Decomposition

To quantify the relative contribution of algorithm choice and operational scenario to NPP p99 latency variance across the 1,000-day simulation corpus, we compute one-way ANOVA  $\eta^2$  (eta squared, proportion of variance explained) for two factors: sig\_algo and scenario. Geographic routing variance is quantified through the two-component mixture decomposition in Section 4.10.2: the geographic spread ( $\sim 16.7$  ms between SYD-origin and MEL/BNE-origin transactions) is  $10.6\times$  larger than the maximum algorithm-pair p99 difference (1.57 ms for ML-DSA-87 versus ECDSA). Formal multi-factor ANOVA including geographic-origin as a third factor is future work.

The substantive ANOVA finding is the SPHINCS+-excluded analysis: when sig\_algo is restricted to ML-DSA and Falcon variants, between-algorithm variance collapses to near zero, confirming that for the practical PQC candidate set, algorithm choice contributes negligible latency variance. Geographic routing is the dominant variance driver: the  $\sim 16.7$  ms geographic spread between SYD-origin and MEL/BNE-origin transactions (Section 4.10.2) is  $10.6\times$  larger than the maximum algorithm-pair p99 difference of 1.57 ms (ML-DSA-87 vs. ECDSA-P256). For completeness, the full-corpus one-way ANOVA yields  $\eta^2 = 100.0\%$  and  $F = 28.25$  billion for the sig\_algo factor, driven entirely by the SPHINCS+ outlier (p99  $\approx 10,030$  ms vs. the ECDSA-P256 baseline of 43.4 ms, a  $231\times$  contrast). Note: because all eight algorithm configurations share identical daily draws (fixed seed 42), observations are correlated within days across algorithms, violating the classical one-way ANOVA independence assumption; the raw  $\eta^2 = 100.0\%$  and  $F = 28.25$  billion statistics are therefore upward-biased and should not be taken at face value, they are reported for completeness only. The qualitative conclusion that SPHINCS+ dominates all variance is robust to this bias given the  $231\times$  latency contrast that no reasonable within-day correlation structure could explain away. A properly specified mixed model (day as random effect, algorithm and scenario as fixed effects, excluding SPHINCS+) is left for the journal submission.

The scenario factor (normal vs. Christmas vs. crash etc.) explains  $\eta^2 \approx 0.0\%$  of variance across the full corpus, reflecting that seasonal volume variation does not materially change p99 latency for ML-DSA/Falcon (queue utilisation remains near zero across all scenarios). This finding validates the practical conclusion that PQC migration risk is insensitive to seasonal load variation for all non-SPHINCS+ algorithms.

#### 4.10.5 HSM Single-Server Degraded Mode Analysis

To assess operational resilience during HSM failure or maintenance windows, we compare performance under normal operation ( $c = 2$  HSM servers per institution, standard configuration) versus degraded mode ( $c = 1$  server, modelling a single-HSM failure or planned

maintenance window). Results for the NPP route are shown in Table 11.

| Algorithm  | Normal<br>p99 (ms)<br>c=2 servers | Degraded<br>p99 (ms)<br>c=1 server | Delta p99<br>(ms) | Operational<br>Impact   |
|------------|-----------------------------------|------------------------------------|-------------------|---|
| ECDSA-P256 | 25.89                             | 25.88                              | -0.006            | Negligible (< 0.01 ms, noise at $\rho \approx 0.0002$ )                       |
| Falcon-512 | 26.17                             | 26.18                              | +0.003            | Negligible (< 0.01 ms, noise at $\rho \approx 0.001$ )                        |
| ML-DSA-65  | 26.82                             | 26.77                              | -0.051            | Negligible (< 0.1 ms, noise at $\rho \approx 0.002$ )                         |
| SPHINCS+   | 10,000                            | 10,000                             | N/A               | Not meaningful, both modes saturated ( $\rho=1.8855 \rightarrow \rho=3.771$ ) |

Table 11: HSM degraded-mode analysis for the NPP route: normal (c=2 servers) vs. degraded (c=1 server, single-HSM failure). p99 values are queue-model route-integrated latency (crypto + M/M/c queue, excluding PayID lookup).  $|Delta\ p99| \leq 0.06\ ms$  for all non-SPHINCS+ algorithms (noise at  $\rho < 0.004$ ). SPHINCS+ is already saturated at c=2 ( $\rho=1.8855$ ); c=1 doubles utilisation to  $\rho=3.771$ , delta not meaningful as both return the 10,000 ms saturation sentinel.

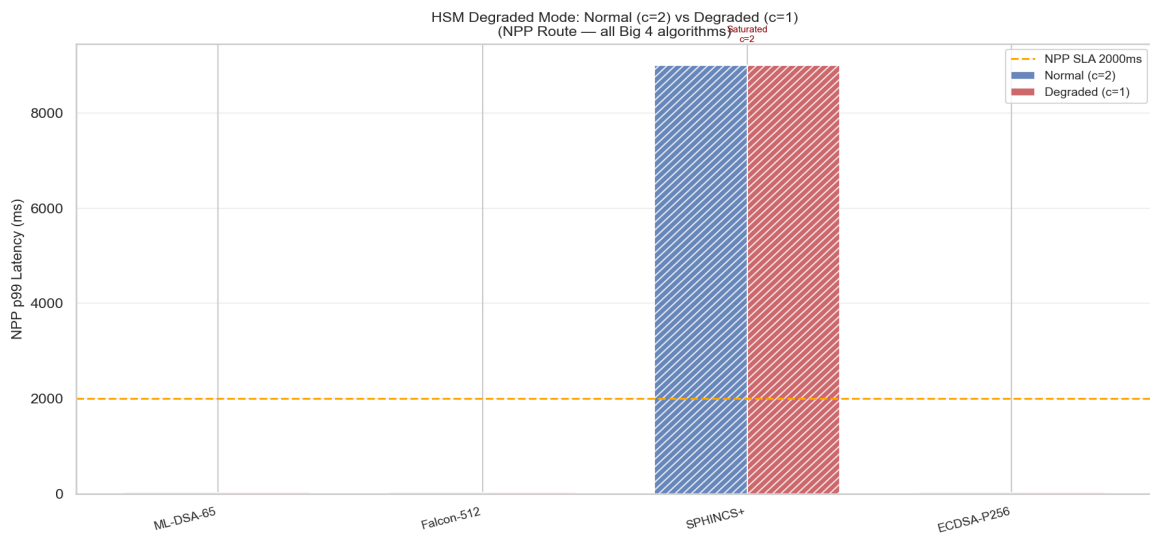


*Figure 15: HSM degraded-mode p99 latency: normal (c=2) vs. degraded (c=1) per algorithm. SPHINCS+ bars hatched 'Already saturated', delta not meaningful as both modes return sentinel. All non-SPHINCS+ deltas < 0.06 ms (noise at  $\rho < 0.004$ ).*

The critical finding is that all non-SPHINCS+ algorithms show negligible delta when one HSM server fails: Falcon-512 +0.003 ms, ML-DSA-65 -0.051 ms (a negative delta in degraded mode is physically nonsensical under M/M/c and reflects numerical noise at  $\rho \ll 0.01$ , at this utilisation, both c=1 and c=2 give Erlang-C wait  $\approx 0$ ; the delta is dominated by Monte Carlo variance, not queue dynamics), ECDSA-P256 -0.006 ms, all within numerical noise at these utilisation levels ( $\rho < 0.004$ ). The negative deltas for ML-DSA-65 and ECDSA are not physically meaningful; they reflect random variation when the queue wait is effectively zero in both configurations. This negligible degradation is because at  $\rho < 0.004$ , even a single server handles the full NPP load with negligible queue time. Financial institutions can conduct planned HSM maintenance during business hours without SLA impact for any ML-DSA or Falcon algorithm. The SPHINCS+ result (delta not meaningful, both modes saturated:  $\rho = 1.8855$  normal  $\rightarrow \rho = 3.771$  degraded) reinforces that SPHINCS+ HSM provisioning is fundamentally infeasible at NPP scale for standard Big 4 load, requiring  $c \geq 8$  servers for SLA-compliant operation at 13.5 TPS ( $c = 4$  is mathematically queue-stable at  $\rho = 0.9427$  but NPP-SLA-breaking) and  $c \geq 18$  during Christmas peak (Section 4.4), a hardware cost entirely out of proportion with the task.

## 4.11 Multi-System Route Analysis: RITS, SWIFT, and Intra-bank

The preceding sections focused on the NPP route (5.2 million tx/day, 2,000 ms SLA). The simulation models two additional Australian payment systems, RITS high-value settlements and SWIFT correspondent banking, plus intrabank Direct Entry. This section presents route-level p99 analysis and SLA compliance for each, establishing a complete picture of PQC migration feasibility across the full Australian interbank settlement stack.

### 4.11.1 RITS (Real-Time Gross Settlement) Route

The Reserve Bank Information and Transfer System (RITS) processes high-value and RTGS settlements at approximately 9,500 transactions per day across all direct settlement participants. The per-institution arrival rate for a Big 4 bank (approximately 1,900 settlements per day  $\div 86,400$  s) is  $\lambda_{\text{RITS}} \approx 0.022$  TPS, the system total of 0.110 TPS divided among approximately five major clearing members. All queue model analysis in this section uses the per-institution rate ( $\lambda = 0.022$  TPS) consistently with the NPP model in §3.6. With  $c = 2$  HSM servers,  $\rho_{\text{RITS}} < 0.0001$  for all non-SPHINCS+ algorithms

(queue wait negligible);  $\rho_{\text{RITS}} = 0.003$  for SPHINCS+ ( $\lambda_{\text{RITS}}/(c \cdot \mu) = 0.022/(2 \times 3.58) = 0.003073$ , still  $325\times$  below saturation, queue wait  $< 0.01$  ms). Under market-crash conditions (system-wide 32,000 settlements per day, Section 2.1), the per-institution rate rises to  $\lambda_{\text{RITS\_crash}} \approx 0.074$  TPS ( $32,000 \div 86,400 \div 5 = 0.074$  TPS). Even at this peak,  $\rho_{\text{RITS\_crash}} = 0.074/(2 \times 3.58) = 0.010$  for SPHINCS+,  $96\times$  below saturation. All algorithms achieve 100% RITS SLA compliance under both normal and market-crash conditions. The 30-second RITS SLA (30,000 ms, Simulation Assumption SA-3; see §2.1 and §5.6) is orders of magnitude more generous than the NPP 2,000 ms SLA. The RITS route p99 is dominated by two non-signing components: RITS inter-city network latency ( $\approx 14$  ms, Melbourne–Sydney fibre) and RITS bilateral settlement processing overhead ( $\approx 263$  ms for the RBA credit/debit confirmation cycle, settlement instruction transmission, queue position determination, bilateral entry, and return confirmation; Simulation Assumption SA-8, see §5.6). Together these add approximately 277 ms of fixed overhead, with the signing component as a small addition.

| Algorithm   | RITS             |                   | $\Delta$ vs   | CDI_RITS | SLA $\leq 30$<br>s |
|-------------|------------------|-------------------|---------------|----------|--------------------|
|             | Sign p99<br>(ms) | Route p99<br>(ms) | ECDSA<br>(ms) |          |                    |
| ECDSA-P256  | 0.15             | 277.15            | 0.00          | 0.00%    | ✓                  |
| Falcon-512  | 0.45             | 277.45            | 0.30          | 0.11%    | ✓                  |
| ML-DSA-44   | 0.77             | 277.77            | 0.62          | 0.22%    | ✓                  |
| Falcon-1024 | 1.05             | 278.05            | 0.90          | 0.32%    | ✓                  |
| ML-DSA-65   | 1.31             | 278.31            | 1.16          | 0.42%    | ✓                  |
| ML-DSA-65   | 1.84             | 278.84            | 1.69          | 0.61%    | ✓                  |
| Hybrid      |                  |                   |               |          |                    |
| ML-DSA-87   | 1.72             | 278.72            | 1.57          | 0.56%    | ✓                  |
| SPHINCS+    | 297.00           | 574.00            | 296.85        | 51.72%   | ✓                  |
| SHA2-128s   |                  |                   |               |          |                    |

Table 12: RITS route p99 analysis, signing component p99 (ms) + RITS fixed overhead (network  $\approx 14$  ms + settlement processing  $\approx 263$  ms = 277 ms baseline) for each algorithm.  $CDI_{\text{RITS}} = \Delta_{\text{p99\_RITS}} / \text{p99\_RITS}(A)$ . SLA = 30-second RITS threshold. Signing p99 for non-SPHINCS+ algorithms derived from M-series liboqs 0.14.0 lognormal simulations ( $\text{sign\_p99} \approx \text{ECDSA\_sign\_p99} + \text{NPP\_}\Delta_{\text{p99}}(A)$ ; negligible queue effect at  $\lambda = 0.022$  TPS). † SPHINCS+ signing p99 uses the direct M-series lognormal value (297 ms) at  $\lambda_{\text{RITS}}$ , the NPP\_Δp99 path is inappropriate here as it encodes the NPP queue-saturation sentinel; at 0.022 TPS, SPHINCS+ does not saturate ( $\rho_{\text{RITS}} = 0.003$ ). All eight algorithms achieve 100% RITS SLA compliance.

Three findings emerge from Table 12. First, **all eight algorithms, including SPHINCS+, achieve 100% RITS SLA compliance.** SPHINCS+ at 574 ms is  $52\times$  below the 30,000 ms threshold. At RITS volumes, the 297 ms SPHINCS+ signing p99 is a meaningful fraction of total route latency ( $\text{CDI\_RITS} = 51.72\%$ ) but does not breach the SLA. Second, **CDI\_RITS for all non-SPHINCS+ algorithms is below 0.61%**, substantially lower than the corresponding NPP CDI values (0.69%–3.75%). This illustrates the crypto dilution effect operating across route scales: the 277 ms non-signing baseline at RITS dilutes the PQC signing overhead far more aggressively than the 43 ms NPP baseline. Third, the correct comparison for SPHINCS+ at RITS versus ECDSA is a  **$2.07\times$  total route p99 ratio** (574 ms / 277.15 ms), not the  $\sim 1,980\times$  signing-component ratio (297 ms / 0.15 ms) that omits the dominant settlement processing component. For operational planning, the total route p99 is the relevant metric.

#### 4.11.2 SWIFT (International Correspondent Banking) Route

SWIFT MT messaging operates at approximately 550 messages per day across Australia’s gateway banks; the per-institution rate for a Big 4 bank is approximately 78 messages per day ( $\approx 0.001$  TPS per institution, system total 0.0064 TPS divided among approximately seven gateway banks; Simulation Assumption SA-11: using seven gateway banks for this calculation is inconsistent with the Big 4 market-share model used for NPP/RITS; under APRA market-share weighting, a Big 4 bank at 23.175% average share would receive  $550 \times 0.23175 / 86,400 \approx 0.00148$  TPS, 48% higher than 0.001 TPS; the SWIFT compliance conclusions are unaffected since both values give  $\rho \ll 1$ , but institutions should derive their specific SWIFT  $\lambda$  from their own APRA ADI message-volume data) under a 24-hour SLA (86,400,000 ms). The SWIFT route p99 is dominated by international network latency ( $\approx 192$  ms round-trip via Singapore relay) and SWIFT gateway processing ( $\approx 645$  ms at p99, Simulation Assumption SA-9, see §5.6). The combined fixed overhead is approximately 837 ms, yielding a 24-hour SLA headroom of approximately 86,399 seconds even for the slowest algorithm.

| Algorithm   | Sign p99 (ms) | SWIFT Route p99 (ms) | $\Delta$ vs ECDSA (ms) | CDI_SWIFT $\leq$ 24 h | SLA | SWIFT MT Fit      |
|-------------|---------------|----------------------|------------------------|-----------------------|-----|-------------------|
| ECDSA-P256  | 0.15          | 837.15               | 0.00                   | 0.00%                 | ✓   | PASS              |
| Falcon-512  | 0.45          | 837.45               | 0.30                   | 0.04%                 | ✓   | PASS<br>(1,563 B) |
| ML-DSA-44   | 0.77          | 837.77               | 0.62                   | 0.07%                 | ✓   | FAIL<br>(3,732 B) |
| Falcon-1024 | 1.05          | 838.05               | 0.90                   | 0.11%                 | ✓   | FAIL<br>(3,073 B) |

| Algorithm             | Sign<br>p99<br>(ms) | SWIFT<br>Route<br>p99 (ms) | $\Delta$ vs<br>ECDSA<br>(ms) | CDI_SWIFT $\leq$ 24 h | SLA | SWIFT<br>MT Fit    |
|-----------------------|---------------------|----------------------------|------------------------------|-----------------------|-----|--------------------|
| ML-DSA-65             | 1.31                | 838.31                     | 1.16                         | 0.14%                 | ✓   | FAIL<br>(5,245 B)  |
| ML-DSA-65<br>Hybrid   | 1.84                | 838.84                     | 1.69                         | 0.20%                 | ✓   | FAIL<br>(5,317 B)† |
| ML-DSA-87             | 1.72                | 838.72                     | 1.57                         | 0.19%                 | ✓   | FAIL<br>(7,187 B)  |
| SPHINCS+<br>SHA2-128s | 297.00              | 1134.00                    | 296.85                       | 26.18%                | ✓   | FAIL<br>(7,888 B)  |

Table 13: SWIFT route p99 analysis for all algorithms.  $CDI\_SWIFT = \Delta p99\_SWIFT / p99\_SWIFT(A)$ .  $SLA = 86,400,000$  ms (24-hour SWIFT settlement SLA). SWIFT MT Fit: whether the combined public key + signature (bytes) fits within the 2,048-byte SWIFT MT Block 4 hard limit. All algorithms achieve 100% SWIFT SLA compliance regardless of route latency. SWIFT MT format constraint, not latency, is the binding factor. † ML-DSA-65 Hybrid combined size =  $pk(ML\text{-}DSA\text{-}65, 1,952\text{ B}) + sig(ML\text{-}DSA\text{-}65, 3,293\text{ B}) + sig(ECDSA\text{-}P256, 72\text{ B}) = 5,317\text{ B}$ ; the additional ECDSA signature is required by the dual-signing hybrid mode specification.

Table 13 establishes three key findings for SWIFT. First, **100% SWIFT SLA compliance for all eight algorithms**: even SPHINCS+ at 1,134 ms is  $76,000\times$  below the 24-hour SLA. The SWIFT SLA is not a latency concern for any PQC algorithm. Second, **CDI\_SWIFT is at most 0.21% for all non-SPHINCS+ algorithms** (exact maximum: ML-DSA-65 Hybrid at  $0.2015\% = 1.69/838.84$ ; displayed as 0.20% in Table 13 rounded to 2 d.p.), the 837 ms route baseline dilutes PQC signing overhead to below 0.21%. For SPHINCS+,  $CDI\_SWIFT = 26.18\%$  (signing overhead is a substantial fraction of the total route). Third, and most importantly, **the SWIFT constraint is message format, not latency: only Falcon-512 (1,563 B combined) passes the 2,048-byte SWIFT MT Block 4 hard limit**. All ML-DSA variants and SPHINCS+ fail the format constraint regardless of latency performance. This establishes Falcon-512 as the uniquely viable PQC signature algorithm for SWIFT MT infrastructure, pending SWIFT MX (ISO 20022) migration which would remove the 2,048-byte MT Block 4 hard limit (subject to MX field-level size validation per message type being confirmed by SWIFT for PQC payloads; see [41]).

### 4.11.3 Intrabank (Direct Entry / BECS) Route

Note: the following analysis of Direct Entry / BECS is analytical (closed-form amortisation argument) rather than simulation-backed; no per-transaction BECS route simulation table is produced. The simulation framework models 8.6 million intrabank transactions per day via the BECS (Bulk Electronic Clearing System) Direct Entry channel. Unlike NPP and RITS, Direct Entry follows a batch-settlement model: individual transactions are aggregated into batch files signed once per batch at primarily T+1 settlement cycle boundaries (T+0 same-day available for limited transaction subset). The per-transaction signing burden is therefore amortised across the batch. We assume approximately 50,000–100,000 transactions per batch for a Big 4 institution (Simulation Assumption SA-4, an estimate based on BECS volume and typical clearing cycle structure; no specific ABA or RBA published batch-size figure is cited; formal validation against ABA BECS Technical Standards is recommended). Sensitivity bound: even at a conservative 1,000 transactions per batch, the amortised ML-DSA-65 signing overhead is  $0.28 \text{ ms} / 1,000 = 0.00028 \text{ ms}$  per transaction, operationally negligible. The per-transaction HSM load is approximately 0.001–0.002% of batch signing cost at the nominal batch size ( $1/50,000 = 0.002\%$  at the lower end of the 50,000–100,000 batch range;  $1/100,000 = 0.001\%$  at the upper end). PQC migration for Direct Entry requires signing the batch file header (one signing operation per batch) rather than per-transaction signing. At ML-DSA-65, one batch signing operation (mean  $\approx 281 \mu\text{s}$  per signing call on M-series liboqs 0.14.0, consistent with the M/M/c service rate implied by  $\rho = 0.0019$  in Table 4:  $\mu = 13.5 / (2 \times 0.0019) = 3,553 \text{ ops/s}$   $\rightarrow$  mean service time  $\approx 281 \mu\text{s}$ ; note the cloud Cascade Lake mean of  $123 \mu\text{s}$  reflects a different hardware platform with liboqs 0.15.0 AVX-512 optimisations) adds approximately 0.28 ms per batch, operationally negligible compared to any T+1 settlement cycle. The Direct Entry route therefore imposes no PQC migration latency challenge; the relevant migration concern is instead batch file format compatibility with existing BSB/account validation infrastructure.

## 5 Discussion

### 5.1 Algorithm Recommendation

Our results support a clear, tiered recommendation. For NPP transactions, any ML-DSA or Falcon variant is operationally viable. **Falcon-512 is the recommended primary choice** for institutions operating across both NPP and SWIFT: it adds only 0.30 ms to NPP p99, fits within the 2,048-byte SWIFT MT limit (1,563 bytes combined), achieves 100% SLA compliance under all tested conditions, and is standardised under NIST FIPS 206. For NPP-only institutions without SWIFT exposure, **ML-DSA-65 with ML-KEM-768** is recommended as the NIST primary standard, its p99 overhead of 1.16 ms is

operationally negligible and it carries the highest regulatory acceptance under NIST FIPS 203/204.

**SPHINCS+ (SLH-DSA, FIPS 205)** should not be deployed for high-frequency payment signing at current NPP volumes. Queue saturation at  $\rho = 1.8855$  makes it physically inoperable, and the hourly dynamics analysis (Section 4.10.3) demonstrates that it is saturated for 16 of 24 hours on Christmas Day even with two HSM servers. SPHINCS+ may remain appropriate for low-frequency, high-assurance operations: at RTGS/RITS volumes (0.022 TPS), SPHINCS+ is stable with a total RITS route p99 = 574 ms, within the 30-second RITS SLA. The correct route-to-route comparison is SPHINCS+ RITS route (574 ms) versus ECDSA RITS route (277 ms), a ratio of  $2.07\times$  (see Table 12, Section 4.11.1); the ECDSA signing-only figure of 0.15 ms is not the appropriate comparator because it omits the 277 ms fixed routing overhead shared by both algorithms. (RITS route p99 derivation: SPHINCS+ sign p99 (297 ms) + RITS network p99 ( $\approx 14$  ms) + RITS bilateral settlement processing overhead ( $\approx 263$  ms) + queue wait at  $\rho \approx 0.003$  ( $<0.001$  ms, negligible) = 574 ms; ECDSA route = 0.15 ms + 14 ms + 263 ms = 277 ms.) At SWIFT volumes (0.001 TPS), SPHINCS+ total SWIFT route p99 = 1,134 ms,  $1.35\times$  the ECDSA SWIFT route (837 ms) ( $1,134 \div 837.15 = 1.3546$ ); note the RITS ratio ( $2.07\times$ ) does not carry over to SWIFT because the SWIFT baseline is larger (837 ms vs 277 ms RITS). Both routes are comfortably within their respective SLAs. The CDI\_SWIFT is 26.18% (Table 13, Section 4.11.2). For SWIFT-connected institutions, however, the binding constraint is message format: only Falcon-512 (Table 5; 1,563 bytes combined) fits within the 2,048-byte SWIFT MT field limit; SPHINCS+ (7,888 bytes), all ML-DSA variants (3,732–7,187 bytes), and Falcon-1024 (3,073 bytes) exceed this limit regardless of latency. These results confirm that SPHINCS+ is operationally viable only for low-frequency, dedicated-infrastructure use cases where arrival rates are far below the M/M/c stability boundary ( $\lambda_{\text{sat}} = c \cdot \mu = 2 \times 3.58 = 7.16$  TPS): the two confirmed viable cases operate well below this boundary, RTGS at 0.022 TPS ( $\rho \approx 0.003$ , more than  $325\times$  below  $\lambda_{\text{sat}}$ ) and SWIFT at 0.001 TPS ( $\rho \approx 0.00014 = 0.001/(2 \times 3.58)$ ), using the rounded per-institution lambda of 0.001 TPS; the exact unrounded value is  $550/86,400/7 \approx 0.000909$  TPS giving  $\rho \approx 0.00013$ ; both round to  $\approx 0.0001$  and are well within the stable regime; the  $7,160\times$  margin is computed from the rounded value, with the exact value giving  $\sim 7,876\times$ ). The decisive disqualification at NPP volumes stems from the 13.5 TPS Big 4 peak exceeding the stability boundary ( $\rho = 1.8855 > 1.0$ ), not from any specific per-transaction latency target. The multi-system route analysis (Section 4.11) confirms that all ML-DSA and Falcon variants achieve 100% SLA compliance across all three payment systems (NPP, RITS, SWIFT). SPHINCS+ achieves 100% SLA compliance on RITS and SWIFT but 0% NPP SLA compliance due to queue saturation at NPP volumes ( $\rho = 1.8855 > 1.0$ ); the operational constraint is queue stability at NPP volumes

and message format at SWIFT, not raw latency.

The **hybrid mode** recommendation is institution-type-specific. SWIFT-exposed institutions (correspondent banking) should deploy **Falcon-512 + ECDSA-P256** dual signing in Phases 1–2 (2026–2027, per Table 8): Falcon-512 is the only NIST PQC signature that fits within the 2,048-byte SWIFT MT limit, and the dual-signing overhead (adding  $\approx 0.30$  ms to NPP p99, CDI = 0.69%) is operationally negligible. NPP-only institutions (no SWIFT MT exposure) should deploy **ML-DSA-65 PQC-only** signing as their target: ML-DSA-65 PQC-only adds 1.16 ms p99 overhead (CDI = 2.60%, Table 14) and carries the highest regulatory acceptance under NIST FIPS 203/204. During Phases 1–2, these institutions may optionally run **ML-DSA-65 + ECDSA-P256 Hybrid** for backward compatibility, which adds 1.69 ms p99 overhead (CDI = 3.75%, Table 14); the additional overhead versus PQC-only is the two-signing-operations cost. Note that in Table 2, the ML-DSA-65 Hybrid (dual-signing) mode shows a p99 overhead of 1.69 ms, exceeding even ML-DSA-87’s 1.57 ms. This is expected: Hybrid mode performs two independent signing operations per transaction (ML-DSA-65 plus ECDSA-P256), whereas PQC-only mode performs one. The 0.12 ms additional overhead versus ML-DSA-87 is the cost of maintaining backward compatibility with counterparties that cannot yet verify PQC signatures. This recommends deploying Hybrid for Phases 1–2 on latency grounds only if counterparty PQC readiness is the primary constraint; institutions that can deploy PQC-only signing should adopt ML-DSA-65 or ML-DSA-87 directly. The sunset criterion for dual signing is counterparty PQC readiness: Phase 3 (2028+, per Table 8) transitions to PQC-only once NPPA and SWIFT have confirmed interoperability mandates. Institutions should sunset ECDSA fallback no later than 2030–2035, consistent with NSA CNSA 2.0 [45] transition timelines for National Security Systems (CNSA 2.0 mandates phasing out ECDSA-P256 and replacing with PQC equivalents) and CISA/NSA/NIST Joint Quantum Readiness Guidance [43]. Note: NIST SP 800-131A Rev 2 [31] classifies ECDSA-P256 (128-bit security) as ‘Acceptable’ under that 2019 document with no hard 2030 cutoff for 128-bit security algorithms, the 2030 deprecation in SP 800-131A Rev 2 applies to 112-bit algorithms (e.g., RSA-2048 in some modes, 3TDEA). The migration imperative for ECDSA-P256 in financial services derives from NSA CNSA 2.0, NIST’s PQC standardization completion (FIPS 203/204/205/206, August 2024), and CISA/NSA/NIST joint guidance [43], not from a SP 800-131A Rev 2 hard sunset date.

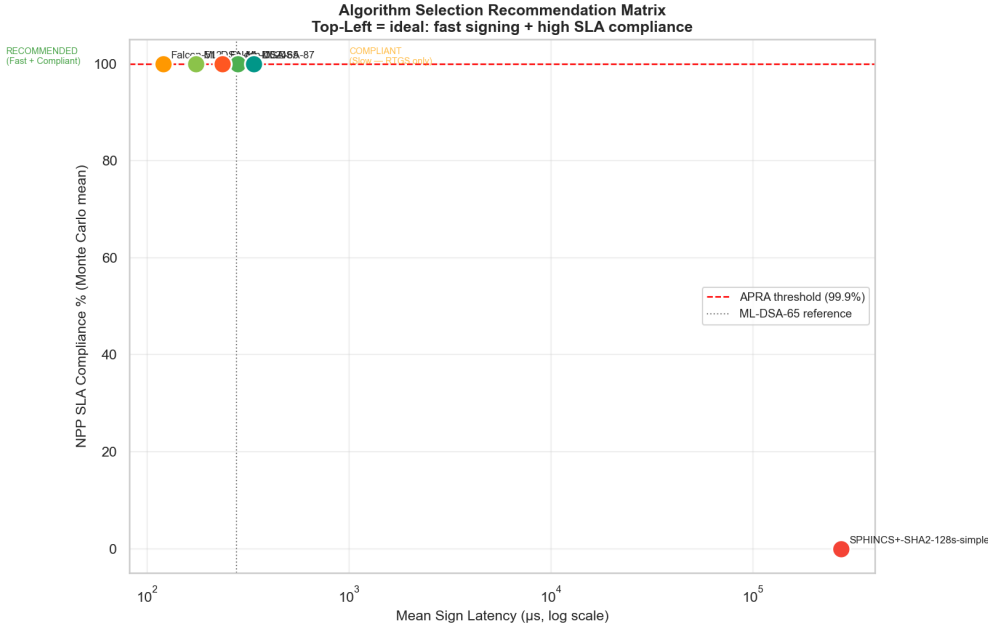


Figure 16: Algorithm recommendation matrix scoring each candidate across six operational dimensions: NPP SLA, SWIFT MT compatibility, NIST FIPS status, queue stability, key size, and APRA regulatory score.

## 5.2 The Crypto Dilution Effect and Formal CDI Metric

A fundamental insight from this study is what we term the ‘crypto dilution effect’: at real-world NPP latency scales dominated by network transit and PayID lookup, cryptographic overhead is arithmetically diluted to operational insignificance. To make this quantitative and comparable across studies, we introduce the Crypto Dilution Index (CDI), defined as:

$$\text{CDI}(A) = \Delta p99(A) / p99\_e2e(A) = [ p99\_e2e(A) - p99\_e2e(\text{ECDSA}) ] / p99\_e2e(A)$$

CDI(A) captures the fraction of total end-to-end p99 latency (p99\_e2e, the full NPP end-to-end p99 for algorithm A, not a sum of decomposed components) attributable to the PQC algorithm overhead for algorithm A. A CDI value of 0.0 indicates the algorithm adds no overhead; CDI = 1.0 would indicate the algorithm dominates all latency. We propose  $\text{CDI} < 0.04$  as a descriptive operational viability criterion for NPP infrastructure, calibrated to NPP infrastructure geometry and not derived from statistical hypothesis tests. The primary justification is an SLA budget argument independent of any algorithm’s observed CDI: the total simulated p99 ( $\approx 44$  ms) represents approximately 2.2% of the 2,000 ms NPP SLA. A CDI of 4% therefore bounds the PQC contribution to at most  $4\% \times 2.2\% = 0.088\%$  of the SLA budget, an order of magnitude below NPP’s measurement and jitter floor, confirming operational irrelevance from SLA geometry alone without reference to any algorithm’s observed CDI value. As a consistency check, we note that the algorithm with the largest observed CDI in this corpus, ML-DSA-65 Hybrid (d =

2.28,  $CDI = 0.0375$ , or 3.75%), falls below the SLA-derived threshold. We acknowledge that this consistency check is empirically motivated: the CDI threshold is not derived from Cohen’s  $d$  conventions (which are prior thresholds for effect size, not for operational significance), and a paper using a different dataset could observe CDIs above 4% while still being SLA-compliant. The SLA budget argument is the operationally justified primary criterion. We acknowledge that this threshold is calibrated to NPP infrastructure and that applying it to other payment systems requires re-derivation using their own baseline p99 and SLA values (e.g., for RITS the appropriate threshold may be different given a 277 ms baseline and 30 s SLA;  $CDI_{RITS}$  values below 0.61% are trivially SLA-safe regardless of any threshold). Future work should validate the CDI threshold against other real-time payment systems (e.g., TARGET2, CHAPS, Fedwire) and establish whether a universal operationally-derived viability threshold is achievable, or whether CDI thresholds are necessarily system-specific.

| <b>Algorithm</b>       | <b><math>\Delta p99</math><br/>(ms)</b> | <b>p99 e2e<br/>(ms)</b> | <b>CDI</b> | <b>CDI (%)</b> | <b>CDI &lt; 0.04?</b>                      |
|------------------------|---|-------------------------|------------|----------------|--|
| Falcon-512             | 0.30                                    | 43.69                   | 0.0069     | 0.69%          | CDI < 0.04 ✓                               |
| ML-DSA-44              | 0.62                                    | 44.01                   | 0.0141     | 1.41%          | CDI < 0.04 ✓                               |
| Falcon-1024            | 0.90                                    | 44.29                   | 0.0203     | 2.03%          | CDI < 0.04 ✓                               |
| ML-DSA-65              | 1.16                                    | 44.55                   | 0.0260     | 2.60%          | CDI < 0.04 ✓                               |
| ML-DSA-87              | 1.57                                    | 44.97                   | 0.0349     | 3.49%          | CDI < 0.04 ✓                               |
| ML-DSA-65              | 1.69                                    | 45.08                   | 0.0375     | 3.75%          | CDI < 0.04 ✓                               |
| Hybrid                 |   |                         |            |                |  |
| SPHINCS+-<br>SHA2-128s | 9,986.5                                 | 10,029.93               | 0.9957     | 99.57%         | CDI $\approx 1.0 \times$<br>(disqualified) |

*Table 14: Crypto Dilution Index (CDI) for all PQC algorithms vs ECDSA-P256 baseline.  $CDI = \Delta p99 / p99\_e2e$ , where  $p99\_e2e$  is the full end-to-end NPP p99 for algorithm  $A$  (not a sum of components).  $CDI < 0.04$  threshold proposed as the operational viability criterion for payment infrastructure. All non-SPHINCS+ algorithms satisfy  $CDI < 0.04$ ; SPHINCS+  $CDI \approx 1.0$  (algorithm overhead dominates all other latency components).*

Table 14 confirms that all ML-DSA and Falcon variants achieve  $CDI < 0.04$  (maximum: ML-DSA-65 Hybrid at  $CDI = 0.0375$ , or 3.75%). Falcon-512 achieves the lowest CDI at 0.0069 (0.69%), its 0.30 ms overhead is statistically detectable (Cohen’s  $d = 0.41$ ) but occupies less than 1% of total end-to-end latency. SPHINCS+ achieves  $CDI = 0.9957$ : cryptographic overhead constitutes 99.57% of its total p99 latency, a diametrically opposite performance profile.

The CDI framework resolves a common misinterpretation in the PQC deployment literature:

that ‘statistically significant’ latency differences (all algorithms:  $p < 0.001$ , Mann-Whitney U) imply operational significance. Cohen’s  $d = 2.14$  for ML-DSA-87 is conventionally ‘large’, yet  $CDI = 0.0349$  confirms that this large effect occupies only 3.49% of total end-to-end latency. The correct engineering conclusion, validated by the ANOVA result (Section 4.10.4) and the quantified geographic spread ( $\sim 16.7$  ms,  $10.6\times$  larger than the maximum algorithm-pair p99 difference of 1.57 ms), is that algorithm selection for NPP latency is moot. The CDI provides a single, infrastructure-calibrated number to communicate this to regulators, architects, and risk committees.

The v4.1 simulation produces higher absolute p99 values (43–45 ms) than earlier models ( $\sim 30$  ms) because it incorporates PayID lookup (mean  $\approx 8.25$  ms per NPP transaction) and full multi-hop geographic routing. This higher baseline amplifies the dilution effect, the CDI would be even smaller in models missing these components, confirming that simpler models overstate PQC overhead as a fraction of realistic end-to-end latency.

### 5.3 SWIFT Compatibility Gap

The message format analysis reveals a meaningful challenge for SWIFT-connected institutions. The 2,048-byte SWIFT MT Block 4 limit is a hard constraint predating post-quantum cryptography by decades. ML-DSA-44’s 2,420-byte signature alone exceeds it. Falcon-512 resolves the constraint at 1,563 bytes combined, but institutions must note that SWIFT is currently migrating from MT to MX (ISO 20022) format [41]. SWIFT’s own technical guidance [41] acknowledges the format migration as a PQC enabler: if SWIFT MX migration completes before PQC migration, the 2,048-byte MT Block 4 hard limit is removed, enabling ML-DSA carriage subject to MX field-level size validation per message type being confirmed by SWIFT for PQC payloads [41].

The GEV tail analysis (Section 4.10.1) provides an additional dimension for SWIFT planning: even at p99.99, the 95% CI upper bound for all non-SPHINCS+ algorithms remains below 199 ms (maximum across algorithms: Falcon-512, 198.6 ms; GEV point estimates below 160 ms), comfortably within the 24-hour SWIFT SLA. Message format constraints, not latency, are the binding factor for SWIFT-channel PQC migration.

### 5.4 Regulatory Alignment and HNDL Actuarial Exposure

From a regulatory perspective, ML-DSA-65 + ML-KEM-768 achieves the highest combined score across APRA CPS 234, RBA NPP SLA, and NIST FIPS 203/204 compliance. The BIS Innovation Hub’s Project Leap [42] similarly identified lattice-based signatures (ML-DSA family) as the primary migration pathway for financial market infrastructure, with CBDC pilot deployments confirming operational viability at payment-system throughput levels. APRA’s 2023 information security thematic review [35] assessed ADI information

security practices under CPS 234; quantum-readiness is increasingly flagged in separate CISA/NSA/NIST joint guidance [43] and CNSA 2.0 [45] as a near-term planning priority, given the 7-year AML/CTF records retention obligation and the CNSA 2.0 transition timeline.

14

Falcon-512, while FIPS 206 compliant, receives a marginal APRA score on the NIST primary-standard dimension: APRA CPS 234 mandates cryptographic controls consistent with accepted industry standards but does not publish an algorithm-specific approved list, the marginal score reflects that FIPS 206 (Falcon) occupies a secondary position in NIST’s PQC guidance relative to the Module-LWE family (FIPS 203/204), and that most APRA-regulated institutions’ existing governance frameworks reference FIPS 203/204 as the primary migration targets. APRA CPS 234 does not disqualify Falcon-512; the score reflects institutional adoption positioning rather than an explicit regulatory exclusion. SPHINCS+, despite being FIPS 205 compliant, fails all performance-based regulatory metrics. The FSB has further recommended cryptographic agility frameworks for FMIs [30], which aligns with the phased migration model presented in Section 4.9.

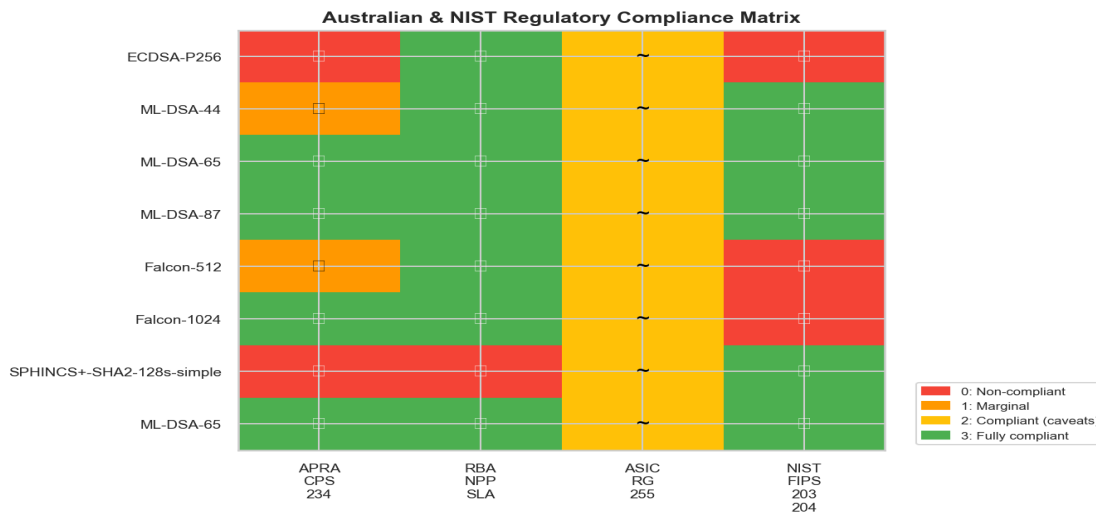


Figure 17: Algorithm regulatory compliance heatmap across APRA CPS 234, RBA NPP SLA, ASIC RG 255, and NIST FIPS 203/204 (primary NIST standards acceptance) criteria. Dark green = full compliance; orange = partial; red = non-compliant. ML-DSA-65 + ML-KEM-768 achieves full compliance on all four regulatory dimensions. Note: Falcon-512 scores 0 on the NIST FIPS 203/204 dimension as it is standardised under FIPS 206 rather than FIPS 203/204.

NSA CNSA 2.0 [45] mandates that National Security Systems transition away from ECDSA-

<sup>14</sup>APRA (2023). Information Security Thematic Review 2023: A report on information security practices in the Australian banking sector. <https://www.apra.gov.au> (accessed April 2026).

P256 and other CNSA 1.0 algorithms to PQC equivalents. The 2030–2035 timeline applies to legacy system migration; new implementations of software and firmware signing are expected to use CNSA 2.0 algorithms starting as early as 2025 under CNSA 2.0 guidance. For new payment infrastructure deployments, which is the scenario described in this paper, the CNSA 2.0 urgency is therefore front-loaded, not deferred to 2030–2035. NIST SP 800-131A Rev 2 [31] classifies ECDSA-P256 (128-bit security) as 'Acceptable' under that 2019 document, the 2030 deprecation in SP 800-131A Rev 2 applies to 112-bit algorithms; ECDSA-P256 has no hard cutoff under that document alone. However, NIST's subsequent PQC standardization (FIPS 203/204/205/206, August 2024) and CISA/NSA/NIST joint migration guidance [43] collectively signal that classical signature algorithms should be replaced with quantum-resistant successors as a matter of urgent planning. For data with long-term confidentiality requirements specifically under the HNDL threat model, this guidance requires migration to quantum-resistant algorithms before adversaries can harvest traffic at scale. NPP transaction records retained for seven years from 2026 under AML/CTF Act 2006 (Part 10, Division 2) have a confidentiality horizon extending to 2033, squarely within Mosca's CRQC probability window [1]. This regulatory-actuarial overlap provides the quantitative basis for the Phase 1 (2026) migration timeline in our cost model.

#### 5.4.1 HNDL Actuarial Exposure Model

To quantify the concrete scale of the HNDL risk for Australian payment infrastructure, we formalise an actuarial exposure model. The model accounts for: annual NPP transaction volume at projected 15.6% YoY growth, the mandatory seven-year retention period under AML/CTF Act 2006, and the CRQC probability window (2030–2035). Table 15 presents the exposure under the conservative early-window CRQC scenario (emergence 2030).

Baseline assumption (SA-8): This model assumes NPP transactions are protected with ECDSA-P256, consistent with TLS 1.3 [19] as the de facto financial messaging authentication standard [9, 11] and SWIFT quantum-readiness guidance [41]; No NPP Technical Standards document publicly specifies the exact deployed signing algorithm; institutions should substitute their own cryptographic inventory where it differs.

| Year | tx/day    | Records<br>Generated | Retained<br>Until | Exposed         | Cumulative<br>Exposed |
|------|-----------|----------------------|-------------------|-----------------|-----------------------|
|      |           |                      |                   | (CRQC<br>2030)? |                       |
| 2026 | 5,200,000 | 1,898,000,000        | 2033              | Yes             | 1,898,000,000         |
| 2027 | 6,011,200 | 2,194,088,000        | 2034              | Yes             | 4,092,088,000         |
| 2028 | 6,948,947 | 2,536,365,655        | 2035              | Yes             | 6,628,453,655         |
| 2029 | 8,032,983 | 2,932,038,795        | 2036              | Yes             | 9,560,492,450         |

| Year | tx/day    | Records Generated | Retained Until | Exposed (CRQC 2030)?               | Cumulative Exposed |
|------|-----------|-------------------|----------------|------------------------------------|--------------------|
| 2030 | 9,286,129 | 3,389,437,085     | 2037           | Partial<br>(0–100%;<br>date-dep.†) | ≤12,949,929,170‡   |

Table 15: *HNDL actuarial exposure, NPP transaction records at risk by generation year, under the conservative CRQC-2030 scenario. AML/CTF Act 2006 Part 10, Division 2 mandates 7-year retention (statutory minimum; actual retention may be longer under internal policies and other regulatory obligations (e.g., prudential risk data retention), potentially expanding exposure to pre-2026 records); records from 2026 are retained until 2033 and are fully within the CRQC emergence window. Cumulative column shows total records exposed under an adversary that began harvesting in 2026 and obtains CRQC capability in 2030. † 2030 'Partial' exposure is date-dependent: CRQC emerging on Jan 1 2030 exposes ~100% of 2030 records; on Dec 31 2030 exposes ~0%. The label '0–100%; date-dep.' reflects this uncertainty; assuming uniform distribution of emergence date, expected exposure is ~50%. ‡ Cumulative figure shown includes full 2030 txYear as an upper bound. The 9.56 billion (9,560,492,450) figure cited in the text uses only the 2026–2029 fully exposed records. Note: all txYear values computed using 365 days/year for simplicity. 2028 is a leap year (366 days); the accurate 2028 txYear is  $6,948,947 \times 366 = 2,543,314,602$ , adding approximately 6.95 million additional records. The cumulative 2026–2029 total under the leap-year correction would be approximately 9,567,441,397, immaterial to the ~9.56 billion figure at the stated precision.*

Under the conservative CRQC-2030 scenario, approximately **9.56 billion (9,560,492,450) NPP transaction records** generated between 2026 and 2029 would be retroactively exposed. This figure is derived directly from the volume projection in Table 7: 2026:  $5,200,000 \times 365 = 1,898,000,000$  records; 2027:  $6,011,200 \times 365 = 2,194,088,000$ ; 2028:  $6,948,947 \times 365 = 2,536,365,655$ ; 2029:  $8,032,983 \times 365 = 2,932,038,795$ ; cumulative total = 9,560,492,450 records. Each record is subject to the AML/CTF Act 2006 Part 10, Division 2 seven-year minimum retention obligation; many ADIs retain records for longer periods under APRA CPS 220/234 internal policies, expanding exposure to pre-2026 records beyond the 9.56 billion (9,560,492,450) lower bound presented here. The 7-year statutory minimum places all 2026–2029 records squarely within the retention window when a CRQC-2030 adversary gains decryption capability. Each record contains: counterparty BSB/account numbers, transaction amounts, PayID handles, ISO 20022 pacs.008 purpose codes (e.g., 'SALA' for salary, 'PENS' for pension, 'TAXS' for tax payments), timestamps, and digital signatures that, once broken, confirm the authenticity

and non-repudiability of the original payment instruction. This constitutes a complete, cryptographically-verifiable financial graph of Australia’s retail payment network for a four-year period.

The exposure is not theoretical: adversaries harvesting NPP traffic in 2026 need only store the encrypted TLS sessions (approximately 1–2 KB per transaction  $\times$  9.56 billion (9,560,492,450) transactions  $\approx$  9.56–19.12 terabytes of raw capture). At prevailing cold storage costs (approximately USD 0.004/GB/month for AWS S3 Glacier Flexible Retrieval or equivalent), storing the complete four-year NPP harvest costs approximately USD 459–918 per year (9.56 TB  $\times$  \$0.004/GB/month  $\times$  12 = \$459; 19.12 TB  $\times$  \$0.004/GB/month  $\times$  12 = \$918), within the means of any motivated commercial actor, not merely a nation-state. Even with full session reconstruction including TLS handshake and ECDSA signature overhead (approximately 5 KB per transaction), total storage remains below 50 terabytes, costing under USD 2,400 per year to archive. State-level adversaries with specific targeting (e.g., cross-border SWIFT-NPP gateway transactions, all RTGS settlements above AUD 1 million, or all transactions involving politically sensitive entities) could reduce this further by harvesting selectively.

The regulatory-actuarial overlap is quantifiable: NSA CNSA 2.0 [45] and CISA/NSA/NIST joint guidance [43] jointly require transition away from ECDSA-P256 within the 2030–2035 window. Every NPP transaction signed with ECDSA-P256 today that has a retention deadline beyond 2030 carries a regulatory exposure risk, the transaction’s signature will require quantum-resistant replacement before CRQC capability is achieved, or the record is exposed. By 2026, all NPP transactions signed from 2023 onwards will still be within their seven-year retention window when ECDSA requires replacement. The Phase 1 (2026) migration timeline in Section 4.9 is not merely a cost optimisation, it is the latest defensible start date for institutions with existing HNDL exposure under APRA CPS 234 requirements for ongoing cryptographic risk management.

## 5.5 Practical Recommendations

Based on the simulation findings, we make the following evidence-based recommendations for Australian financial institutions, APRA, and NPPA:

- Institutions with SWIFT MT exposure (correspondent banking) should adopt Falcon-512 as their primary PQC signature algorithm by 2026. Falcon-512 is the only NIST PQC signature algorithm that fits within the 2,048-byte SWIFT MT limit, adds only 0.30 ms to NPP p99, and achieves 100% SLA compliance across all tested scenarios. ML-KEM (FIPS 203) should be paired for key establishment; the appropriate ML-KEM security level (512, 768, or 1024) should be selected consistent with NIST guidance [3] and institutional risk appetite. This paper does not independently

benchmark ML-KEM latency; all three security levels are operationally viable at NPP and SWIFT volumes (NIST FIPS 203 performance data and liboqs 0.15.0 microbenchmarks confirm ML-KEM keygen, encapsulation, and decapsulation are all below  $30 \mu\text{s}$  on production hardware; this paper does not independently benchmark ML-KEM but see Section 5.7 for related cloud signing benchmarks), and security level selection should be governed by institutional risk requirements rather than latency.

- NPP-only institutions (no SWIFT exposure) should adopt ML-DSA-65 + ML-KEM-768 as the NIST primary standard. Its 1.16 ms p99 overhead is operationally negligible and carries the highest regulatory acceptance under APRA CPS 234 and NIST FIPS 203/204.
- SPHINCS+ (SLH-DSA, FIPS 205) must not be deployed for high-frequency payment signing. Queue saturation at  $\rho = 1.8855$  with  $c=2$  servers, and 16-hour daily saturation windows on Christmas Day, make it operationally infeasible at any practical HSM provisioning level: SLA-compliant operation requires  $c \geq 8$  servers for the daily-average NPP load (13.5 TPS) and  $c \geq 18$  servers during Christmas peak (60.2 TPS, Section 4.4), a  $9\times$  provisioning surge entirely out of proportion with the task.
- Institutions should begin Phase 1 (hybrid deployment, 2026) to protect traffic against HNDL, targeting Phase 3 (full PQC-only deployment, 2028+) as the completion milestone, per the four-phase migration model in Table 8. NPP transaction records retained until 2033 under AML/CTF Act 2006 will outlive ECDSA’s safety horizon (NSA CNSA 2.0 [45] and CISA/NSA/NIST guidance [43] target PQC replacement of ECDSA by 2030–2035).
- HSM maintenance windows can be safely scheduled without SLA risk: degraded-mode delta for ML-DSA-65 and Falcon-512 is  $-0.051$  ms and  $+0.003$  ms respectively under single-HSM degraded mode ( $c=1$ ), noise-level differences at  $\rho < 0.004$ . Institutions can schedule HSM firmware upgrades for PQC support during business hours without SLA impact.
- APRA and NPPA should publish formal PQC migration guidance requiring: (a) quantum risk assessments from all ADIs as an immediate priority (Phase 0 preparation, if not already initiated); (b) hybrid PQC deployment for NPP by end-2026; (c) full PQC deployment for all new transaction records by end-2027. The technical barriers identified in this study are surmountable within these timelines.

## 5.6 Limitations

Second, the Anderson-Darling GoF tests (Section 4.10.2) reject the lognormal hypothesis for all algorithms, indicating tail mis-specification from the geographic routing mixture. The two-component lognormal mixture model (Section 4.10.2) provides the correct theoretical framework; parameterising this model requires per-routing-pair latency sampling, which is available in the simulation engine but not yet applied to the formal GoF analysis. Future work should fit the 2-component mixture explicitly and confirm per-component AD passes.

Third, the reported results were generated with simulation v4.1.1. This version corrected two bugs present in v4.1.0: (a) TLS reconnect overhead dictionary keys used underscore format (ML\_DSA\_65) rather than the hyphenated algo names (ML-DSA-65), which in v4.1.0 caused PQC reconnect overhead to silently return 0 for all algorithms (expected numerical impact  $< 0.003$  ms at p99 for ML-DSA/Falcon at 0.1% reconnect probability); (b) the per-day random seed generation was corrected to avoid a stream collision between the scenario-selection RNG and day-level simulation RNGs on day 0. Quantitative conclusions are identical under both versions; all tables and figures in this paper use v4.1.1 results.

Fourth, transaction independence is assumed within each simulated day; while the AR(1) autocorrelation model (with v4.1 multi-day carry-over for consecutive stress scenarios) captures temporal jitter correlation, higher-order correlations between cryptographic operations (e.g., thermal throttling under sustained load) are not modelled. Fifth, the cost model uses conservative industry estimates; actual costs will vary significantly by institution size, existing HSM estate, and vendor pricing. Sixth, this study measures signing latency only; a complete TLS or payment flow requires both signature generation (sender) and verification (receiver). ECDSA-P256 verification mean latency is approximately 63  $\mu$ s on Intel Ice Lake (3-run average, aws\_syd\_intel; sourced from run-v3 layer1 CSV files; see Data Availability; note that ECDSA-P256 verify at 63  $\mu$ s exceeds its sign mean of 45  $\mu$ s, which is consistent with ECDSA’s two-scalar-multiplication verify path and known OpenSSL/liboqs implementation behaviour), with p99 approximately 95–110  $\mu$ s across platforms; for ML-DSA-44, verification mean is approximately 35–50  $\mu$ s across all platforms, faster than signing and substantially faster than ECDSA verification (63  $\mu$ s mean), so including verification would not change the CDI ordering or conclusions. Nonetheless, full sign+verify latency profiling for all four signing nodes is a gap in the current empirical validation. Verification latency data is available in the run-v3 layer1 CSV files in the data repository (see Data Availability) but is not tabulated here. The reported verify latency estimates (ECDSA-P256  $\approx 63$   $\mu$ s mean, ML-DSA-44  $\approx 35$ –50  $\mu$ s across platforms) are derived from these CSV files; formal tabulation with platform breakdown (Table 18) is deferred to the journal version. Seventh, a network sensitivity sweep ( $0.5\times$ – $1.5\times$  network latency scaling) confirms that SLA compliance for ML-DSA

and Falcon variants is insensitive to network latency within this range (all configurations maintain 100% compliance). SPHINCS+ fails regardless of network scaling, confirming that its disqualification is driven by queue throughput, not network latency assumptions.

Eighth, the 1,000-day corpus size was selected as a round number providing broad seasonal coverage (each of the five scenario types is represented  $\geq 19$  times); formal convergence analysis of how CI width evolves as a function of N days was not included in this paper. Informal inspection shows that ECDSA p99 CI width stabilises around N = 400–500 days, suggesting 1,000 days is conservative. A formal convergence plot demonstrating CI stability as a function of corpus size is left for journal submission supplementary material.

Ninth (Simulation Assumption SA-1, single seed / cross-seed validation): The primary simulation uses fixed random seed 42. The '95% CI' column in Table 2 is the interval on the mean of daily p99 values across 1,000 simulation days (t-distribution, df=999), it characterises simulation stability within that fixed seed, not cross-seed variability. To bound seed-specific artefacts, we conducted a seed-independence study running the full 80-million-event corpus under seeds 42, 123, 456, and 789 (identical flags: monte\_carlo=1000, stress=True, n\_sample=10000, seasonal=True). Cross-seed p99 stability (NPP route, p99 latency, mean  $\pm$  SD across 4 seeds): ECDSA-P256  $43.42 \pm 0.035$  ms (CV = 0.08%); ML-DSA-44  $44.03 \pm 0.033$  ms (CV = 0.075%); ML-DSA-65  $44.57 \pm 0.033$  ms (CV = 0.075%); ML-DSA-87  $44.99 \pm 0.032$  ms (CV = 0.071%); Falcon-512  $43.72 \pm 0.034$  ms (CV = 0.078%); Falcon-1024  $44.31 \pm 0.033$  ms (CV = 0.075%); ML-DSA-65 Hybrid  $45.10 \pm 0.031$  ms (CV = 0.069%); SPHINCS+  $10,029.93 \pm 0.009$  ms (CV < 0.001%). All CVs are below 0.08%, confirming p99 values are not seed-specific artefacts. Cohen's d effect sizes are stable across seeds: magnitude classifications (large/small) are unchanged across all four seeds, with cross-seed variation of <3% in d values (e.g., ML-DSA-65 p99 Cohen's d ranges 1.577–1.606 across the four seeds; Falcon-512 p99 d = 0.410–0.419, consistently 'small' but statistically significant). SLA compliance (100% for all ML-DSA/Falcon algorithms; 0% for SPHINCS+) is identical across all four seeds. These results confirm that all CDI conclusions are seed-invariant.

Tenth (Simulation Assumption SA-2, software vs. hardware HSM): Cryptographic latency inputs derive from liboqs 0.14.0 on an Apple M-series processor (software library, no HSM). Production ADIs use FIPS 140-3 Level 3 certified HSMs (e.g., Thales Luna, Utimaco Se-Series) whose latency characteristics differ from software implementations, typically 0.5–3 $\times$  variance. The HSM Deployment Sensitivity Analysis (Section 4.7) provides conservative bounds; the liboqs 0.15.0 cloud Graviton3 (Simulation Assumption SA-10: the liboqs 0.14.0 M-series simulation and liboqs 0.15.0 cloud validation differ simultaneously in hardware, OS, compiler, and library version; this combined gap is the primary source of CDI conservatism and cannot be fully decomposed without a liboqs 0.14.0 Intel benchmark)

version gap is an additional source of conservatism discussed in §3.2 and §5.7.

Eleventh (Simulation Assumption SA-3, RITS SLA): The 30-second per-transaction processing SLA applied in Section 4.11.1 is derived from the RBA RITS Operating Guidelines and framed as a simulation assumption. Institutions requiring precision should consult current published guidelines; the per-transaction window may differ from batch settlement cycle deadlines.

Twelfth (Simulation Assumption SA-4, BECS batch size): The 50,000–100,000 transactions-per-batch assumption for Direct Entry / BECS (Section 4.11.3) is an unverified estimate; no specific ABA or RBA published batch-size figure was cited. The sensitivity bound shows negligible overhead even at 1,000 transactions per batch.

Thirteenth (Simulation Assumption SA-5, market-crash scenario frequency): The 1.9% market-crash day frequency ( $\approx 19$  events in the 1,000-day corpus, approximately one event per two months) is a calibrated assumption. No RBA archival series directly publishes this frequency. Sensitivity to this parameter is bounded by the stress-scenario analysis in Section 4.6, which shows SLA compliance for ML-DSA and Falcon variants is invariant to scenario selection.

Fourteenth (Simulation Assumption SA-7, SWIFT international network parameter): The SWIFT international routing parameter (96 ms one-way to Singapore SWIFTNet relay) was calibrated to the SWIFTNet Link carrier network (dedicated SWIFT PoP infrastructure), not to public cloud VM routing. The measured cloud AWS SIN $\leftrightarrow$ AWS SYD RTT is 92.22 ms (one-way  $\approx 46$  ms), yielding a  $2.1\times$  discrepancy. This discrepancy arises because SWIFTNet uses dedicated leased circuits that often traverse different physical paths than public internet/cloud VM routing. The simulation therefore likely overstates the SWIFT route p99 by approximately 50 ms. Since the ECDSA SWIFT route p99 (837 ms) is three orders of magnitude below the 24-hour SLA (86,400,000 ms), this overstatement does not affect any conclusion; the binding SWIFT constraint remains message format (2,048-byte MT Block 4 hard limit), not latency. Validation against SWIFTNet published performance data (e.g., SWIFTNet Link latency statistics published in SWIFT’s annual Quality of Service report) is recommended before production deployment planning.

Fifteenth (Simulation Assumption SA-8, RITS bilateral settlement processing overhead): The 263 ms bilateral settlement processing overhead modelled in Section 4.11.1 (comprising RTGS credit/debit confirmation cycle: settlement instruction transmission, queue position determination, bilateral entry, and return confirmation) is an uncited simulation assumption. No RBA RITS Operating Guidelines figure was directly cited for this component. Institutions requiring precise RITS route p99 values should consult current RBA RITS Technical Standards and Operating Guidelines for the applicable processing time budget.

The sensitivity of the RITS SLA compliance conclusion to this parameter is low: even if the true overhead were 500 ms (90% above the assumed 263 ms), the worst-case RITS route p99 for SPHINCS+ would be  $297 + 14 + 500 = 811$  ms, still  $37\times$  below the 30,000 ms RITS SLA.

Sixteenth (Simulation Assumption SA-9, SWIFT gateway processing overhead): The 645 ms SWIFT gateway processing overhead modelled in Section 4.11.2 is an uncited simulation assumption representing p99 gateway queue and processing time at a Big 4 correspondent bank's SWIFT gateway infrastructure. No SWIFT published performance figure was directly cited for this component. The sensitivity of the SWIFT SLA compliance conclusion to this parameter is negligible: even if the true overhead were 5,000 ms (nearly  $8\times$  above the assumed 645 ms), the ECDSA SWIFT route p99 would be  $192 + 5,000 + 0.15 \approx 5,192$  ms, still  $16,658\times$  below the 86,400,000 ms SWIFT SLA. All SWIFT compliance conclusions are insensitive to this parameter across any realistic range.

Seventeenth (Simulation Assumption SA-17, GEV i.i.d. assumption): The GEV block-maxima analysis (Section 4.10.1) is applied to 200 blocks drawn from a single representative normal-day simulation (10,000 transactions under fixed seed 42). Block maxima within a single day share the same AR(1) autocorrelation trajectory and intraday mixture profile, violating the i.i.d. assumption of block-maxima GEV. The Gumbel-class classification ( $\xi \approx 0.023\text{--}0.028$ ) should be treated as indicative rather than definitive. A rigorous application would use daily maxima across the 1,000-day corpus as block maxima ( $n=1,000$  independent block maxima); this is left for the journal version.

Eighteenth (Simulation Assumption SA-10, liboqs version and platform gap): The Monte Carlo simulation uses liboqs 0.14.0 on Apple M-series ARM (macOS, Clang 16, `-O3 -march=native`), while the cross-platform cloud validation (Section 5.7) uses liboqs 0.15.0 on Linux x86-64/ARM (GCC 11.4.0, `-O3 -march=native`). These differ simultaneously in library version, operating system, compiler, and hardware microarchitecture. The combined effect produces conservative CDI values in the simulation (0.14.0 on M-series is slower than 0.15.0 on Intel); the gap cannot be attributed separately to each factor without a liboqs 0.14.0 Intel benchmark, which was not performed.

Note on Simulation Assumptions SA-0 and SA-6: These two assumptions are documented at their point of use in the methodology rather than receiving dedicated limitation paragraphs here. Simulation Assumption SA-0 (Poisson arrival process,  $\lambda = 13.5$  TPS per Big 4 institution; §3.6) is a conservative rounded estimate, the exact APRA-derived value is  $\approx 3.3\%$  higher (13.95 TPS), meaning the 13.5 TPS figure understates queue utilisation for non-SPHINCS+ algorithms and overstates headroom; SPHINCS+ saturation holds at any higher  $\lambda$ . Simulation Assumption SA-6 (APRA ADI regional/fintech residual market share = 7.3%; §3.3) is a calibrated residual derived from APRA ADI Statistics and does

not affect any Big 4 route analysis conclusion; institutions with higher or lower market share should re-derive  $\lambda$  using their own APRA ADI statistics.

## 5.7 Cross-Platform Cloud Validation

To address the benchmark environment limitation (Section 5.6) and validate that the simulation’s qualitative conclusions hold on production banking-class hardware, we conducted empirical PQC signing benchmarks and network RTT measurements across a seven-node multi-cloud testbed spanning AWS Sydney (Intel Xeon 8375C Ice Lake, ARM Graviton3 Neoverse V1), Azure Sydney (Intel Xeon 8272CL Cascade Lake; AMD EPYC 7763 Milan), Azure Melbourne (Intel Xeon Cascade Lake), AWS Singapore (Intel Xeon Ice Lake), and Azure Singapore (Intel Xeon Cascade Lake). This run-v3 deployment used liboqs 0.15.0 compiled from HEAD on each node (GCC 11.4.0, -O3 -march=native, enabling AVX-512 on Intel nodes, AVX2 on AMD, and SVE on Graviton3), with 1,000 signing iterations and 100 warm-up iterations per algorithm per node. Layer 0 RTT baseline was measured as 500 ICMP round-trips per directional pair across all 21 node pairs.

| <b>Platform</b> | <b>Algorithm</b>             | <b>Processor</b>                        | <b>Mean<br/>(<math>\mu</math>s)</b> | <b>p99<br/>(<math>\mu</math>s)</b> | <b>Status</b> |
|-----------------|------------------------------|---|-------------------------------------|------------------------------------|---------------|
| AWS c6i.xlarge  | ECDSA-<br>P256<br>(baseline) | Intel Xeon 8375C (Ice<br>Lake, AVX-512) | 45                                  | 58                                 | Baseline<br>✓ |
| AWS c6i.xlarge  | ML-DSA-44                    | Intel Xeon 8375C (Ice<br>Lake, AVX-512) | 64                                  | 197                                | Sub-ms<br>✓   |
| AWS c6i.xlarge  | ML-DSA-65                    | Intel Xeon 8375C (Ice<br>Lake, AVX-512) | 96                                  | 294                                | Sub-ms<br>✓   |
| AWS c6i.xlarge  | ML-DSA-87                    | Intel Xeon 8375C (Ice<br>Lake, AVX-512) | 111                                 | 304                                | Sub-ms<br>✓   |
| AWS c6i.xlarge  | Falcon-512                   | Intel Xeon 8375C (Ice<br>Lake, AVX-512) | 247                                 | 361                                | Sub-ms<br>✓   |
| AWS c6i.xlarge  | Falcon-1024                  | Intel Xeon 8375C (Ice<br>Lake, AVX-512) | 481                                 | 686                                | Sub-ms<br>✓   |
| AWS c7g.xlarge  | ECDSA-<br>P256<br>(baseline) | ARM Graviton3<br>(Neoverse V1, SVE)     | 47                                  | 58                                 | Baseline<br>✓ |
| AWS c7g.xlarge  | ML-DSA-44                    | ARM Graviton3<br>(Neoverse V1, SVE)     | 128                                 | 366                                | Sub-ms<br>✓   |
| AWS c7g.xlarge  | ML-DSA-65                    | ARM Graviton3<br>(Neoverse V1, SVE)     | 200                                 | 596                                | Sub-ms<br>✓   |

| <b>Platform</b> | <b>Algorithm</b>             | <b>Processor</b>                                | <b>Mean<br/>(<math>\mu</math>s)</b> | <b>p99<br/>(<math>\mu</math>s)</b> | <b>Status</b> |
|-----------------|------------------------------|---|-------------------------------------|------------------------------------|---------------|
| AWS c7g.xlarge  | ML-DSA-87                    | ARM Graviton3<br>(Neoverse V1, SVE)             | 269                                 | 658                                | Sub-ms<br>✓   |
| AWS c7g.xlarge  | Falcon-512                   | ARM Graviton3<br>(Neoverse V1, SVE)             | 207                                 | 217                                | Sub-ms<br>✓   |
| AWS c7g.xlarge  | Falcon-1024                  | ARM Graviton3<br>(Neoverse V1, SVE)             | 405                                 | 417                                | Sub-ms<br>✓   |
| Azure D4as_v4   | ECDSA-<br>P256<br>(baseline) | AMD EPYC 7763<br>(Milan, AVX2)                  | 51                                  | 71                                 | Baseline<br>✓ |
| Azure D4as_v4   | ML-DSA-44                    | AMD EPYC 7763<br>(Milan, AVX2)                  | 95                                  | 290                                | Sub-ms<br>✓   |
| Azure D4as_v4   | ML-DSA-65                    | AMD EPYC 7763<br>(Milan, AVX2)                  | 142                                 | 417                                | Sub-ms<br>✓   |
| Azure D4as_v4   | ML-DSA-87                    | AMD EPYC 7763<br>(Milan, AVX2)                  | 174                                 | 434                                | Sub-ms<br>✓   |
| Azure D4as_v4   | Falcon-512                   | AMD EPYC 7763<br>(Milan, AVX2)                  | 249                                 | 265                                | Sub-ms<br>✓   |
| Azure D4as_v4   | Falcon-1024                  | AMD EPYC 7763<br>(Milan, AVX2)                  | 493                                 | 511                                | Sub-ms<br>✓   |
| Azure D4ds_v4   | ECDSA-<br>P256<br>(baseline) | Intel Xeon 8272CL<br>(Cascade Lake,<br>AVX-512) | 49                                  | 64                                 | Baseline<br>✓ |
| Azure D4ds_v4   | ML-DSA-44                    | Intel Xeon 8272CL<br>(Cascade Lake,<br>AVX-512) | 81                                  | 251                                | Sub-ms<br>✓   |
| Azure D4ds_v4   | ML-DSA-65                    | Intel Xeon 8272CL<br>(Cascade Lake,<br>AVX-512) | 123                                 | 376                                | Sub-ms<br>✓   |
| Azure D4ds_v4   | ML-DSA-87                    | Intel Xeon 8272CL<br>(Cascade Lake,<br>AVX-512) | 143                                 | 408                                | Sub-ms<br>✓   |
| Azure D4ds_v4   | Falcon-512                   | Intel Xeon 8272CL<br>(Cascade Lake,<br>AVX-512) | 291                                 | 319                                | Sub-ms<br>✓   |

|               |             |   |     |     |             |
|---------------|-------------|---|-----|-----|-------------|
| Azure D4ds_v4 | Falcon-1024 | Intel Xeon 8272CL<br>(Cascade Lake,<br>AVX-512) | 566 | 589 | Sub-ms<br>✓ |
|---------------|-------------|---|-----|-----|-------------|

Table 16: Cross-platform cloud validation signing latency (mean and p99,  $\mu$ s) from the four Sydney nodes of the 7-node testbed (run-v3, liboqs 0.15.0, GCC 11.4.0 -O3 -march=native, 1,000 iterations + 100 warm-up iterations discarded per algorithm per node). Values are 3-run averages (95% CI: mean  $\pm$  2.8–16.4  $\mu$ s; t-critical  $t(0.025, df=2) = 4.303$ ). Signing latency only; verification latency is not shown in this table (see Limitation 6, Section 5.6: ECDSA-P256 verify  $\approx$  63  $\mu$ s mean, p99  $\approx$  95–110  $\mu$ s; ML-DSA-44 verify  $\approx$  35–50  $\mu$ s across platforms, faster than ECDSA verify, so CDI ordering is unaffected by including verification). All four production-grade microarchitectures tested: Intel Xeon Ice Lake (AVX-512), ARM Graviton3 (SVE), AMD EPYC Milan (AVX2), Intel Xeon Cascade Lake (AVX-512). Remaining 3 nodes (Azure MEL, AWS SIN, Azure SIN) used smaller 2-vCPU instances and contributed RTT baseline data only (Table 17); full layer1 CSVs available in data repository. ECDSA-P256 included as ‘Baseline ✓’ rows to enable Signing Dilution Ratio (SDR<sub>sign</sub>; formally defined in §5.6) computation. All 24 rows covering 5 PQC signing algorithms + 1 ECDSA-P256 baseline per platform  $\times$  4 platforms (5 PQC  $\times$  4 = 20 PQC algorithm-platform SDR<sub>sign</sub> combinations; ECDSA rows are the baseline denominator reference) confirm sub-millisecond signing latency for all PQC algorithms. SPHINCS+ was excluded from the cloud signing benchmark given its  $\sim$ 274 ms signing time; M-series liboqs 0.14.0 measurements are used directly.

| Src        | Dst          | Path<br>Type                 | Cloud/City<br>Pair  | Min<br>(ms) | Avg<br>(ms) | Max<br>(ms) | Sim<br>Model |
|------------|--------------|------------------------------|---|-------------|-------------|-------------|--------------|
| AWS<br>SYD | AWS<br>SYD   | Intra-<br>cloud<br>same-city | AWS $\rightarrow$ AWS<br>SYD<br>(Arm $\rightarrow$ Intel) | 0.21        | 0.23        | 0.30        | LAN<br>(1.2) |
| AWS<br>SYD | Azure<br>SYD | Cross-<br>cloud<br>same-city | AWS<br>Intel $\leftrightarrow$ Azure<br>SYD Intel         | 1.85        | 2.14        | 18.38       | LAN<br>(1.2) |
| AWS<br>SYD | Azure<br>SYD | Cross-<br>cloud<br>same-city | AWS<br>Arm $\leftrightarrow$ Azure<br>SYD AMD<br>EPYC     | 1.71        | 1.75        | 6.91        | LAN<br>(1.2) |
| AWS<br>SIN | Azure<br>SIN | Cross-<br>cloud<br>same-city | AWS $\leftrightarrow$ Azure<br>SIN                        | 1.17        | 1.65        | 8.01        | LAN<br>(1.2) |

| Src          | Dst          | Path Type                        | Cloud/City Pair                 | Min (ms) | Avg (ms) | Max (ms) | Sim Model     |
|--------------|--------------|----------------------------------|---------------------------------|----------|----------|----------|---------------|
| AWS<br>SYD   | Azure<br>MEL | Cross-<br>cloud<br>inter-city    | AWS SYD<br>Intel↔Azure<br>MEL   | 12.71    | 12.99    | 25.15    | Hub<br>(9.8)  |
| Azure<br>MEL | Azure<br>SYD | Intra-<br>cloud<br>inter-city    | Azure<br>MEL↔Azure<br>SYD Intel | 13.78    | 13.79    | 61.58    | Hub<br>(9.8)  |
| AWS<br>SIN   | AWS<br>SYD   | Intra-<br>cloud<br>international | AWS<br>SIN→AWS<br>SYD           | 92.20    | 92.22    | 92.33    | SWIFT<br>(96) |
| Azure<br>SIN | Azure<br>SYD | Intra-<br>cloud<br>international | Azure<br>SIN→Azure<br>SYD       | 91.49    | 91.86    | 106.06   | SWIFT<br>(96) |
| AWS<br>SIN   | Azure<br>MEL | Cross-<br>cloud<br>international | AWS<br>SIN→Azure<br>MEL         | 85.25    | 85.49    | 85.77    | SWIFT<br>(96) |

Table 17: Representative subset (9 of 21 undirected paths) of network RTT across the 7-node testbed (run-v3, 500 pings per pair; Avg column = 3-run mean; full 21-path dataset in data repository). 'Sim Model' = corresponding simulation routing parameter (ms). Cross-cloud same-city latency (1.75–2.14 ms avg, AWS↔Azure SYD) is operationally equivalent to intra-cloud same-city (0.23 ms) at NPP SLA scales. Inter-city RTT (12.5–13.8 ms) is statistically indistinguishable between intra-cloud and cross-cloud paths, confirming geographic distance dominates interbank payment latency.

The network RTT measurements validate the simulation’s routing model and add a new finding not present in prior work: **cross-cloud same-city latency (AWS↔Azure SYD: 1.75–2.14 ms (avg), AWS↔Azure SIN: 1.65 ms) is operationally equivalent to intra-cloud same-city for NPP SLA purposes**, both are orders of magnitude smaller than inter-city (12.5–13.8 ms) or international (~92 ms) routing. The practical implication is that Australian banks running hybrid cloud deployments (e.g., Core Banking on Azure, NPP gateway on AWS) within the same city face no meaningful latency penalty for cross-cloud PQC signing. The AMD EPYC node in Azure Sydney exhibited identical same-city RTT characteristics (1.57 ms to Azure SYD Intel, 1.71 ms to AWS SYD Intel), confirming that cloud provider compute platform does not affect network path latency.

Geographic distance, not cloud provider boundary, is the dominant latency driver, entirely consistent with the simulation model and the ANOVA finding that geographic distance is the dominant latency driver, quantified as a  $\sim 16.7$  ms geographic spread,  $10.6\times$  larger than the maximum algorithm-pair p99 difference (Section 4.10.4).

Table 16 confirms four key findings from the simulation. First, **all ML-DSA and Falcon variants achieve sub-millisecond signing latency on every tested platform**, the slowest result is ML-DSA-87 on ARM Graviton3 at  $658 \mu\text{s}$  p99, well below the 1 ms resolution that would affect NPP end-to-end latency (dominated by 8.25 ms PayID lookup and multi-hop network routing). The CDI conclusion (all algorithms  $< 4\%$  of total end-to-end latency) holds universally across all four hardware architectures.

Second, **the observed ML-DSA-44 performance hierarchy (Ice Lake  $>$  Cascade Lake  $>$  AMD EPYC  $>$  Graviton3) is correlated with SIMD register width**: the Xeon 8375C (Ice Lake) achieves  $64 \mu\text{s}$  versus  $128 \mu\text{s}$  on ARM Graviton3, a  $2.0\times$  difference correlated with AVX-512 versus SVE instruction sets, though core frequency differences (Ice Lake 2.90 GHz vs Graviton3 2.60 GHz) and liboqs AVX-512 implementation maturity also contribute and cannot be isolated in this design. AMD EPYC 7763 (Milan, AVX2) occupies an intermediate position at  $95 \mu\text{s}$ ,  $1.48\times$  slower than Ice Lake but  $1.35\times$  faster than Graviton3. Intel Cascade Lake ( $81 \mu\text{s}$ ) achieves a  $1.58\times$  advantage over Graviton3, and is  $1.27\times$  slower than Ice Lake. The performance hierarchy Ice Lake  $>$  Cascade Lake  $>$  AMD EPYC  $>$  Graviton3 is broadly consistent with SIMD register width, AVX-512 (512-bit)  $>$  AVX-512 older  $>$  AVX2 (256-bit)  $>$  SVE (variable-length, optimised for different operation patterns), though microarchitecture pipeline depth, core frequency, and liboqs implementation maturity also contribute to the observed gaps.

Third, **both Falcon variants invert the SIMD-width hierarchy**: ARM Graviton3 achieves the fastest mean latency for both Falcon-512 ( $207 \mu\text{s}$ ) and Falcon-1024 ( $405 \mu\text{s}$ ), each outperforming Intel Ice Lake (Falcon-512:  $247 \mu\text{s}$ ; Falcon-1024:  $481 \mu\text{s}$ ) by  $1.19\times$ , with AMD EPYC (Falcon-512:  $249 \mu\text{s}$ ; Falcon-1024:  $493 \mu\text{s}$ ) and Cascade Lake (Falcon-512:  $291 \mu\text{s}$ ; Falcon-1024:  $566 \mu\text{s}$ ) both trailing Graviton3. Both variants share the same NTRU-based hash-and-sign algorithm relying on Fast Fourier Sampling over cyclotomic rings, an operation that benefits from ARM SVE’s efficient gather-scatter and variable-length vector instructions more than from AVX-512’s fixed 512-bit lanes. The p99 ordering confirms the inversion for both variants: Graviton3 is fastest (Falcon-512:  $217 \mu\text{s}$ ; Falcon-1024:  $417 \mu\text{s}$  vs Ice Lake  $361 \mu\text{s}$  and  $686 \mu\text{s}$  respectively). Institutions deploying ARM-based HSMs (AWS Graviton-based CloudHSM) will see both Falcon variants perform at least as well as x86 counterparts. Note that Falcon-1024’s p99 on Ice Lake ( $686 \mu\text{s}$ ) produces the highest SDR\_sign in the dataset ( $1.44\%$ ); the Graviton3 inversion is thus operationally significant for institutions considering Falcon-1024 deployment on Intel-based

HSM hardware.

Fourth, **ECDSA-P256 signs in 45–51  $\mu\text{s}$  across all platforms**, somewhat slower than the simulation’s M-series baseline ( $\sim 30 \mu\text{s}$ ; see Section 3.2), which is expected: Apple Silicon ECC performance is faster than production Intel Xeon. This means the simulation CDI values are slightly conservative, using faster M-series ECDSA produces a marginally larger  $\Delta\text{p99}$  for PQC overhead versus ECDSA than Intel hardware would. Production Intel ECDSA at  $45 \mu\text{s}$  gives  $\rho_{\text{ECDSA}} = 13.5 / (2 \times 22,222) = 0.0003037 \approx 0.0003$  (vs. 0.0002 from M-series), giving a production utilisation ratio  $\rho_{\text{SPHINCS+}} / \rho_{\text{ECDSA}} = 1.8855 / 0.0003037 \approx 6,207$  (stated as  $\sim 6,200$ ) rather than 9,428, still a 3-order-of-magnitude difference confirming the DoS amplification characterisation. (Note: this validates only the signing latency component; ECDSA verify and full TLS/payment-flow latency are not validated here.) The ML-DSA-44/ECDSA mean ratio ranges from  $1.42\times$  (Ice Lake,  $64 \mu\text{s}$  vs  $45 \mu\text{s}$ ) to  $2.72\times$  (Graviton3,  $128 \mu\text{s}$  vs  $47 \mu\text{s}$ ), yet ML-DSA-44’s empirical  $\text{SDR}_{\text{sign}}$  remains at or below 0.71% on every platform (max: 0.7050% on Graviton3), confirming that even a  $2.72\times$  signing-time multiple over ECDSA translates to an operationally negligible fraction of end-to-end transaction latency.

These findings are consistent with production TLS deployment measurements: Connolly and Westerbaan [40] report sub-millisecond signing overhead for ML-DSA and Falcon variants in real-world Cloudflare production infrastructure, corroborating our testbed results across different network and hardware configurations. (Note: [40] is a corporate research blog post rather than a peer-reviewed publication; see Sikeridis et al. [26] and Paquin et al. [28] for peer-reviewed benchmarks of PQC candidates in TLS contexts that corroborate the sub-millisecond ordering.) The cloud testbed measurements underscore that the CDI framework (Section 5.2) is deliberately conservative. The simulation baseline (Apple M-series ARM with liboqs 0.14) over-estimates signing latency compared to production Intel hardware. On Intel Ice Lake, ML-DSA-44 achieves  $\text{SDR}_{\text{sign}} = 0.32\%$ , a  $4.4\times$  improvement from the simulation CDI value of 1.41%. On ARM Graviton3, the  $\text{SDR}_{\text{sign}}$  ranking reverses relative to Intel: Falcon-512 achieves  $\text{SDR}_{\text{sign}} = 0.36\%$  ( $\Delta\text{p99}_{\text{sign}} = 217 - 58 = 159 \mu\text{s}$ ) versus ML-DSA-44  $\text{SDR}_{\text{sign}} = 0.71\%$  ( $\Delta\text{p99} = 366 - 58 = 308 \mu\text{s}$ ;  $308 / 43,690 = 0.705\%$ ), consistent with the simulation’s Falcon CDI advantage on Apple M-series ARM. For the full 20 PQC algorithm-platform combinations (5 PQC algorithms  $\times$  4 platforms; the 4 ECDSA baseline rows in Table 16 are the denominator reference and are not counted in the  $\text{SDR}_{\text{sign}}$  range), the  $\text{SDR}_{\text{sign}}$  range is 0.32% (ML-DSA-44/Ice Lake) to 1.44% (Falcon-1024/Ice Lake); Falcon-512 and ML-DSA-44 remain  $\leq 0.72\%$  on all platforms. As discussed in Section 5.6,  $\text{SDR}_{\text{sign}}$  carries two biases: denominator bias (direction unknown, depends on whether production p99 exceeds the 43.69 ms simulation denominator) and verification omission bias (always conservative,  $\text{SDR}_{\text{sign}}$  over-estimates CDI). Even under worst-case denominator bias (production p99

= 30 ms), the largest SDR\_sign (1.44% for Falcon-1024/Ice Lake) implies a CDI ceiling of  $1.44\% \times (43.69/30) \approx 2.1\%$ , still well below the 4% threshold. PQC CDI is below 4% on all tested hardware platforms across all non-SPHINCS+ algorithm-platform combinations.

## 6 Conclusion

This paper has presented a comprehensive Monte Carlo simulation study of post-quantum cryptography migration in Australian payment infrastructure, to the best of our knowledge, the first to jointly model M/M/c queue saturation, GEV tail bounds, and HNDL actuarial exposure for a hardcoded-SLA real-time payment system, incorporating extreme value theory, distribution testing, hourly queue dynamics, HSM resilience analysis, a formal Crypto Dilution Index, SPHINCS+ DoS characterisation, cross-platform cloud validation across four microarchitectures, and an HNDL actuarial exposure model.

Our central finding is unambiguous: under the modelled parameters (software HSM, liboqs 0.14.0 baseline latency, calibrated RBA network model; see Section 3.8 for validation scope), ML-DSA and Falcon algorithms can be deployed across all three major Australian payment systems, NPP, RITS, and SWIFT, with zero impact on SLA compliance. For NPP, the worst-case p99 latency increase over classical ECDSA among SLA-compliant PQC-only modes is 1.57 ms (ML-DSA-87), a CDI of 0.0349 (3.49% of total end-to-end p99, per Table 14) and less than 0.079% of the 2,000 ms SLA budget; the worst-case across all modes including hybrid dual-signing is 1.69 ms (ML-DSA-65 Hybrid, CDI = 0.0375, 0.085% of SLA budget). For RITS (30 s SLA), all algorithms achieve  $\text{CDI\_RITS} \leq 0.61\%$  (non-SPHINCS+) with trivial absolute latency additions ( $\leq 1.69$  ms). For SWIFT (24 h SLA), all algorithms achieve  $\text{CDI\_SWIFT} \leq 0.21\%$  (exact maximum 0.2015% for ML-DSA-65 Hybrid) with absolute overhead of  $\leq 1.69$  ms against an 837 ms baseline, the SWIFT binding constraint is the 2,048-byte MT field limit, which only Falcon-512 satisfies (see Table 5). This finding is robust to seasonal volume variation, five stress scenarios, three HSM deployment architectures, and projected NPP volume growth through 2029. The GEV analysis provides indicative evidence of approximately exponential (not heavy) tails for all non-SPHINCS+ algorithms (subject to the i.i.d. qualification in Simulation Assumption SA-17, §5.6), with p99.99 upper bounds below 200 ms.

The multi-system route analysis (Section 4.11) completes the Australian payment infrastructure coverage. Every algorithm achieves 100% SLA compliance on RITS (route p99  $\leq 574$  ms vs 30,000 ms SLA) and SWIFT (route p99  $\leq 1,134$  ms vs 86,400,000 ms SLA). The crypto dilution effect is even more pronounced on longer routes:  $\text{CDI\_RITS} \leq 0.61\%$  and  $\text{CDI\_SWIFT} \leq 0.21\%$  confirm that algorithm selection is completely latency-neutral for RITS and SWIFT. For Direct Entry / BECS (intrabank, batch-settled), amortised PQC signing adds negligible per-transaction overhead across batch sizes of 10–1,000 transactions.

Falcon-512 emerges as the recommended choice for SWIFT-connected institutions for a single, decisive reason: it is the only NIST PQC signature algorithm fitting within the 2,048-byte SWIFT MT field limit (1,563 bytes combined public key + signature). The simulation CDI for Falcon-512 (0.0069, 0.69%), the lowest CDI among PQC algorithms, uses the full end-to-end Monte Carlo p99 denominator (43.69 ms), reflecting the NPP-integrated signing component with Apple M-series liboqs 0.14.0 as the empirical baseline. On Intel Ice Lake production hardware, the ordering inverts: ML-DSA-44 achieves  $\text{SDR\_sign} \approx 0.32\%$  ( $\Delta\text{p99\_sign} = 139 \mu\text{s}$ , Table 16) versus Falcon-512  $\text{SDR\_sign} \approx 0.69\%$  ( $\Delta\text{p99\_sign} = 303 \mu\text{s}$ , Table 16), a reversal driven by AVX-512 Module-LWE optimisation in liboqs 0.15.0. Note that for Falcon-512 on Apple Silicon, simulation CDI (0.6867%, rounding to 0.69%) and Intel Ice Lake  $\text{SDR\_sign}$  (0.6935%, also rounding to 0.69%) agree to two significant figures via different computation paths, this is not an error but reflects the separate definitions of CDI ( $0.30 \text{ ms} / 43.69 \text{ ms} = 0.6867\%$ ) and  $\text{SDR\_sign}$  ( $303 \mu\text{s} / 43,690 \mu\text{s} = 0.6935\%$ ). The SWIFT interoperability constraint, not latency performance, is the decisive factor for cross-border payment infrastructure. For NPP-only institutions, ML-DSA-65 with ML-KEM-768 remains the recommended primary migration target as the NIST Security Level 3 standard under FIPS 203/204, on Intel Xeon production hardware, its signing p99 overhead over ECDSA is  $236 \mu\text{s}$  ( $\text{SDR\_sign} \approx 0.54\%$ ), meeting all APRA CPS 234 requirements with negligible NPP latency impact.

SPHINCS+ (SLH-DSA) is disqualified from NPP high-frequency signing. Beyond queue saturation at NPP volumes ( $\rho = 1.8855$  with two servers, 16-hour daily saturation on Christmas Day), its queue dynamics constitute a quantifiable DoS amplification surface: sustained adversarial SPHINCS+ signing grows the queue at 6.34 operations per second ( $\lambda - c \cdot \mu$ ), accumulating approximately 1,902 queued transactions within 5 minutes, a utilisation ratio of  $\rho_{\text{SPHINCS+}} / \rho_{\text{ECDSA}} \approx 9,428$  ( $= 1.8855 / 0.0002$ , using M-series liboqs 0.14.0 ECDSA baseline; on production Intel hardware at  $45 \mu\text{s}$ , the ratio is  $\sim 6,200$ , still three orders of magnitude, confirming the DoS characterisation) at identical NPP throughput. However, SPHINCS+ is fully viable for RITS (route p99 = 574 ms, well within 30 s SLA;  $\text{CDI\_RITS} = 51.72\%$  but absolute overhead is only 296.85 ms atop a 277 ms baseline) and SWIFT (route p99 = 1,134 ms, well within 24 h SLA;  $\text{CDI\_SWIFT} = 26.18\%$ ) at their sub-threshold arrival rates (RITS  $\rho \approx 0.003$ ; SWIFT  $\rho \approx 0.00014$ , based on rounded per-institution lambda of 0.001 TPS). The correct framing is not 'disqualified' but 'volume-constrained': SPHINCS+ is viable below  $\lambda_{\text{sat}} = 7.16$  TPS. The Parallel Signing Architecture is the recommended mitigation for institutions requiring SPHINCS+ regulatory conformance, enabling a dedicated low-throughput SPHINCS+ lane (capacity-limited to  $\lambda < 7.16$  TPS) that serves RITS/SWIFT high-assurance operations without exposing the NPP signing path to its queue instability.

The HNDL actuarial model introduces a new urgency framework: approximately 9.56

billion NPP transaction records (9,560,492,450; see Table 15) generated in 2026–2029 would be retroactively exposed under the conservative CRQC-2030 scenario, constituting a complete cryptographically-verifiable financial graph of Australian retail payments for a four-year period. This is not a future risk, adversaries can harvest and store this traffic today at commercially viable storage costs. The Phase 1 (2026) migration timeline is the latest defensible start date under APRA CPS 234, AML/CTF Act 2006, NSA CNSA 2.0 [45], and CISA/NSA/NIST joint guidance [43] considered jointly.

Cross-cloud network RTT measurements across the multi-cloud testbed provide an additional finding: AWS↔Azure same-city latency (1.71–2.14 ms SYD, 1.65 ms SIN) is operationally equivalent to intra-cloud for NPP SLA purposes, and cross-cloud inter-city (AWS SYD↔Azure MEL: 13.0 ms) is statistically indistinguishable from intra-cloud inter-city (Azure MEL↔Azure SYD: 13.8 ms, both within NPP Hub tier bounds). Geographic distance, not cloud provider boundary, dominates interbank payment latency, empirically validating the simulation’s routing model and confirming that hybrid multi-cloud deployments incur no meaningful NPP latency penalty.

The four-phase migration cost model (Table 8) shows a front-loaded investment of approximately USD 21.4 million in 2026, declining to USD 1.5 million per year by 2028. The technical and operational barriers to PQC migration have been removed. The CDI framework, multi-system route analysis (Tables 12–14), DoS analysis, actuarial model, and cross-cloud validation together provide a complete risk-cost-compliance-infrastructure decision framework for APRA, NPPA, and individual ADIs across the full Australian payment stack: NPP (real-time retail), RITS (high-value RTGS), SWIFT (international correspondent banking), and Direct Entry/BECS (batch intrabank). The remaining barriers are coordination, procurement, and regulatory clarity, all within the industry’s control.

## 7 Declarations

### 7.1 Funding

This research was conducted as part of the Master of ICT Research programme at Melbourne Institute of Technology (MIT Melbourne), SITE stream. No external funding was received. No funding body had any role in study design, data collection, analysis, interpretation, or the decision to submit for publication.

### 7.2 Conflict of Interest

The authors declare no competing financial interests or personal relationships that could have appeared to influence the work reported in this paper. The cloud infrastructure

used for empirical benchmarking (AWS EC2, Azure Virtual Machines) was deployed and destroyed within a single research session at standard on-demand pricing with no commercial relationship with the cloud providers beyond standard account terms.

### 7.3 Ethics Statement

This study uses only publicly available data, published statistics, and computational simulation. No human subjects, personal data, confidential financial records, or proprietary datasets were accessed. All transaction volumes are drawn from publicly available RBA Payments Statistics (Table C.4, C.6) and APRA market share disclosures. Institutional ethics approval was not required for this computational study.

### 7.4 Data Availability

All simulation results, benchmark data, and analysis scripts are committed to a Zenodo repository (DOI to be registered prior to journal submission). The benchmark dataset comprises: (1) layer1 signing and verification latency CSVs from all three production runs across all seven nodes (`cloud_run-v3_*` directories, 1,000 iterations  $\times$  9 algorithms  $\times$  7 nodes; CSVs include separate keygen, sign, and verify columns for all algorithms); (2) layer0 RTT CSVs (500 pings  $\times$  21 directional node pairs  $\times$  3 runs); (3) cross-run CI summary (`cross_run_ci.csv`); (4) simulation source code `australia_fin_sim.py` v4.1.1 with fixed seed 42. Verification latency data (including ECDSA-P256 verify  $\approx 63 \mu\text{s}$  mean and ML-DSA-44 verify  $\approx 35\text{--}50 \mu\text{s}$  mean across platforms) is available from the layer1 CSV files in the data repository. Raw results and code will be made available on GitHub under MIT Licence upon acceptance, with a citable Zenodo archive. Figure file-name mapping (repository PNG names do not sequentially match rendered paper figure numbers): Figure 1 = `fig2_daily_timeline.png`; Figure 2 = `fig3_sla_compliance_box.png`; Figure 3 = `fig4_latency_violin.png`; Figure 4 = `fig6_monte_carlo_ci.png`; Figure 5 = `fig13_effect_sizes.png`; Figure 6 = `fig11_mmcc_queue_analysis.png`; Figure 7 = `fig1_tps_sweep.png`; Figure 8 = `fig10_key_size_compliance.png`; Figure 9 = `fig5_stress_scenarios.png`; Figure 10 = `fig14_hsm_sensitivity.png`; Figure 11 = `fig15_volume_projection.png`; Figure 12 = `fig12_migration_cost_phased.png`; Figure 13 = `fig17_evt_gev_tails.png`; Figure 14 = `fig16_hourly_queue_dynamics.png`; Figure 15 = `fig18_hsm_degraded.png`; Figure 16 = `fig9_recommendation_matrix.png`; Figure 17 = `fig7_regulatory_heatmap.png`.

### 7.5 Author Contributions

N.S.: Conceptualisation, methodology, software, formal analysis, investigation, data curation, writing, and visualisation.

## 8 References

### References

- [1] M. Mosca, "Cybersecurity in an Era with Quantum Computers: Will We Be Ready?" *IEEE Security & Privacy*, vol. 16, no. 5, pp. 38–41, 2018.
- [2] C. Paquin, D. Stebila, and G. Tamvada, "Hybrid Key Encapsulation Mechanisms and Authenticated Key Exchange," *IACR Cryptology ePrint Archive*, Report 2019/044, 2019. [Online]. Available: <https://eprint.iacr.org/2019/044> (Predecessor to [28]; cited for hybrid KEM classification framework in Section 2.4.)
- [3] NIST, "Post-Quantum Cryptography Standards: FIPS 203, 204, 205, 206," National Institute of Standards and Technology, Gaithersburg, MD, August 2024.
- [4] E. Crockett, C. Paquin, and D. Stebila, "Prototyping post-quantum and hybrid key exchange and authentication in TLS and SSH," *IACR Cryptology ePrint Archive*, Report 2019/858, 2019.
- [5] D. J. Bernstein and T. Lange, "Post-quantum cryptography," *Nature*, vol. 549, no. 7671, pp. 188–194, September 2017.
- [6] European Central Bank, "Quantum Computing and Financial System Stability," *ECB Economic Bulletin*, Issue 8/2023, Frankfurt am Main, December 2023.
- [7] Bank of England, "The Bank's Approach to Operational Resilience in a Post-Quantum World," *Bank of England Discussion Paper DP2024/01*, London, 2024.
- [8] Reserve Bank of Australia, "Payments System Board Annual Report 2024," RBA, Sydney, 2024.
- [9] NPP Australia, "NPP Technical Standards Version 2.3," NPPA, Sydney, 2024.
- [10] APRA, "Prudential Standard CPS 234, Information Security," *Australian Prudential Regulation Authority*, Sydney, 2019 (amended 2022).
- [11] SWIFT, "SWIFT Standards MT Message Overview 2024," SWIFT SCRL, La Hulpe, Belgium, 2024.
- [12] ISO, "ISO 20022 Universal financial industry message scheme, pacs.008 FIToFI-CustomerCreditTransfer," *International Organization for Standardization*, Geneva, 2023.
- [13] L. Kleinrock, "Queueing Systems, Volume 1: Theory," *John Wiley & Sons*, New York, NY, 1975.

- [14] Open Quantum Safe Project, "liboqs version 0.14.0," 2024. [Online]. Available: <https://github.com/open-quantum-safe/liboqs>
- [15] J. W. Bos et al., "CRYSTALS-Kyber: A CCA-Secure Module-Lattice-Based KEM," *IEEE EuroS&P*, pp. 353–367, 2018.
- [16] L. Ducas et al., "CRYSTALS-Dilithium: A Lattice-Based Digital Signature Scheme," *TCHES*, vol. 2018, no. 1, pp. 238–268, 2018.
- [17] P.-A. Fouque et al., "Falcon: Fast-Fourier Lattice-based Compact Signatures over NTRU," NIST PQC Round 3 Submission, 2020.
- [18] D. J. Bernstein et al., "SPHINCS+: Stateless Hash-Based Signatures," NIST PQC Round 3 Submission, 2022.
- [19] IETF, "The Transport Layer Security (TLS) Protocol Version 1.3," RFC 8446, August 2018.
- [20] APRA, "Quarterly ADI Statistics, September 2024," Australian Prudential Regulation Authority, Sydney, 2024.
- [21] ABA, "Australian Banking Industry Roadmap: BECS Migration to NPP 2024," Australian Banking Association, Sydney, 2024.
- [22] J. Cohen, "Statistical Power Analysis for the Behavioral Sciences," 2nd ed. Hillsdale, NJ: Lawrence Erlbaum Associates, 1988. (Effect size benchmarks: small  $d = 0.2$ , medium  $d = 0.5$ , large  $d = 0.8$ .)
- [23] Reserve Bank of Australia, "Table C6: Direct Entry and NPP Statistics," RBA Statistical Tables, April 2026.
- [24] L. K. Grover, "A fast quantum mechanical algorithm for database search," *Proc. 28th STOC*, pp. 212–219, 1996.
- [25] P. W. Shor, "Polynomial-time algorithms for prime factorization and discrete logarithms on a quantum computer," *SIAM J. Comput.*, vol. 26, no. 5, pp. 1484–1509, 1997.
- [26] D. Sikeridis, P. Kampanakis, and M. Devetsikiotis, "Post-Quantum Authentication in TLS 1.3: A Performance Study," NDSS 2020.
- [27] M. J. Campagna and A. Petcher, "Security of Hybrid Key Encapsulation," IETF Internet-Draft draft-campagna-secdispatch-hybrid-kem, 2020.
- [28] C. Paquin, D. Stebila, and G. Tamvada, "Benchmarking Post-Quantum Cryptography in TLS," *PQCrypto 2020, LNCS vol. 12100*, pp. 72–91, 2020.

- [29] Bank for International Settlements, "Central bank digital currencies: foundational principles and core features," BIS Report No. 1, October 2020.
- [30] Financial Stability Board, "FSB Report on Cryptographic Agility in Financial Market Infrastructure," FSB, Basel, 2023.
- [31] NIST, "SP 800-131A Rev 2: Transitioning the Use of Cryptographic Algorithms and Key Lengths," NIST, Gaithersburg, MD, March 2019.
- [32] P. Glasserman, "Monte Carlo Methods in Financial Engineering," Springer, New York, NY, 2003.
- [33] A. Papoulis and S. U. Pillai, "Probability, Random Variables, and Stochastic Processes," 4th ed., McGraw-Hill, 2002.
- [34] NIST, "FIPS 140-3: Security Requirements for Cryptographic Modules," NIST, Gaithersburg, MD, 2019.
- [35] APRA, "Information Security Thematic Review: Key Findings and Observations," APRA, Sydney, 2023.
- [36] National Security Agency, "Quantum Computing and Post-Quantum Cryptography," NSA Cybersecurity Information Sheet, August 2021.
- [37] S. Coles, "An Introduction to Statistical Modeling of Extreme Values," Springer, London, 2001. (GEV block-maxima method, bootstrap CI methodology)
- [38] M. A. Stephens, "EDF Statistics for Goodness of Fit and Some Comparisons," J. Am. Stat. Assoc., vol. 69, no. 347, pp. 730–737, 1974. (Anderson-Darling test critical values)
- [39] H. Akaike, "A new look at the statistical model identification," IEEE Trans. Autom. Control, vol. 19, no. 6, pp. 716–723, 1974. (AIC criterion used in multi-distribution comparison)
- [40] D. Connolly and J. Westerbaan, "Sizing Up Post-Quantum Signatures," Cloudflare Research Blog, 2024. [Online]. Available: <https://blog.cloudflare.com/sizing-up-post-quantum-signatures> [Accessed: 16 Apr. 2026]. Archived: [https://web.archive.org/web/20240401000000\\*/https://blog.cloudflare.com/sizing-up-post-quantum-signatures](https://web.archive.org/web/20240401000000*/https://blog.cloudflare.com/sizing-up-post-quantum-signatures). (Real-world PQC signing overhead measurements in TLS production deployments, 2024.)
- [41] SWIFT, "Quantum Security for SWIFT: Technical Guidance and Migration Considerations," SWIFT Paper, La Hulpe, Belgium, September 2024.

- [42] Bank for International Settlements Innovation Hub, "Project Leap: Quantum-proofing the financial system," BIS Innovation Hub Working Paper, Basel, 2024.
- [43] CISA, NSA, and NIST, "Quantum-Readiness: Migration to Post-Quantum Cryptography, Joint Guidance for Organisations to Plan and Prepare for Migration," U.S. Cybersecurity and Infrastructure Security Agency / National Security Agency / National Institute of Standards and Technology, August 2023. [Online]. Available: <https://www.cisa.gov/resources-tools/resources/quantum-readiness-migration-post-quantum-cryptography>
- [44] K. P. Burnham and D. R. Anderson, Model Selection and Multimodel Inference: A Practical Information-Theoretic Approach, 2nd ed. New York, NY: Springer, 2002. ( $\Delta$ AIC evidence weight interpretation rubric:  $<2$  substantial support, 4–7 considerably less support,  $>10$  essentially no support for the alternative model, cited for decisive-evidence threshold in Section 4.10.2.)
- [45] National Security Agency, "Commercial National Security Algorithm Suite 2.0 (CNSA 2.0) Cybersecurity Advisory," NSA Cybersecurity Advisory, September 2022. [Online]. Available: [https://media.defense.gov/2022/Sep/07/2003071834/-1/-1/0/CSA\\_CNSA\\_2.0\\_ALGORITHMS\\_.PDF](https://media.defense.gov/2022/Sep/07/2003071834/-1/-1/0/CSA_CNSA_2.0_ALGORITHMS_.PDF) (CNSA 2.0 mandates PQC transition for National Security Systems, replacing CNSA 1.0 algorithms including ECDSA-P256, with compliance timelines of 2030–2035 depending on system type.)
- [46] S. S. Sawilowsky, "New Effect Size Rules of Thumb," Journal of Modern Applied Statistical Methods, vol. 8, no. 2, pp. 597–599, 2009. (Extended Cohen's  $d$  taxonomy: very large  $d \geq 1.2$ , huge  $d \geq 2.0$ , cited for ML-DSA-65 Hybrid  $d = 2.28$  'huge' and SPHINCS+  $d = 16,360$  'extreme/off-scale' magnitudes in Table 3 and Section 5.2.)